Influence of cGMP signaling on VSMC growth and its dependence on fibronectin in cultured VSMCs and development of atherosclerosis

Dissertation

der Mathematisch-Naturwissenschaftlichen Fakultät

der Eberhard Karls Universität Tübingen

zur Erlangung des Grades eines

Doktors der Naturwissenschaften

(Dr. rer. nat.)

vorgelegt von

Hyazinth Gregor Dobrowinski

aus Tczew (Polen)

Tübingen

2019

Gedruckt mit Genehmigung der Mathematisch-Naturwissenschaftlichen Fakultät der Eberhard Karls Universität Tübingen.

Tag der mündlichen Qualifikation: 28.06.2019
Dekan: Prof. Dr. Wolfgang Rosenstiel
1. Berichterstatter: Prof. Dr. Robert Feil
2. Berichterstatter: Prof. Dr. Robert Lukowski

Table of contents

Zusammenfassung

Der im Jahr 1963 erstmals beschriebene sekundäre Botenstoff cyclisches Guanosin 3´5´-Monophosphat (cGMP) ist ein intrazelluläres Signalmolekül mit vielen Funktionen. Zu den bekanntesten physiologischen Wirkungen von cGMP gehört die Regulation des Blutflusses durch die Relaxation der vaskulären Glattmuskelzellen (VSMCs). cGMP-modulierende Medikamente werden bereits seit mehr als einem Jahrhundert für die Behandlung vasokonstriktiver Erkrankungen verwendet. In Säugetieren erfolgt die Bildung von cGMP entweder durch (1) cytosolische Stickstoffmonoxid (NO)-sensitive Guanylyl-Cyclasen (NO-GCs) oder durch (2) transmembrane "partikuläre" Guanylyl-Cyclasen (pGCs). Letztere werden u.a. infolge der Bindung natriuretischer Peptide wie atriales natriuretisches Peptid (ANP) oder C-Typ natriuretisches Peptid (CNP) aktiviert. In VSMCs werden viele Effekte von cGMP durch die cGMP-abhängige Proteinkinase Typ I (cGKI) vermittelt. Neben der Regulation des Gefäßtonus sind VSMCs auch am vaskulären Umbau im Rahmen kardiovaskulärer Erkrankungen wie Atherosklerose und Restenose beteiligt. Unter physiologischen Bedingungen zeigen VSMCs meist einen kontraktilen Phänotyp. Bei pathophysiologischen Veränderungen wechseln VSMCs jedoch verstärkt in einen sog. synthetischen Phänotyp. Dieser unterscheidet sich vom kontraktilen Phänotyp durch eine gesteigerte Sekretion extrazellulärer Matrix (ECM)-Proteine, den Verlust kontraktiler Markerproteine, sowie eine erhöhte Proliferation. Ob eine Aktivierung des cGMP-Signalwegs den Vorgang der phänotypischen Modulation von VSMCs fördert oder inhibiert und somit die Entstehung vaskulärer Erkrankungen beschleunigt oder verlangsamt, wird kontrovers diskutiert. Bisherige Studien mit Knockout-Mausmodellen verschiedener Komponenten des cGMP-Signalweges weisen auf eine pro-atherosklerotische Wirkung des Signalweges in VSMCs hin.

Im ersten Teil dieser Arbeit wurde der Effekt von cGMP auf das Wachstum von primären VSMCs untersucht. Anders als in vorhergehenden Wachstumsuntersuchungen, deren Ergebnisse auf konventionellen Endpunktmessungen (WST, MTS) beruhten, wurde in dieser Arbeit eine neue Impedanz-basierte Messtechnik mit der Bezeichnung xCELLigence verwendet. Diese Methode ermöglichte es, das Wachstumsverhalten von VSMCs in Echtzeit zu verfolgen und somit ein besseres Verständnis der Wachstumsregulation über den cGMP-Signalweg zu erhalten. Durch den Vergleich von Wildtyp-VSMCs mit NO-GC- und cGKI-defizienten VSMCs konnte gezeigt werden, dass NO (75 µM DETA-NO) das Wachstum von VSMCs durch die Aktivierung der NO-GC-cGMP-cGKI Signalkaskade stark beschleunigt.

In der verwendeten Konzentration hatte NO keinen signifikanten Einfluss auf die Vitalität der Zellen. Im Gegensatz zu NO bewirkte die Stimulation mit ANP nur eine moderate Erhöhung der Wachstumsrate, hatte aber einen stark positiven Effekt auf die Vitalität der VSMCs. Diese Ergebnisse weisen darauf hin, dass es in VSMCs unterschiedliche cGMP-Kompartimente gibt, nämlich NO-induziertes globales cGMP und durch ANP ausgelöste lokale cGMP-Signale, welche unterschiedliche Effekte auf Zellwachstum und Vitalität vermitteln. Darüber hinaus konnte gezeigt werden, dass der cGMP-induzierte Wachstumseffekt am stärksten ist, wenn die Aktivierung des cGMP-Signalwegs direkt bei der Aussaat der Zellen erfolgt. Diese Beobachtung lässt darauf schließen, dass cGMP vor allem in frühen Phasen des Wachstums, insbesondere beim adhärieren der Zellen, eine wichtige Funktion hat.

Im zweiten Teil dieser Arbeit wurde analysiert, welchen Einfluss das ECM-Protein Fibronektin (Fn) auf das Wachstumsverhalten und die phänotypische Modulation von VSMCs ausübt und ob es evtl. mit dem cGMP-Signalweg in Verbindung steht. cGMP-Messungen mit dem FRET-basierten cGMP-Sensor cGi500 zeigten, dass in Gegenwart von Fn gewachsene VSMCs stärker auf CNP als auf ANP reagieren. Mittels Immunfluoreszenz-Färbungen konnte gezeigt werden, dass Zellen, die verstärkt auf CNP reagieren, eine reduzierte Expression kontraktiler Markerproteine (wie z.B. SMαA) haben und demzufolge einen eher synthetischen Phänotyp aufweisen. Schließlich wurde durch die Generierung eines Glattmuskel-spezifischen Fn Knockouts (Fn-smko) untersucht, inwiefern das Fn aus VSMCs die Entstehung von Atherosklerose beeinflusst. Interessanterweise wurde in VSMC-Kulturen aus Fn-smko Mäusen ein erhöhtes Zellwachstum beobachtet. Eine Western Blot-Analyse der Phosphorylierung von VASP (ein Indikator für die Aktivität von cGKI) sowie FRET-basierte cGMP-Messungen (Konzentrations-Wirkungs-Analyse von NO) wiesen darauf hin, dass VSMCs aus Fn-smko Mäusen eine erhöhte NO-GC Aktivität besitzen, was deren erhöhtes Zellwachstum erklären könnte. In Übereinstimmung mit den *in vitro* Daten zeigten *in vivo* Untersuchungen von Fn-smko Mäusen eine Zunahme atherosklerotischer Plaques. Diese Plaques waren im Vergleich zu Plaques aus der Fn-exprimierenden Kontrollgruppe durch eine höhere Stabilität (SMαA > Mac2 positive Fläche eines Plaques) gekennzeichnet. Zusammenfassend weisen diese Ergebnisse darauf hin, dass die genetische Ablation von Fn in Glattmuskelzellen zu einer Amplifikation der wachstumsfördernden cGMP Signalkaskade in VSMCs führt, welche wiederum die Entwicklung stabiler atherosklerotischer Plaques mit einem hohen Anteil an VSMCs fördert.

Summary

Cyclic guanosine 3´-5´-monophosphate (cGMP) is an intracellular second messenger with many functions, first identified in 1963. The role of cGMP in blood flow regulation due to relaxation of vascular smooth muscle cells (VSMCs) is well known and cGMP-modulating drugs are used to treat vasoconstrictive diseases for more than a century. In mammals, cGMP is generated either by (1) cytosolic nitric oxide (NO)-sensitive guanylyl cyclases (NO-GCs) or by (2) transmembrane "particulate" guanylyl cyclases (pGCs). The latter are activated by natriuretic peptides such as atrial natriuretic peptide (ANP) or C-type natriuretic peptide (CNP). In VSMCs, many of the cGMP-induced effects are mediated by the cGMP-dependent protein kinase type I (cGKI). Besides their role in the regulation of blood flow, VSMCs are also involved in vascular remodeling during vascular diseases such as atherosclerosis and restenosis. In a physiological environment VSMCs display a contractile phenotype, whereas during pathophysiological changes VSMCs can switch into a synthetic phenotype. In contrast to the contractile phenotype, the synthetic phenotype is characterized by extensive expression of extracellular matrix (ECM) proteins, loss of contractile marker proteins and high proliferative activity. Whether activation of the cGMP signaling cascade promotes or inhibits the phenotypic modulation of VSMCs and, therefore, accelerates or reduces the development of vascular diseases, is controversially discussed. Previous studies with knockout mice of components of the cGMP pathway suggest a pro-atherosclerotic function of cGMP signaling in VSMCs.

In the first part of this study, the effect of cGMP on the growth behavior of primary VSMCs was investigated. Differently from most previous studies that were based on conventional end-point assays (WST, MTS), the present study used a new impedance-based technique called xCELLigence. This method allowed us to monitor the growth of VSMCs in real-time, thereby gaining a better understanding of cell growth regulation by the cGMP signaling pathway. By comparing wildtype VSMCs with NO GC- and cGKI-deficient VSMCs, we were able to show that NO (75 µM DETA-NO) strongly promoted the growth of VSMC via activation of the NO-GC-cGMP-cGKI signaling cascade. The same concentration of NO had no significant effect on cell viability. In contrast to NO, stimulation with ANP did only result in a moderate promotion of cell growth, but had a strong pro-survival effect on VSMCs. These observations indicate that VSMCs might have distinct cGMP pools, i.e., a global NO-induced pool and a local ANP-stimulated pool, which mediate different effects on cell growth and survival. Furthermore, we demonstrated that the growth-promoting effect of cGMP is strongest when the signaling cascade is already activated during plating of the cells. This observation

implies that cGMP has an important function during early stages of cell growth, especially during adhesion.

In the second part of this study we investigated the role of the ECM protein fibronectin (Fn) on growth behavior and phenotypic modulation of VSMCs and whether it might be connected to cGMP signaling. cGMP measurements with the FRET-based cGMP biosensor cGi500 showed that VSMCs that were grown in the presence of Fn responded stronger to CNP than to ANP. Immunofluorescence staining demonstrated that CNP-preferring cells expressed relatively low levels of contractile marker proteins (e.g. SMαA) indicative of a synthetic phenotype. To investigate to what extent Fn from VSMCs influences the development of atherosclerosis, we generated smooth muscle-specific Fn knockout (Fn-smko) mice. Interestingly, VSMC cultures from Fn-smko mice showed increased cell growth. Western blot analysis of VASP phosphorylation (an indicator of cGKI activity) and FRET-based cGMP measurements (dose-response analysis for NO) indicated that VSMCs from Fn-smko mice had an increased activity of NO-GC, which might explain their increased growth. In accordance to the *in vitro* results, the *in vivo* analysis of Fn-smko mice showed an increase of atherosclerotic plaques. In comparison to plaques from the Fn-expressing control group, plaques from Fn-smko mice were characterized by a greater stability (SMαA > Mac-2 positive plaque area). In summary, these results indicate that genetic ablation of Fn from smooth muscle cells leads to an amplification of the growth-promoting cGMP signaling cascade in VSMCs, which promotes the development of stable atherosclerotic plaques with a high amount of VSMCs.

Danksagung

Als erstes möchte ich mich von ganzem Herzen bei Prof. Dr. Robert Feil und Dr. Susanne Feil bedanken. Und zwar dafür, dass sie mir damals die Möglichkeit gegeben haben, meine Doktorarbeit in Ihrem Labor zu machen. Zu Beginn meiner Arbeit hatte ich so gut wie keinerlei Erfahrung im Bereich der Zellbiologie und Transgener Tiere und auf dem Papier gab es sicherlich bessere Kandidaten. Trotzdem haben mir beide diese Chance gegeben. Wofür ich Ihnen auf immer dankbar sein werde, schließlich hat es mein weiteres Leben maßgeblich beeinflusst.

Ich möchte mich auch vor allem bei Moritz Lehners und Michael Paolillo bedanken. Wir haben beinahe fünf Jahre miteinander verbracht und sind gemeinsam durch viele Höhen aber auch Tiefen gegangen. Moritz ist eine der hilfsbereitesten Personen, die ich kenne und ich hoffe, dass er diese Eigenschaft niemals verlieren wird. Michael ist zu der Person geworden, die mich am stärksten dazu gedrängt hat auch einmal über den Tellerrand hinaus zu schauen und Sachen zu hinterfragen. Beide sind für mich zu richtigen Freunden geworden und ich wünsche mir, dass, wohin es uns auch führen sollte, diese Freundschaft für immer bestehen bleibt.

Ein großes Dankeschön geht auch an Barbara Birk (alias Frau Birkenstock). Sie stand mir vor allem zu Beginn meiner Promotion zur Seite und hat mir vieles beigebracht.

Natürlich möchte ich mich auch beim gesamten verbliebenen Feil Labor bedanken. Nicht nur für den wissenschaftlichen Austausch. Ich finde wir sind ein tolles Team gewesen und hoffe, dass das Feil Labor immer aus solch tollen Menschen bestehen wird.

Vor allem möchte ich mich aber auch bei meiner Mutter und meinem Vater bedanken. Wir sind niemals eine wohlhabende Familie gewesen und es gab Zeiten, in denen es schwer war. Nichtsdestotrotz haben mir meine Eltern geholfen, wo es nur ging. Ohne sie wäre ich niemals da wo ich jetzt stehe.

List of figures

List of tables

List of abbreviations

8-Br-cGMP	8- Bromoguanosine- 3', 5'- cyclic monophosphate, sodium salt
ACh	acetylcholine
ANP	atrial natriuretic peptide
APS	ammonium persulfate
ATP	adenosine triphosphate
BNP	brain natriuretic peptide
BSA	bovine serum albumin
Ca^{2+}	calcium
cAK	cAMP-dependent protein kinase
cAMP	cyclic 3' 5' adenosine monophosphate
CFP	cyan fluorescent protein
cGi	cGMP indicator
cGK	cGMP-dependent protein kinase
cGMP	cyclic 3' 5' guanosine monophosphate
CNG	cyclic nucleotide-gated ion channel
CI	cell index
CNP	C-type natriuretic peptide
CO_2	carbon dioxide
Cre	cyclisation/recombination site-specific recombinase
DEA-NO	2-(N,N-diethylamino)-diazenolate-2-oxide diethylammonium salt
DETA-NO	(Z)-1-[N-(2-aminoethyl)-N-(2-ammonioethyl)amino]diazen-1-ium 1,2-diolate
DMEM	Dulbecco's modified Eagle medium
DMSO	dimethyl sulfoxide
DNA	deoxyribonucleic acid
dNTP	deoxynucleotide triphosphate
ECM	extracellular matrix
EDRF	endothelium-derived relaxing factor
EDTA	ethylenediaminetetraacetic acid
eNOS	endothelial nitric oxide synthase
EtOH	ethanol

FBS	fetal bovine serum
FCS	fetal calf serum
Fn	fibronectin
Fn-smko	smooth muscle-specific fibronectin knockout
FRET	Förster (fluorescence) resonance energy transfer
GC-A	guanylyl cyclase A
GC-B	guanylyl cyclase B
GC-C	guanylyl cyclase C
GFP	green fluorescent protein
GMP	guanosine monophosphate
GTP	guanosine triphosphate
iNOS	inducible nitric oxide synthase
IP3	inositol-1,4,5-trisphosphate
IRAG	IP3 receptor-associated cGMP-kinase substrate
ko	knockout
loxP	locus of X-over in P1
Mac-2	galectin-3
MLC	myosin light chain
MLCK	myosin light chain kinase
MLCP	myosin light chain phosphatase
MYPT	myosin targeting unit
NDS	normal donkey serum
NO	nitric oxide
NO-GC	NO-sensitive guanylyl cyclase
nNOS	neuronal nitric oxide synthase
NOS	nitric oxide synthase
NP	natriuretic peptide
OD	optical densitry
PBS	phosphate buffered saline
PCR	polymerase chain reaction
PDE	phosphodiesterase
Pen/Strep	Penicillin/Streptomycin
pGC	particulate guanylyl cyclase
PMSF	phenylmethylsulfonylfluorid

RNA	ribonucleic acid
ROCK	Rho kinase
ROI	region of interest
ROSA	reverse orientation splice acceptor
RT	room temperature
SMC	smooth muscle cell
SMαA	smooth muscle α-actin
SM22	transgelin
SOA	start of adhesion
Tris	Tris(hydroxymethyl)aminomethane
VASP	vasodilator-stimulated phosphoprotein
VSMC	vascular smooth muscle cell
wt	wildtype
YFP	yellow fluorescent protein

1 Introduction

1.1 Nitric oxide in the cardiovascular system and the role of cGMP signaling

Organic nitrates have been used for over a century for the treatment of the vasoconstrictive disease angina pectoris [1, 2]. In the 1970s, Murad and co-workers discovered that the gaseous signaling molecule (NO) is released by nitroglycerin and other NO-releasing agents and thereby induces vasodilation [3]. By that time, it was still unclear how and where NO is generated in the body. In the 1980s, Furchgott and Zawadzki demonstrated that acetylcholine (ACh) only produces relaxation of isolated blood vessels *in vitro* when the intimal layer was still intact [4]. In cases where the intimal layer was damaged, ACh did not induce vasorelaxation. From this observation they concluded that ACh stimulates the relaxation of blood vessels by activating endothelial cells, subsequently releasing unknown substance(s) (endothelium-derived relaxing factor; EDRF) leading to vasodilation by acting on an unknown target in smooth muscle cells (SMCs) [4]. Further research conducted by several groups demonstrated that NO is identical to EDRF [5, 6]. In 1977, it was reported that NO-induced vasodilation was related to NO's stimulatory effect on guanylyl cyclase, which in turn generates cyclic guanosine 3´-5´ monophosphate (cGMP) [3]. However, the scientific interest in cGMP signaling remained relatively modest until 1998, when Furchgott, Ignarro, and Murad were awarded the Nobel Prize in Physiology or Medicine for their discoveries regarding the action of NO in the cardiovascular system.

cGMP is a versatile intracellular second messenger first identified in 1963 [7]. It is present in many cell types, such as SMCs, platelets, neurons, cardiomyocytes, and many more. It controls numerous physiological processes including cardiovascular homeostasis, inflammation, sensory transduction, cellular growth and survival, and others [8, 9]. The role of cGMP has been extensively studied in the cardiovascular system in relation to vasodilation and blood pressure regulation. It is well known now that cGMP affects these processes through its function in vascular smooth muscle cells (VSMCs) [10, 11].

The effects of cGMP are mediated by its binding to at least three different classes of effector proteins: (1) Cyclic nucleotide-gated (CNG) cation channels, (2) cGMP-dependent protein kinases, also known as cGKs or PKGs **(see chapter 1.3)**, and (3) cGMP-regulated phosphodiestereases (PDEs) **(Figure 1)**. The role of CNG channels is more restricted to the sensory system, whereas PDEs and cGKs play a role in many tissues [10, 12, 13]. PDEs control

cGMP levels by hydrolyzing it to guanosine-monophosphate (GMP); in VSMCs mainly due to PDE5 [14, 15]. In addition, the enzymatic activity of some PDEs that hydrolyze cyclic adenosine 3´-5´ monophosphate (cAMP) is regulated by binding of cGMP, thereby, enabling a crosstalk of cGMP and cAMP signaling. For example, in the presence of high cGMP concentrations cAMP hydrolysis by PDE3 is inhibited resulting in increased cAMP concentrations and changes of cellular functions [16, 17].
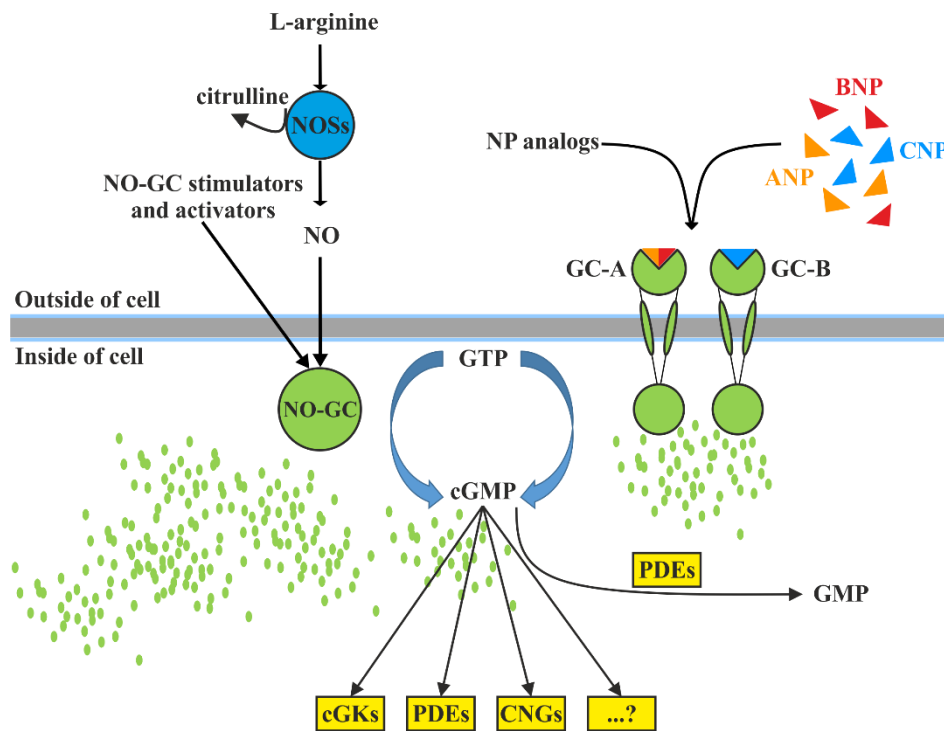
Figure 1. cGMP signaling pathway

Shown here are cGMP generators (green), cGMP (green dots), and cGMP effectors (yellow). NOSs, nitric oxide synthases; GC-A and GC-B, guanalyl cyclase A and B, respectively; NO, nitric oxide; ANP, BNP and CNP, atrial, B-type and C-type natriuretic peptide, respectively; NO-GC, NO-sensitive guanylyl cyclase; cGKs, cGMP-dependent protein kinases; PDEs, phosphodiesterases; CNGs, cyclic nucleotide-gated cation channels. For details see text.

1.2 cGMP generators

In mammals, there exist two families of guanylyl cyclases (GCs) that generate cGMP from guanosine-triphosphate (GTP). They differ in their subcellular localization and are activated by different ligands: (1) Intracellular 'soluble' NO-sensitive GCs (NO-GCs) are stimulated by NO, which is generated by NO synthases (NOSs) [18]; (2) transmembrane 'particulate' GCs (pGCs) are activated by natriuretic peptides (NPs). For example, GC-A binds

atrial and B-type natriuretic peptide (ANP, BNP), GC-B binds C-type natriuretic peptide (CNP) **(Figure 1)** and GC-C is activated by guanylin and uroguanylin [19].

NOSs convert the amino acid arginine into citrulline and NO **(Figure 1)** [20]. To date, these enzymes are classified into three different isoforms, namely endothelial NOS (eNOS), neuronal NOS (nNOS) and inducible NOS (iNOS). eNOS is present in endothelial cells including those from the central nervous system [21]. nNOS generates NO mainly in neurons, but also in some non-neuronal tissues such as skeletal muscle. iNOS is associated with immune responses and has been reported in macrophages and microglia [21, 22]. In contrast to iNOS, both eNOS and nNOS demonstrate calcium (Ca^{2+})-dependent regulation [22, 23]. Compared to eNOS and iNOS the N-terminus (220 amino-acids) of nNOS contains a binding site for the post synaptic density protein 95 (PSD-95), termed PDZ domain. The term PDZ comes from the first letters of the first three proteins discovered with said domain, namely **P**SD-95, drosophila disc large tumor suppressor (**D**lg1), and zonula occludens-1 protein (**z**o-1) [22]. It allows nNOS to interact with N-methyl-D-aspartic acid (NMDA) receptors [24, 25]. Researchers have postulated that agonist-induced NMDA receptor stimulation activates nNOS and thus NO generation in neurons, pointing to a neuronal activity-dependent modulation of cGMP signaling.

Binding of NO to NO-GCs triggers the generation of cGMP **(Figure 1)**. NO-GCs are heterodimers consisting of an α subunit and a heme-containing β subunit. In mammals, two functional NO-GC isoforms are known to exist, namely NO-GC1 (α1β1 subunit combination) and NO-GC2 (α2β1 subunit combination) [26]. There has also been homology analysis which identified a β2 subunit [27], but until now there is a lack of evidence that this subunit is functional and so far it is regarded to be a "pseudogene" [26]. While NO-GC1 is expressed in most tissues, especially in the cardiovascular system, NO-GC2 expression is primarily restricted to the brain, lung, colon, heart, spleen, uterus and placenta. [28]. Neither biochemical characterization (catalytic activity, sensitivity to NO) nor physiological analyses of these two isoforms revealed striking differences [29]. However, different subcellular localization might determine the functional role of the respective isoform. Namely, the C-terminus of the α2 domain of NO-GC2 provides a platform for interaction with the PDZ domains of various proteins located at the cell membrane [26]. Finally, it should be mentioned that although NO mediates many of its effects via the cGMP signaling pathway, NO can also function independently of cGMP, for example, due to S-nitrosylation of cysteine residues from intracellular proteins [30]. Such direct, cGMP-independent effects of NO should be considered, and appropriate control experiments be performed, to avoid misinterpretation of results.

As previously stated, cGMP generation cannot only be elicited by binding of NO to intracellular NO-GCs. Binding of extracellular peptide hormones to membrane bound pGCs also leads to cGMP generation **(Figure 1)**. The family of pGCs consists of seven members, GC-A through GC-G [19]. In contrast to NO-GCs, which act as heterodimers, all known pGCs form homodimers. They share similar protein topology composed of an intracellular region, an extracellular region (≈500 amino acids each) and a short hydrophobic transmembrane domain (21 – 25 amino acids) [19]. The extracellular region is responsible for ligand binding and specificity. The intracellular region is responsible for signal transduction and is composed of two ≈250 amino acid long domains: (1) The juxtamembraneous protein kinase-homology domain (KHD), (2) and a cGMP-generating GC domain [31, 32]. Until now, no research has shown that the KHD domain exerts kinase activity and the specific function of this region remains unknown [19].

In contrast to the retinal (GC-E and GC-F) and olfactory (GC-D and GC-G) GCs, which are stimulated by Ca^{2+} or CO_2 and low temperatures, respectively, GC-A through GC-C respond to natriuretic peptides [33]. GC-A is mainly expressed in vasculature, endothelium, heart, adrenals glands, spleen, kidney, central and peripheral nervous system [33], generates cGMP upon stimulation with ANP and BNP, and regulates blood pressure and metabolism. GC-B is expressed in vasculature, endothelium, heart and bone, generates cGMP upon stimulation with CNP, and regulates vascular regeneration, cardiomyocyte growth and endochondral ossification [33]. GC-C is expressed in the kidney and intestinal epithelium and is stimulated upon binding of heat-stable entero toxins and the intestinal peptides guanylin and uroguanylin. GC-C is implicated in electrolyte/water transport regulation and epithelial cell growth and differentiation [33]. Finally, the natriuretic peptide receptor C, also called clearance receptor NPR-C (not to be confused with GC-C), has no guanylyl cyclase activity and is thought to be responsible for the internalization and degradation of NPs [34].

1.3 Structure, tissue distribution and function of cGMP-dependent protein kinases

In principle, the effects of cGMP are mediated by its binding to CNGs, PDEs, and cGKs. As cGKs, also known as protein kinases G (PKGs), are the principle cGMP effectors in most tissues, they will be explained in more detail. They belong to the family of serine/threonine kinases and are present in a variety of organisms [11]. In mammals, two genes encode three different cGKs: cGKIα, cGKIβ, and cGKII. cGKII is encoded by *prkg2* and cGKI is encoded by *prkg1*. The N-terminal region (≈ amino acids 1 to 100) of cGKI is encoded by two alternative

15

5'-exons resulting in expression of two isoforms, cGKIα and cGKIβ, which differ only in their N-terminal domains [11, 35-37]. cGKIα is ≈10-fold more sensitive to cGMP stimulation than cGKIβ [38]. cGKI (≈75 kDa per subunit) as well as cGKII (≈85 kDa per subunit) are homodimers. Each subunit is composed of three domains; (1) The N-terminal domain is responsible for homodimerization (via a leucine zipper), interaction with other proteins, and autoinhibition of kinase activity in the absence of cGMP; (2) The regulatory domain controls the kinase activity by binding of cGMP. It contains two non-identical cGMP-binding pockets, namely the high affinity pocket cGMP I and low affinity pocket cGMP II; (3) The kinase domain catalyzes the transfer of γ-phosphate from ATP to the hydroxyl group of a serine/threonine side chain of the target protein [11, 39]. To enable efficient phosphorylation of target proteins, the regulatory domain must bind two cGMP molecules at each subunit (four molecules in total), which leads to the release of the catalytic domain from the N-terminal autoinhibitory/pseudosubstrate domain [39] **(Figure 2)**.

cGKII is anchored to the plasma membrane by N-terminal myristoylation and has been found to be expressed in renal cells, chondrocytes, lung, kidney, several brain nuclei, intestinal mucosa and others [11, 37, 40]. cGKII has been shown to be involved in the modulation of neurobehavioral effects of alcohol [41], vesicle endo- and exocytosis in cerebellar granule neurons [42], and bone growth [43, 44]. In line with its weak/undetectable expression in the cardiovascular system, a function of cGKII in SMCs has not been reported to date.

In contrast to cGKII, cGKI is predominantly localized in the cytosol and is expressed in many cell types of the cardiovascular system. Particularly high concentrations (> 0.1 µM) of cGKI are found in SMCs and platelets [11]. It is also expressed in cardiomyocytes, fibroblasts, immune cells, neurons, and many other cell types. In line with its broad expression profile, cGKI is involved in various physiological processes. It controls platelet aggregation and thrombosis [45, 46], and in the heart, cGKI was shown to mediate the negative inotropic effect of NO/cGMP signaling [11, 47]. Furthermore, cGKI was reported to have a pro-angiogenic function in blood vessel formation [48-50]. The most thoroughly investigated effect of cGKI is its impact on blood pressure regulation via the relaxation of VSMCs [36, 51, 52] **(see chapter 1.4)**. Moreover, cGKI was found to play important roles in the sensitization of nociceptive neurons and distinct forms of synaptic plasticity and learning [53, 54]. Emerging evidence indicates that the cGMP-cGKI signaling pathway might also be involved in the progression of cancer and that the cGMP signaling pathway might be a new target for cancer therapy [55-58]. As the cardiovascular system is the focus of this work, the impact of cGMP-cGKI on SMCs will be explained in more detail in the following chapters.
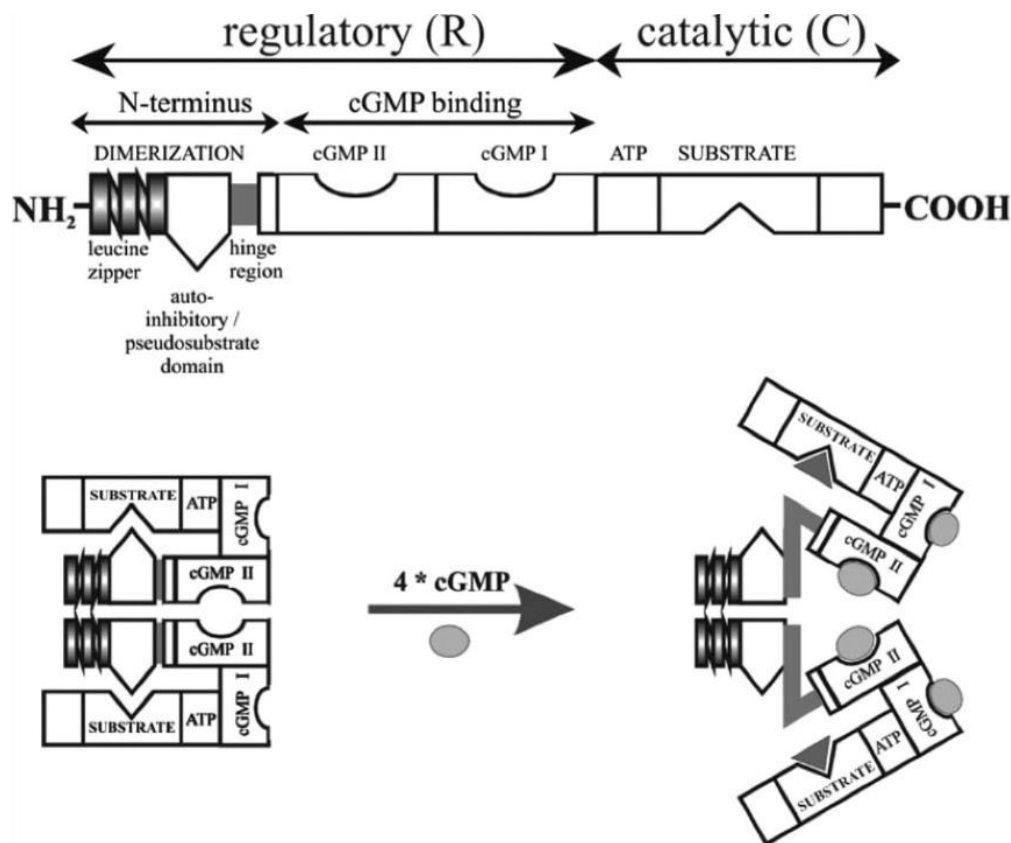
Figure 2. Structure of cGMP dependent protein kinases

cGKs are homodimers and each subunit is composed of three domains. (1) The N-terminal domain, responsible for homodimerization and protein interaction; (2) The regulatory domain, which activates the kinase activity by binding of cGMP; (3) The kinase domain, which catalyzes phosphorylation of serine/threonine side-chains of target proteins. Upon binding of 4 cGMP molecules, the catalytic domain is released from the autoinhibitory N-terminal domain. For further details see text. Taken from Hofmann et al. 2009 [39].

1.4 cGMP-cGKI-mediated effects on vascular tone

The role of cGMP-cGKI for the regulation of vascular tone and blood pressure is one of the best studied but also most poorly understood aspects of this signaling cascade. Vascular cGMP levels are increased in response to stimulation with NO and ANP. Thereby, small arteries and arterioles relax and blood pressure decreases [10, 11, 51]. The relationship between cGMP and blood pressure regulation was confirmed by studies with knockout mice for various components of the cGMP signaling cascade. For example, mice became hypertensive when they lacked eNOS [59, 60], NO-GC [61-63], ANP [64] or its corresponding receptor GC-A [65]. In contrast, the analysis of cGKI-deficient mice indicated that cGKI is most likely not essential for basal blood pressure homeostasis but mediates acute blood pressure drops in response to NO-releasing drugs [36, 52]. These findings suggest that both acute and basal blood pressure regulation are cGMP-dependent processes, but mediated by different effector proteins.

17

Even though its role for endogenous blood pressure control is questionable, it is well accepted that activation of cGKI in VSMCs results in vasodilation via relaxation of VSMCs [36, 66]. There are multiple targets of cGKI that are associated with the contractility of VSMCs: (1) The release of (Ca^{2+}) from intracellular stores might be inhibited by phosphorylation of the membrane-anchored protein, inositol trisphosphate receptor-associated cGMP-kinase substrate (IRAG), thereby, inhibiting inositol 1,4,5-triphosphate (IP3)-induced Ca^{2+} release [67, 68]; (2) Activation of the Ca^{2+}-activated K^+ channel (BK_{Ca}) either through direct phosphorylation or indirectly via cGKI's action on a protein phosphatase (probability of opened channel might be increased) might lead to a hyperpolarization of the membrane, thereby, reducing Ca^{2+} influx and inducing relaxation of SMCs [51]; (3) Moreover, cGKI might promote the re-uptake of cytosolic Ca^{2+} into the endoplasmic reticulum by targeting the sarco/endoplasmic reticulum Ca^{2+}-ATPase (SERCA) regulator, phospholamban [69]; (4) cGKI-induced vasorelaxation might be achieved via a Ca^{2+}-independent signaling mechanism by phosphorylation of the regulatory subunit 1 (MYPT1) of myosin light-chain phosphatase (MLCP). In consequence, MLCP is activated, which leads to a dephosphorylation of the myosin light chain (MLC) [70, 71] culminating in relaxation of VSMCs [72]; (5) Furthermore, the impact of cGKI on VSMC contraction might be explained by an interplay between the Rho/Rho kinase (ROCK) pathway and myosin MLCP signaling. It has been shown that cGKI inactivates RhoA-GTP through phosphorylation [73, 74], leading to a reduced activity of ROCK, which results in an increased MLCP activity. In sum, activation of cGKI in VSMCs might reduce cytosolic Ca^{2+} and/or increase MLCP activity, ultimately leading to vasorelaxation (**Figure 3**). Overall, dynamically regulated Ca^{2+} transients regulate the contractile status of VSMCs. And in contrast to the Ca^{2+} reducing, vasorelaxing effect of cGKI, the rise in Ca^{2+} calcium transients activates the Ca^{2+}/calmodulin (CaM)-dependent, myosin light-chain kinase (MLCK). Thereby MLC is phosphorylated, leading to the contraction of VSMCs.
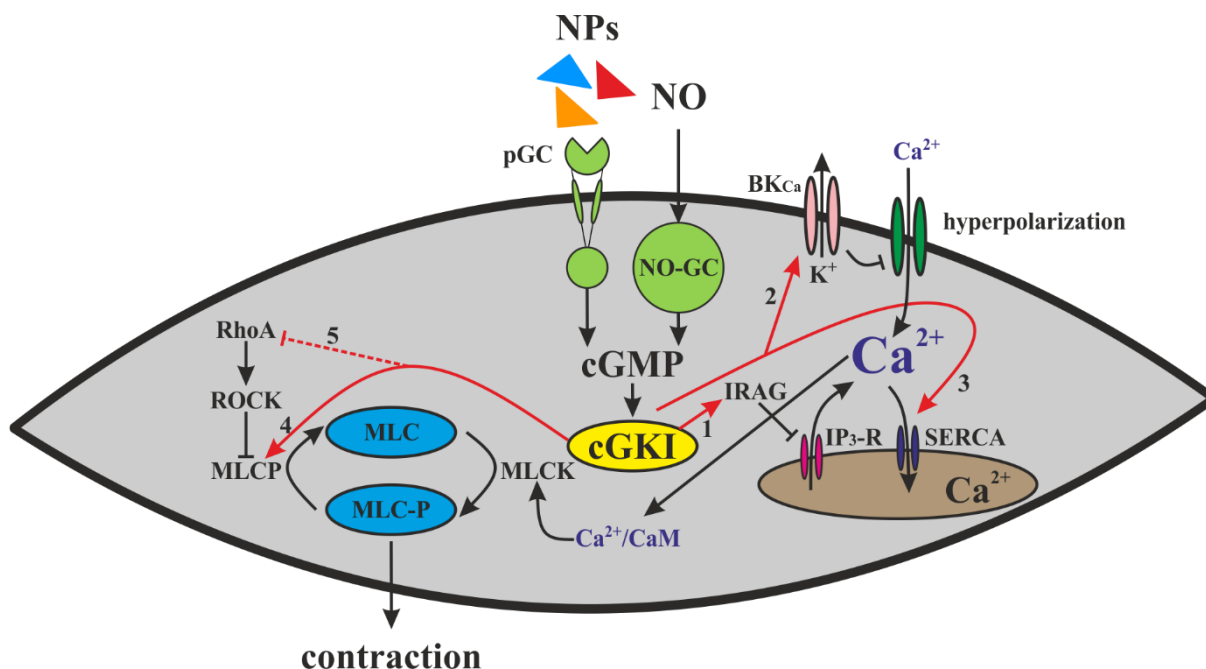
Figure 3. Relaxation of a VSMC in response to cGMP-cGKI activation

The cGMP-cGKI signaling pathway has multiple targets which are associated with the relaxation of vascular VSMCs. (1) Phosphorylation of the inositol trisphosphate receptor-associated cGMP-kinase substrate (IRAG); (2) Hyperpolarization of the membrane due to activation of BK_{Ca} channels; (3) Re-uptake of cytosolic Ca^{2+} into the endoplasmic reticulum; (4) Dephosphorylation of myosin light-chain (MLC); (5) Interaction with Rho/Rho kinase (ROCK) signaling. For further details see text.

1.5 Role of VSMCs during vascular remodeling

In addition to their well described role in acute regulation of blood flow, VSMCs are also involved in long-term vascular remodeling in the context of vascular diseases. In a healthy blood vessel, VSMCs reside in a 'contractile' state with low proliferative activity and strong expression of contractile proteins (e.g. SM α-actin, SM myosin heavy-chain, calponin, SM22α) [75, 76]. Upon pathological changes in their environment, VSMCs have been observed to switch into so-called 'synthetic' cells. The synthetic phenotype of VSMCs is characterized by extensive secretion of extracellular matrix (ECM) proteins, loss of contractile marker protein expression and high proliferative activity **(Figure 4)** [75, 76]. The process of VSMC phenotypic modulation is also known as VSMC plasticity [17]. Before discussing the role of VSMCs and cGMP signaling in the process of vascular remodeling during atherosclerosis, I will talk about cGMP and VSMC plasticity in the *in vitro* situation.

Contractile phenotype
(Contraction and Relaxation)

Synthetic phenotype
(Synthesis of extracellular matrix)

Signalling factors
Extracellular matrix
etc.

Fusiform morphology

Rhomboid morphology

High expression of contractile proteins (e.g. α-smooth muscle actin (αSMA), transgelin (SM22α))

Low expression of contractile proteins (e.g. αSMA, SM22α)

Low proliferation and migration

High proliferation and migration

Figure 4. Phenotypic plasticity of VSMCs

VSMCs can switch from a contractile phenotype (physiological conditions) into a synthetic phenotype (pathophysiological conditions). The contractile phenotype is characterized by a fusiform morphology, high expression of contractile marker proteins, and low proliferation and migration. In contrast, the synthetic phenotype is characterized by a rhomboid morphology, low expression of contractile marker proteins, and high proliferation and migration. For further details see text. Adapted from Beamish et al. 2010 [75].

1.5.1 cGMP and VSMC plasticity in cell culture

Over the last decades, studies have intensively investigated the therapeutic relevance of the NO-cGMP-cGKI signaling axis in VSMC plasticity [11, 77-82]. Phenotypic modulation of VSMCs is involved in the development of vascular diseases such as atherosclerosis and restenosis, and can also be observed in the *in vitro* situation [83, 84]. Primary VSMC cultures (cells isolated from aorta by enzymatic digestion, plated on plastic dishes and grown for 3-7 days) develop a synthetic phenotype, which is further amplified by passaging (subculturing) [85]. However, up to now it remains controversial as into which direction the cGMP signaling pathway pushes VSMCs, namely, whether it promotes or inhibits the phenotypic switch into the synthetic state.

One reason why this controversy is still not solved is the lack of highly specific activators and inhibitors of cGMP signaling, which are suitable for use in intact cells [86]. For example, some of the "specific" cGKI-activating cGMP analogues exert effects which are independent of cGKI [87, 88]. Rp-PET-8-Br-cGMP, which is mistakenly known as one of the

most potent, cell permeable and selective cGKI "inhibitors", was shown to be a partial agonist of cGKIα rather than antagonist [89]. DT-2 another "specific" inhibitor of cGKI was shown to lose its specificity in intact cells [90]. Furthermore, the widely used cGKI "inhibitor" KT5823 appears to rather act as a cGKI stimulator in intact cells [91]. To circumvent the problems associated with the use of these pharmacological tools, many groups started to use RNA knockdown techniques or knockout mice deficient in components of the cGMP signaling cascade [17].

The investigation of VSMC plasticity is further complicated by the fact that primary cells and passaged cells behave differently in response to cGMP stimulation. Many studies were performed with passaged VSMCs. Lincoln and colleagues [78] demonstrated that activation of the NO-cGMP pathway leads to reduced proliferation and/or increased expression of contractile marker proteins, indicating a shift towards the contractile phenotype. YC-1, a NO-GC stimulator [92-95], was shown to reduce the proliferation of passaged VSMCs [96]. In line with these observations, adenoviral transduction of cGKI in passaged rat aortic smooth muscle cells (RASMCs) reduced proliferation, and apoptosis was increased after stimulating the cGMP signaling pathway [97]. Based on these results, cGKI was postulated to promote the contractile VSMC phenotype. But as already mentioned at the beginning of this chapter, the impact of the cGMP signaling pathway on the phenotype of VSMCs strongly depends on the initial state of the cell; whether they are already synthetic (passaged cells) or still share properties of the contractile one (primary cells).

For example Garg and Hassid were able to observe the bilateral effect of cGMP signaling, in passaged and primary cells. They showed that NO-donors or the cGMP analogue 8-Br-cGMP reduced proliferation in passaged RASMCs [98]. Surprisingly, in contrast to their observations made in passaged cells, Hassid and colleagues demonstrated that activation of the NO-cGMP cascade amplified the growth-promoting effect of fibroblast growth factor 2 in primary RASMCs. cGMP analogues were also shown to stimulate the pro-proliferative mitogen-activated protein kinase pathway in freshly isolated RASMCs [99]. These findings support the notion that the outcome of increased cGMP signaling critically depends on the phenotype of the studied VSMCs ("contractile" primary vs. "synthetic" passaged).

More recently, by comparing cGKI-expressing and cGKI-deficient primary VSMCs, the Feil group clearly demonstrated that the growth-promoting effect of NO/cGMP is transduced via activation of cGKI [79]. Interestingly, low concentrations (0.5 µM) of the NO-donor diethylenetriamine NONOate (DETA-NO) increased VSMC growth in a cGKI-dependent manner, whereas high concentrations of DETA-NO (100 µM) inhibited VSMC growth

independent of cGKI expression. A cGMP-independent growth inhibiting effect of high NO concentrations in VSMCs was observed by other groups as well [80, 100]. Extending the results obtained by Wolfsgruber et al. [79], Weinmeister et al. [101] suggested that passaging of VSMCs might result in functional changes of the endogenous NO-cGMP-cGKI signaling cascade and, therefore, result in alterations of the growth response. While 8-Br-cGMP clearly promoted the growth of primary VSMCs, this effect was lost already after the first passage and even reversed into a weak growth-inhibiting effect [101]. This study also addressed the mechanism behind the growth promoting effect of cGMP in primary VSMCs. The signaling pathway predominantly promotes the cell adhesion process by activating $\beta 1$ and $\beta 3$ integrins [101]. Complementing the results obtained with cGKI-deficient VSMCs, Segura-Puimedon and colleagues analyzed the growth behavior of primary VSMCs lacking NO-GC [80]. Consistent with the data obtained with cGKI-knockout VSMCs, NO-GC-deficient VSMCs showed less proliferation, migration and increased expression of contractile marker proteins [80].

Taken together, these observations support a model, in which the NO-cGMP-cGKI signaling axis promotes the growth and survival of primary VSMCs.

1.5.2   Vascular plasticity in atherosclerosis

Atherosclerosis leads to heart attack and stroke, which are the major causes of death in industrialized nations [102]. Although atherosclerosis is heavily investigated, the development of this vascular disease and particularly the impact of the different cell types involved in this process is not well understood [103-106]. Atherosclerosis is induced via a chronic inflammatory condition, which results from complex interactions of modified lipoproteins and various cell types, including cells of the vessel wall and monocyte-derived macrophages [107-109]. The detailed contribution of mature VSMCs residing in the vascular media is controversially discussed [110, 111]. It is well known that the so-called fibrous cap, which covers the atherosclerotic lesion on its luminal side, is built up of VSMCs that are derived from the vascular media and express contractile marker proteins [112]. Generally, the fibrous cap is proposed to be beneficial, stabilizing the plaque via synthesis of ECM. On the other hand, it was a long-standing matter of debate whether VSMCs also contribute to the core region of the plaque [112]. Traditionally, the general view was that the core of a plaque mainly consists of blood monocyte-derived macrophages that invade the lesion, take up cholesterol and become so-called foam cells [112]. The idea that VSMCs might not only supply the fibrous cap of a plaque, but also contribute to its core was not promoted by the scientific community until recently.

To gain a more precise understanding on the role of VSMCs during development of atherosclerosis, the Feil group started in the early 2000s to establish a Cre/loxP-based genetic inducible fate mapping system, which allows researchers to label and track medial VSMCs during atherogenesis. With this elegant method it could be clearly demonstrated that VSMCs indeed contribute to the plaque core region [79, 113]. Excitingly, some of the VSMC-derived plaque cells expressed the macrophage marker galectin-3 (Mac-2) [113]. These *in vivo* results are consistent with data obtained from *in vitro* experiments, where it was shown that loading of VSMCs with cholesterol leads to phenotypic modulation into macrophage-like cells [114]. In 2014, the Feil laboratory confirmed the hypothesis that medial VSMCs have the potential to switch into macrophage-like cells during atherogenesis *in vivo* [115]. Definite lineage tracing and co-staining of VSMC-derived plaque cells with markers for SMCs and macrophages showed that medial VSMCs switch into macrophage-like cells, which may lose expression of SMC markers and make up a major component of the atherosclerotic lesion. Another important finding of this study was that the macrophage-like plaque cells are derived by clonal expansion of few medial progenitor cells [115]. In line with the mouse data, immunostainings of human plaque sections revealed that some intimal cells co-express markers for SMCs and macrophages, suggesting the existence of a VSMC-macrophage chimeric cell type in human lesions [116, 117].

The new concept of clonal VSMC-to-macrophage transdifferentiation in atherosclerosis has been confirmed by several other laboratories [118-121], implying that previous studies that were solely based on immunostainings for marker proteins vastly underestimated the impact of VSMC plasticity on the development of atherosclerosis.

1.5.3   cGMP and atherosclerosis

As mentioned above, the impact of cGMP signaling on VSMC phenotype in the *in vitro* situation is controversially discussed (**see chapter 1.5.1**). To determine the relevance of cGMP-regulated VSMC plasticity in the *in vivo* situation, is obviously even more challenging (**Figure 5**). As shown by genome-wide association studies in humans, minor changes in components of this signaling pathway (e.g., NO-GC, ANP, BNP, PDEs) due to genetic variants, significantly influence blood pressure and cardiovascular disease risk [122-126].

Over the last years, multiple knockout mice were developed to help answer some of the questions regarding the impact of cGMP signaling on VSMC plasticity during development of vascular diseases such as atherosclerosis. Data collected with these mouse models indicate that an increase of cGMP in different cell types can have different, and even opposing, effects [17].
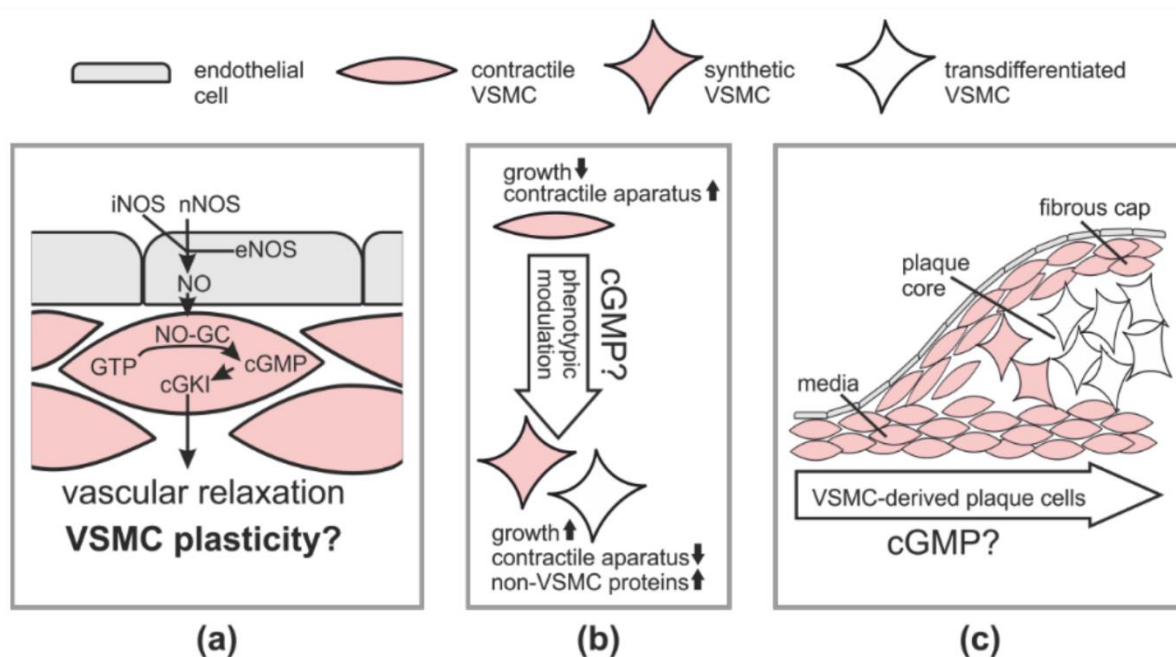
Figure 5. cGMP signaling and VSMC plasticity in atherosclerosis

 (a) The canonical NO-cGMP-cGKI pathway in the vessel wall; **(b)** Concept of VSMC plasticity and **(c)** VSMC-derived cells and VSMC trans-differentiation in atherosclerotic plaques and potential role of cGMP. Note that monocyte-derived macrophages and other plaque cells are not shown. Taken from Lehners, Dobrowinski et al. [17].

NO has an ambivalent role in atherosclerosis. As shown by genetically modified mouse models, NO derived from eNOS [127, 128] or nNOS [129] is atheroprotective, whereas iNOS, which is upregulated under inflammatory conditions, promotes atherosclerosis [130, 131]. The different effects of NO derived from different NOS isoforms might be related to the differences in the spatiotemporal profile of NO, i.e. NO is generated at different times in different cell types and quantities [132]. The opposing roles of NO are further supported by observations that high "pathophysiological" DETA-NO concentrations (100 µM) inhibit VSMC growth in a cGKI-independent manner, while low "physiological" DETA-NO concentrations (0.5 µM) promote VSMC growth **(1.5.1)**.

Interpretation of results obtained from global knockout mice is complicated if the protein is present in multiple cell types and/or mice display multiple phenotypes which might affect each other. For example, eNOS-deficient mice are hypertensive, which may also influence the development of atherosclerosis independent of the effect of NO on VSMC plasticity [127, 133]. Hence, cell type-specific and inducible conditional knockout models were developed to overcome the limitations of conventional knockout mice. Without such models it would not be possible to investigate NO-GC or cGKI in respect to vascular diseases, since mice with a conventional total knockout of those genes have an extremely reduced lifespan [36, 134].

Mice with postnatal SMC-specific ablation of cGKI had smaller plaques compared to cGKI-expressing control mice [79]. By combining the SMC-specific cGKI knockout with fate mapping it has been shown that cGKI-deficient VSMCs were almost exclusively located in the media below atherosclerotic lesions, whereas VSMCs from cGKI-expressing control mice were also present in the fibrous cap and core region of plaques. In line with these findings, it was shown that genetic disruption of NO-GC1 by deleting the α1 subunit reduces the atherosclerotic lesion area [80] Together, these preclinical mouse studies indicate that the NO-cGMP-cGKI pathway in VSMCs promotes the growth and phenotypic modulation of VSMCs and the development of atherosclerotic plaques *in vivo* [79]. Although lesion area is often used to rate atherosclerosis development, an increased plaque size is not necessarily detrimental. Indeed, the cGMP-mediated effect on lesion size appears to be associated with an altered plaque composition, with more VSMC-derived cells in the fibrous cap as well as in the plaque core. Future studies are required to clarify whether cGMP increases or decreases plaque stability [17]. In this context, it will also be interesting to test the effects of cGMP-elevating drugs on atherosclerosis.

1.5.4   Fibronectin and atherosclerosis

The progression of inflammatory diseases of the vasculature, such as atherosclerosis, depends in large part on the surrounding extracellular matrix (ECM). In healthy non-inflamed vessels, the basement membrane consists mainly of collagen type IV and laminin [135, 136], whereas pathological vessels are characterized by the deposition of fibronectin (Fn) [135-137]. Cells can sense the ECM through specialized receptors and respond to it by altered adhesion, morphology, migration, and growth. In 1986, Tamkun et al. were the first to demonstrate that glycoproteins on the cell surface can link the ECM to the cytoskeleton and suggested to name this complex "integrin", denoting the transmembrane interaction between the surrounding ECM and the cytoskeleton [138]. Since then our understanding of integrin signaling has developed rapidly, and today we know that the interaction between integrins and their respective ligands is responsible for myriad (patho-)physiological functions, from embryonic development to immune response to body hemostasis to cancer and many other diseases [139].

Integrins are heterodimers consisting of an α and β subunit. In vertebrates, there are 24 different integrins composed of 18 α and 8 β subunits [140]. Depending on the ligand, these 24 integrins are clustered into four classes [140]: (1) Integrins preferentially binding to ligands with an RGD motif (arginine-glycine-aspartic acid) like Fn; (2) Integrins which act as receptors for the different types of collagen; (3) Laminin recognizing integrins; and (4) Leukocyte-

specific integrins, which mediate cell-cell interaction through counter receptors of the Ig-superfamily [139] **(Figure 6)**.
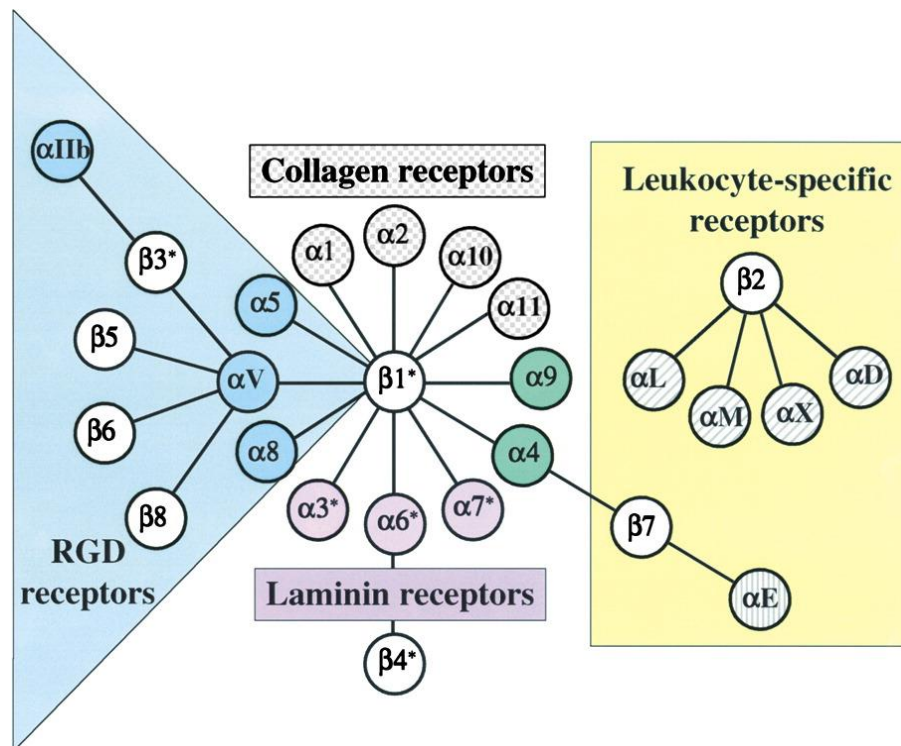
Figure 6. Integrin receptor family

Taken from Hynes et al. 2002 [139]. For further details, see text.

Fn is an important member of the ECM. It is a large protein secreted from multiple cell types. Knockout studies demonstrated that Fn is critical for embryonal development [141]. Fn forms a homodimer of two ≈250 kDa subunits, which are covalently linked by disulfide bonds. The subunits are built of three types of repeating units (type I, type II and type III), which account for around 90% of the protein sequence. In vertebrates up to 20 variants of Fn exist, which are generated by alternative splicing of one single gene. Moreover, Fn can be subdivided into two forms, cellular Fn and plasma Fn. While insoluble cellular Fn (assembled into fibrils) is synthetized by many different cell types, soluble plasma Fn is circulating in the blood and is mainly synthetized by hepatocytes in the liver. Under certain circumstances, plasma Fn can be assembled into fibers as well [142]. Besides its interaction with integrins, Fn can also bind other biologically active compounds such as heparin, collagen or fibrin [143].

As already described **(see chapter 1.5.1)** VSMCs can switch from a contractile into a synthetic phenotype. More than 30 years ago, Hedin and Thyberg studied primary VSMCs grown on Fn-coated surfaces and demonstrated that plasma Fn promotes the synthetic phenotype of VSMCs [144]. In contrast to Fn, laminin, another ECM protein, was shown to

preserve the contractile phenotype of VSMCs to a certain extent [145]. Moreover, in 1989 Glukhova and colleagues showed that atherosclerosis leads to an upregulation of Fn [137]. Consistent with this observation, Astrof and Hynes reviewed, that expression of Fn splice variants containing the EIIIA and EIIIB domains, is upregulated during embryonic vessel formation as well as postnatally during pathological events, such as cardiac hypertrophy, tumorigenesis and atherogenesis [146]. Global ablation of the EIIIA domain led to a reduction of atherosclerotic lesion size in mice [147, 148]. By using a Cre/loxP-based conditional knockout approach, the group of Reinhard Fässler demonstrated that deletion of hepatocyte-derived plasma Fn led to a reduction of Fn deposition at atherosclerotic-prone sites and smaller atherosclerotic lesions compared to control mice [136]. Interestingly, atherosclerotic lesions from mice lacking plasma Fn were not only relatively small, but were also devoid of VSMCs and a fibrous cap suggesting that these plaques were less stable than plaques from wildtype mice [136].

In summary, these findings led to the concept that plasma Fn promotes VSMC growth and the progression of atherosclerosis. However, whether cellular Fn secreted specifically from VSMCs plays a role for atherosclerosis is not known. Thus, one aim of this thesis was to investigate the impact of VSMC-derived Fn on atherosclerosis and its potential interaction with the cGMP signaling pathway in VSMCs.

1.6 Real-time imaging of cGMP using the FRET-based biosensor cGi500

As previously mentioned, VSMCs switch between the contractile and synthetic phenotype [17]. This characteristic leads to a heterogenic population of VSMCs not only in the *in vitro* system, but also in the *in vivo* situation, where VSMCs can switch into macrophage-like cells, contributing to the core region of an atherosclerotic plaque [115]. While the heterogeneity of VSMC populations is scientifically extremely interesting, it also poses a major obstacle to draw clear conclusions about the role of cGMP signaling in each subpopulation. To resolve this issue, it is necessary to investigate the cGMP signaling pathway at the level of individual cells. To a certain extent, this is possible via classical immunostaining of selected components of the signaling pathway. However, antibodies for distinct members of the signaling cascade are not always available or their specificity is questionable. Furthermore, classical immunostainings do not allow to follow dynamic cGMP changes in real-time. To visualize spatiotemporal cGMP signaling in live cells, genetically-encoded cGMP biosensors have been developed [149, 150].

Transgenic mice for cGMP imaging have been generated that express the Förster (fluorescence) resonance energy transfer (FRET)-based cGMP biosensor cGi500 either ubiquitously or in specific cell types [151]. The cGMP sensor mice are very useful tools. They are a convenient source to isolate sensor-expressing primary cells [149, 151-153] and tissues for *ex vivo* cGMP measurements [153-155], and they enable cGMP imaging in anesthetized mice *in vivo* [45, 151, 156]. The cGMP sensor mice allow for cGMP research at a new level by "watching" this signaling pathway in real-time, in individual cells *in vitro* and even *in vivo* under close to native conditions.

cGi500 consists of the tandem cGMP-binding region of cGKI flanked by two fluorescent probes, cyan fluorescent protein (CFP) and yellow fluorescent protein (YFP). In the absence of cGMP, both fluorophores reside in close proximity and FRET occurs from the exited CFP (excitation at 445 nm) to YFP. The transferred energy is emitted by YFP at 535 nm, while non-transferred energy is emitted by CFP at 480 nm. Upon cGMP binding the conformation of the sensor changes and both fluorophores are reoriented. This event results in reduced FRET efficiency between CFP and YFP, leading to an increased CFP emission (at 480 nm) and decreased YFP emission (at 535 nm). The ratio of CFP/YFP emission can be used as a measure of FRET efficiency and, thus, the intracellular cGMP concentration **(Figure 7)**.
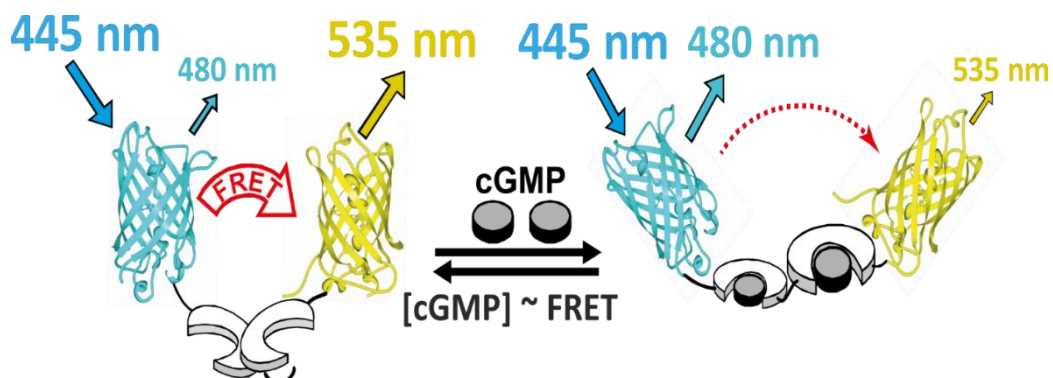
Figure 7. FRET-based cGMP biosensor cGi500

cGi500 is a ratiometric cGMP biosensor consisting of the cGMP-binding domain of bovine cGKI flanked by CFP and YFP. The left image depicts the sensor in the cGMP-free state where FRET occurs at maximal efficiency. The right image depicts the cGMP bound state, which causes a conformational change that reorients CFP and YFP. Thereby, light emission from YFP at 535 nm is reduced, while emission from CFP at 480 nm is increased. The ratio of emission at 480 nm and 535 nm (F480/F535) is used as a measure of FRET efficiency, which represents the intracellular cGMP level. Adapted from Thunemann and Wen et. al. 2013 [149].

1.6 Aim of the work

The aim of the present study was to investigate the cGMP-induced growth behavior of VSMCs in more detail using transgenic mouse and cell models. While previous studies used conventional end-point measurements (e.g. WST, MTS, CellTiter-Glo and nuclei enumeration) depicting the cGMP-induced growth behavior at a single time point, in this work we sought to setup an impedance-based approach, which would allow us to follow VSMC growth in real-time. One goal of this subproject was to investigate whether stimulation of global and local cGMP pools with NO and NPs, respectively, leads to differential effects on VSMC growth and survival. Furthermore, we wanted to investigate whether changes in the ECM surrounding the VSMCs influences their phenotype and cGMP signaling pathway. To this end, primary VSMCs were grown on Fn and characterized via growth experiments and FRET-based cGMP imaging. Another major aim of this work was to investigate the effect of SMC-specific Fn ablation on the development of atherosclerosis *in vivo* and to investigate a potential interaction of Fn and cGMP signaling.

2. Material and Methods

2.1 General materials

2.1.1 Common reagents, compounds and antibodies

Table 1. Common reagents

Reagent	Company	Reagent	Company
0.4% Trypan blue	Life Technologies	KCL	Roth
1 kb plus ladder	Life Technologies	KH_2PO_4	Merck
10x Reaction Buffer S	Bioron	LE Agarose	Biozym
2-mercaptoethanol	Roth	L-glutamate	Roth
Aminocaproic acid	Roth	Methanol	Sigma-Aldrich
APS	Roth	$MgCl_2$	Roth
Bromphenol blue	Roth	Midori Green	Nippon Genetics
BSA	Roth	Milk powder	Roth
$CaCl_2$	Sigma-Aldrich	Na_2HPO_4	Roth
Collagenase	Sigma-Aldrich	NaCl	Roth
D-Glucose	Roth	NDS	Millipore
DMEM medium - Glutamax^{TM}	Gibco	Oil Red O	Roth
dNTPS	Genaxxon	Papain	Sigma-Aldrich
DTT	Roth	Pen/Strep	Gibco
EDTA	Roth	PMSF	Roth
Ethanol	Sigma-Aldrich	Proteinase K	Genaxxon
FCS	Gibco	SDS	Roth
Formaldehyde	Applichem	Taq Polymerase	Bioron
Glycerol	Roth	TEMED	Roth
Glycine	Sigma-Aldrich	Toluene	Roth
Heparin	Roth	Tris-Cl	Roth
HEPES	Roth	Triton X-100	Roth
Hoechst 33258	Sigma-Aldrich	Trypsin	Sigma-Aldrich
Hyaluronidase	Sigma-Aldrich	Xylene xyanol	Roth

Table 2. Common compounds

Compound	Company	Compound	Company
8-Br-cGMP	Biolog	DEA-NO	Enzo
ANP	Tocris	DETA-NO	Enzo
CNP	Tocris	Sildenafil	Sigma-Aldrich
Fibronectin (pure)	Roche		

Table 3. Common antibodies

Antibody	Company	Dilution	Source
Fibronectin	AB2033 Millipore	1:1.000 WB	Rabbit
GAPDH	2118 Cell Signaling	1:1.000 WB	Rabbit
Mac-2	Cl8942 Cedarlane	1:250 IHC	Rat
NO-GC β1 subunit	Donation AG. Friebe	1:10.000 WB	Rabbit
SMαA	A2547 Sigma-Aldrich	1:500 IHC	Mouse
pVASP Ser239	3114 Cell Signaling	1:1000 WB	Rabbit

WB, Western blot; IHC, immunohistochemistry

2.1.2 Common solutions

o 0.5 M EDTA (pH 8.0): Dissolve 186.1 g disodium ethylenediaminetetraacetic acid dihydrate (Roth) in 800 mL H_2O and add NaOH until pH 8.0. Adjust the volume to 1 L with H_2O and store at RT

o 1 M Tris-Cl (pH 8.0): Dissolve 121.14 g tris(hydroxymethyl)aminomethane (Roth) in 800 mL H_2O and add HCl to pH 8.0. Adjust the volume to 1 L with H_2O and store at RT

o 100x Pen/Strep: 10´000 U/mL penicillin (Gibco) and 10´000 µg/mL streptomycin (Gibco) prepare 5 mL aliquots and store at -20°C

o 1000x Hoechst: 1 mg/mL Hoechst 33258 (Sigma-Aldrich) in H_2O prepare 1 mL aliquots and store at -20°C

o 10x Trypsin/EDTA: 0.5% trypsin/EDTA (Gibco) and store at -20°C

o 1x Trypsin/EDTA: Mix 1 part 10x trypsin/EDTA with 9 parts PBS and store at 4°C

o 100 µM ANP: Prepare 100 µM ANP (Tocris) in H_2O. Store in 50 µL aliquots at -20°C

o 100 µM CNP: Prepare 100 µM CNP (Tocris) in H_2O. Store in 50 µL aliquots at -20°C

o 100 mM DEA-NO: Prepare 100 mM DEA-NO (Enzo) in 10 mM NaOH. Store in 50 µL aliquots at -20°C

- 100 mM DETA-NO: Prepare 100 mM DETA-NO (Enzo) in 10 mM NaOH. Store in 50 µL aliquots at -20°C
- 100 mM 8-Br-cGMP: Prepare 100 mM 8-Br-cGMP (Biolog) in H_2O. Store in 50 µL aliquots at -20°C

2.1.3 Common buffers

Table 4. Phosphate-buffered saline (pH 7.4)

NaCl	135 mM (8 g/L)
KCl	3 mM (0.2 g/L)
Na_2HPO_4	8 mM (1.42 g/L)
KH_2PO_4	2 mM (0.24 g/L)
H_2O	to 1 L
pH 7.4	If necessary adjust pH with NaOH or HCl

Table 5. 5x TBE

Tris-Cl	0.25 M (30.29 g/L)
Boric acid	0.25 M (15.46 g/L)
EDTA	0.005 M (10 mL/L) from 0.5 M stock
H_2O	to 10 L

Table 6. 10x TE

Tris-Cl	100 mM (100 mL/L) from 1 M stock
EDTA	10 mM (20 mL/L) from 0.5 M stock
H_2O	to 1 L

2.2 Mouse breeding and husbandry

All mouse lines were housed in the animal facility of the Interfaculty Institute of Biochemistry at the Eberhard-Karls University Tuebingen. The standard conditions of the facility were 22°C and 50 – 60 % humidity with a 12 hour light / 12 hour dark cycle. Type II cages (360 cm²) were used for housing of single animals or groups with a maximal size of 2-3 animals. Type III cages (810 cm²) were used for groups of maximum eight animals. The animals had permanent access to standard rodent chow (Altromin Spezialfutter GmbH & Co. KG, Lage,

Germany and Sniff Spezialdiaten GmbH, Soest, Germany) and tap water. The bedding of a cage consisted of autoclaved shredded wood chips (Tapvei). For environmental enrichments, tissues and wooden tunnels (Tapvei) were used. The animal care takers changed the water and put the mice into clean cages weekly. For breeding, one or two female mice were housed together with one male mice in a Type II cage. The pregnancy lasted for nineteen to twenty-one days. To prevent uncontrolled breeding, female mice were separated into a Type III cage before they gave birth. The pregnant animals received access to breeding chow (Altromin and Sniff). The newborn animals were separated by the gender after 21 days and their ears were tagged for subsequent genotyping.

2.2.1 DNA extraction from mouse tissues for genotyping by PCR

For mouse genotyping, the polymerase chain reaction (PCR) was used. The template deoxyribonucleic acid (DNA) was extracted from ear punches of the young (≈3 weeks old) animals.

1. Prepare PCR lysis buffer **(Table 7)**.
2. Place each ear punch into 50 µL PCR lysis buffer and incubate over night at 55°C.
3. After overnight incubation vortex the sample to dissolve the ear punch completely.
4. Centrifuge the sample at 12´000 rpm for 5 minutes.
5. Transfer the supernatant into a 0.5 mL PCR tube.
6. Denature the DNA and inactivate the Proteinase K at 95°C for 15 minutes.
7. Use 1 – 3 µL of this sample (depending on the specific PCR) immediately for genotyping PCR, or store the DNA containing solution at -20°C.

Table 7. PCR lysis buffer (one reaction)

10 x Reaction buffer S	5 µL
Proteinase K	1 µL
H_2O	44 µL
Total volume	**50 µL**

- Proteinase K (Genaxxon): 50 mg/mL proteinase K in 1x TE buffer, store at -20°C
- 10x Reaction buffer S (Bioron), store at -20°C

2.2.2 PCR for mouse genotyping

Every genotyping PCR had specific conditions depending on the respective annealing temperature of the primer set (Ta) and the expected PCR product length **(Table 24)**.

1. Pipette 1-3 µL of your genomic DNA template into a new PCR tube.
2. Prepare an appropriate volume of the master mix **(Table 8)**.
3. Add 23 µL of the master mix to your DNA sample and pipette several times up and down (Prepare a positive control from an already genotyped DNA sample and a negative control with H_2O instead of DNA).
4. Transfer the samples into the thermocycler (PEQLAB Peqstar 2x; PEQLAB Primus 96 Advanced) and run the respective program.
5. After the PCR add 5 µL of 6x DNA loading dye to the samples.
6. Analyze the PCR products (min. 12 µL) with a 1 kb plus ladder (min. 5 µL) on a Midori Green containing (2 µL per 50 mL agarose gel) 2% agarose gel.

Table 8. PCR master mix (one reaction)

10x RT buffer	2.5 µL
Primer 1	0.3 µL
Primer 2	0.3 µL
Primer 3	0.3 µL
Taq Polymerase	0.3 µL
H_2O	19.3 µL
Total volume	**23 µL**

o dNTP stocks: 100 mM dATP, 100 mM dCPT, 100 mM dGTP, 100 mM dTTP (Genaxxon); store at -20°C

o 10x RT buffer: 100 mM Tris-HCl pH 8.0, 500 mM KCl, 15 mM $MgCl_2$, 2 mM of each dNTP (dATP, dCPT, dGTP, dTTP), in H_2O, store at -20°C

o Primer **(Table 24)**: 25 pmol/µL (Eurofins Genomics) in H_2O, store at -20°C

o Taq Polymerase (Bioron); store at -20°C

o Molecular size marker: Dilute 250 µL 1kb plus ladder (Life Technologies) in 8.25 mL 1x DNA loading dye. Prepare aliquots with a volume of 500 µL and store one aliquot ready to use at 4°C while the other are stored at -20°C

o Midori Green (nucleic acid staining solution, Nippon Genetics); store at 4°C

o 6x DNA loading dye: Glycerol 30%, 10x TE buffer 10%, bromphenol blue 0.05 %,

xylene cyanol 0.05%; store at 4°C

- o 1x TBE buffer: Dilute 2 L of 5x TBE buffer with 8 L H_2O; store at RT
- o LE Agarose (Biozym); store at RT
- o 2% agarose gel: Weight 1 g LE agarose (Biozym) into 50 mL 1x TBE buffer. Put it into the microwave and heat it until the agarose is completely dissolved. Let it cool down (test the temperature by touching the skin of your forearm with the Erlenmeyer flask) and add 2 µL of Midori Green (Nippon Genetics). Dissolve the Midori Green on a magnetic stirrer and poor the agarose gel into a chamber to polymerize.

2.3 Vascular smooth muscle cell culture

Primary VSMCs were isolated from the thoracic aortae of mice with an age from three to eight weeks. Due to the reduced lifespan of NO-GC (β1 subunit) and cGKI knockout mice, the isolation of VSMCs was performed from animals of two weeks of age. Approximately 150,000 VSMCs per aorta were isolated by enzymatic digestion. The cell yield depended highly on the age of the animals and was greater from younger animals. Cells were grown in culture medium containing 10% FCS and Pen/Strep at 37°C with 6% CO_2. Primary VSMCs started to adhere, spread and grow after 24-48 hours. Depending on the amount of cells seeded **(Table 9)**, they reached confluency five to seven days post isolation.

1. Prepare several petri dishes (100 mm) with PBS and put them on ice.
2. Prepare a 35 mm dish with Ca^{2+}-free medium and put on ice.
3. Sacrifice the animals by CO_2. Cut tail tips when needed for re-genotyping.
4. Wet the fur of the animals with 70% ethanol and open abdominal and thoracic cavity.
5. Remove diaphragm, remaining intestines, esophagus and liver as well spleen and lung. To isolate the aorta, grab the heart with the forceps and lift it carefully. Thereby the aorta will stretch under some tension. Carefully cut along the spine towards the tail. Transfer the aorta with the still attached heart into the PBS containing petri dish on ice.
6. Use two forceps and carefully remove the heart from the aorta.
7. Put light pressure on the aorta to get rid of the remaining blood.
8. Remove the surrounding, fat containing tissue by peeling the aorta carefully under a stereomicroscope (Stemi 2000C).
9. Transfer the cleaned aorta into the Ca^{2+}-free medium containing 35 mm dish. Especially when more than one aorta has to be isolated it is important to place this dish on ice to prevent degradation.
10. Use scissors to cut the cleaned aorta into ≈3 mm pieces.

At that point, all following steps should be performed in a culture hood.

11. Transfer the pieces into a 15 mL tube with enzyme solution A (0.5 mL solution for 2 aortae)

12. Incubate for 60 minutes in a 37°C water bath and gently mix the sample every 10 minutes (the mixing will reduce time for the critical incubation in solution B and thereby increase cell yield).

13. Centrifuge at 1000 rpm for 3 minutes.

14. Carefully discard the supernatant and suspend the tissue pellet in enzyme solution B. Use the same volume as for enzyme solution A (0.5 mL solution for 2 aortae).

15. Incubate the sample for max. 12 minutes in a 37°C water bath (this step is critical and should be performed as short as possible). After the first 3 minutes of incubation suspend the mixture occasionally with a 1000 µL pipette. This procedure will reduce the incubation time dramatically and increase the cell yield.

16. Stop the reaction with FCS containing culture medium using 3-4x the volume of enzyme solution B.

17. Centrifuge at 1000 rpm for 8 minutes.

18. Discard the supernatant and suspend the pellet in an appropriate volume of medium (≈0.5 mL per 2 aortae).

19. Mix 18 µL of the cell suspension with 2 µL trypan blue and count viable and dead cells (blue positive) in a Neubauer counting chamber.

20. Adjust the number of VSMCs in culture medium and plate it into the desired format.

21. Grow the cells at 37°C and 6% CO_2.

Table 9. Recommendations for cell plating

Culture format	Cell density plated
Culture dish	≈1.2 x 10^6 cells / 10 mL
6 well plate	≈1,8 x 10^5 cells / 3 mL
12 well plate	≈1x 10^5 cells / 2 mL
24 well plate	≈5x 10^4 cells / 1 mL
96 well plate	≈2x 10^4 cells / 0.2 mL
xCELLigence well plate	≈2x 10^4 cells / 0.2 mL

o Ca^{2+}-free medium (pH 7.4): 85 mM L-glutamate, 60 mM NaCl, 10 mM HEPES, 5.6 mM KCl, 1 mM $MgCl_2$, adjust pH to 7.4 with HCl, autoclave and store at 4°C

- VSMC culture medium: 500 mL DMEM medium -GlutaMAX^{TM} (Gibco) including 50 mL FCS and 5 mL Pen/Strep, store at 4°C
- 10 mg/mL Collagenase: Dissolve 100 mg Collagenase (Sigma-Aldrich) in 10 mL Ca^{2+}-free medium, prepare 0.5 mL aliquots and store at -20°C
- 10 mg/mL Hyaluronidase: Dissolve 100 mg Hyaluronidase (Sigma-Aldrich) in 10 mL Ca^{2+}-free medium, prepare 0.5 mL aliquots and store at -20°C
- 7 mg/mL Papain: Dissolve 100 mg Papain (Sigma-Aldrich) in 14.29 mL Ca^{2+}-free medium, prepare 0.5 mL aliquots and store at -20°C
- 100 mg/mL BSA: Dissolve 0.5 g BSA (Roth) in 5 mL Ca^{2+}-free medium, sterilize by filtration, prepare 0.5 mL aliquots and store at -20°C
- 100 mg/mL DTT: Dissolve 0.5 g DTT (Roth) in 5 mL Ca^{2+}-free medium, sterilize by filtration, prepare 0.5 mL aliquots and store at -20°C
- Enzyme solution A (0.5 mL per 2 aortae): Dilute Papain stock 1/10, BSA stock 1/100 and DTT stock 1/100 in Ca^{2+}-free medium
- Enzyme solution B (0.5 mL per 2 aortae): Dilute Collagenase stock 1/10, Hyaluronidase stock 1/10 and BSA stock 1/100 in Ca^{2+}-free medium

Unless otherwise stated, all experiments were performed with primary VSMCs from wildtype mice.

- Mice for NO-GC knockout (NO-GC β1$^{L1/L1}$) experiments were friendly donated by Prof. Dr. Andreas Friebe (academic chair for vegetative physiology, University of Würzburg)
- Mice with floxed fibronectin gene (Fn$^{L2/L2}$) were friendly donated by Prof. Dr. Reinhard Fässler (Max Planck Institute for Biochemistry, Martinsried)
- Mice for cGKI knockout experiments were bred in the own animal facility

2.4 WST-1 growth assay

The colorimetric WST-1 assay (Roche) was used for quantification of cell viability and cell growth [157]. This assay is based on the metabolic activity of viable cells. Thereby, the tetrazolium salt WST-1 is reduced into a soluble formazan dye. The amount of formazan directly correlates with the number of metabolic active cells **(Figure 8)**. Primary VSMCs were plated into 96-wells and analyzed after three days of growth.

1. Isolate primary VSMCs and plate 2 x 10^4 cells / 200 µL VSMC culture medium **(see chapter 2.3)** into a 96 well plate.
2. Grow the cells for 3 days at 37°C and 6% CO_2.
3. Remove the medium and wash the cells 2x with PBS.
4. Mix 100 µL VSMC culture medium with 10 µL WST-1 solution and pipette into the wells. As blank control, pipette the solution into wells without attached cells.
5. Incubate for 1-4 hours at 37°C with 6% CO_2.
6. Measure OD at 450 nm in the Thermo Multiskan EX plate reader.
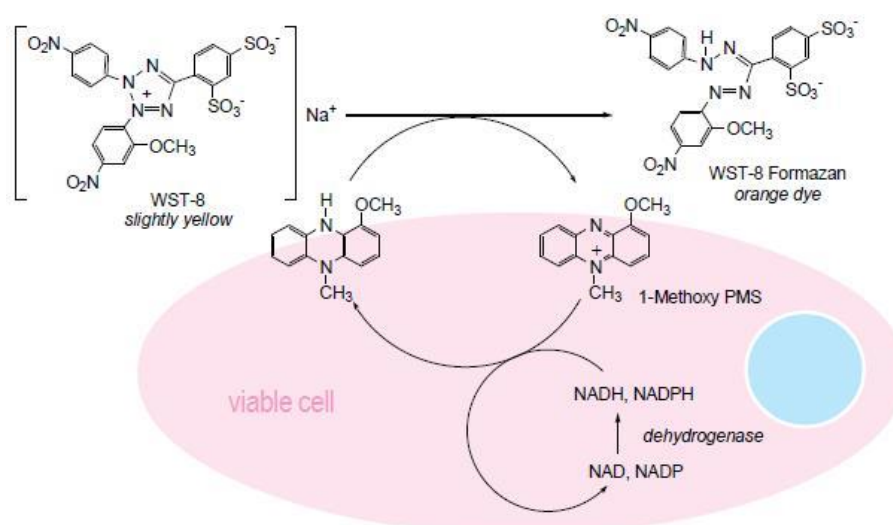
Figure 8. Schematic presentation of the WST-1 growth assay

The colorimetric WST-1 assay is used for quantification of cell viability. The assay is based on the metabolic activity of cells. Thereby water soluble tetrazolium salt (WST-8, slightly yellow) is reduced by dehydrogenases into formazon (WST-8, orange dye). Taken from www.tebu-bio.com [157].

2.5 Impedance based growth assay

The WST-1 assay is an approved method to investigate cell viability. However, with this assay only endpoint measurements are possible. To overcome this limitation and to get a greater insight into the dynamics of cell growth, we utilized an impedance-based growth assay. The impedance based xCELLigence® RTCA DP system (Roche Diagnostics GmbH) allows to monitor the growth behavior of cells in real-time and under label-free conditions. This device measures cell growth in microtiter well plates with gold microelectrodes (E-Plates®) fused to the bottom. These electrodes cover 70-80% of the bottom surface and measure the electron flow through the bulk solution within an individual well **(Figure 9)** [158].
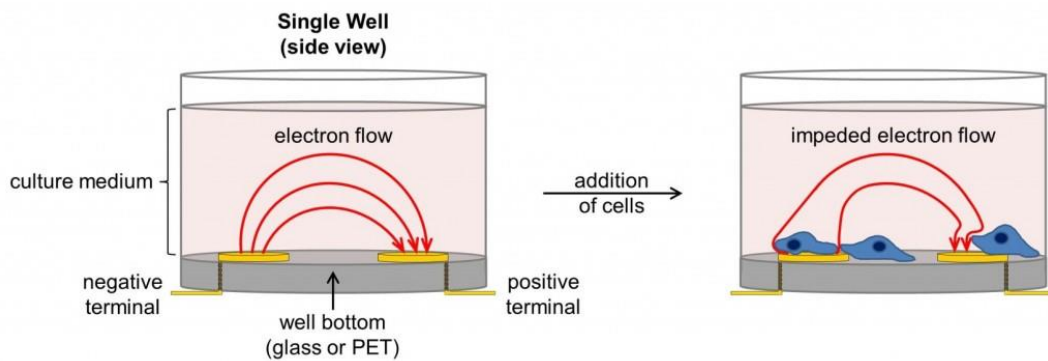
Figure 9. Schematic presentation of impedance measurement in a single well

The bottom surface of each well is covered by 70-80 % with electrodes. In the absence of cells, the electric current flows freely through the medium. When cells are adhered, proliferate and migrate, the electric current is impeded. This provides an extremely sensitive readout about the growth behavior of cells in real time. Taken from www.aceabio.com [158].

When cells attach to the microelectrodes, they imped the electron flow between the negative and positive terminal. This electronic readout is displayed as CI (cell index). The CI is a relative unitless value which is calculated by subtracting the background resistance R_{t0} (experimental start with only medium in the wells) from the resistance at an individual time point R_{tn} (cell index= $(R_{tn} - R_{t0})$ / 15 Ω). The magnitude of impedance can be correlated to processes like cell adhesion, spreading, proliferation, or death [159] **(Figure 10)**.

1. Isolate primary VSMCs and adjust the cell number to 2x 10^4 cells / 100 µL VSMC culture medium **(2.3)**.
2. Add 100 µL pre warmed VSMC culture medium to each well of the E-Plate.
3. Start the RTCA software and create the layout (loading of the E-Plate) and the schedule (sweeps and intervals for the measurement). One E-Plate consist of 16 wells. At least 4

wells per condition should be prepared. To monitor VSMC growth at least 700 sweeps with 15 minutes intervals should be measured.

4. Insert the E-Plate into the RTCA DP analyzer and make sure it is properly aligned. Otherwise in the message box of the software a notice will appear.

5. Start the experiment (step1). The first step is responsible for background measurement (CI of every single well without VSMCs inside).

6. Remove the E-Plate and add 100 µL of the cell suspension (2x 10^4 cells / 100 µL). Pipette several times up and down to dispense the cells in the total volume of 200 µL.
   Desired drugs are dissolved in the cell suspension before adding them to the wells.

7. Place the E-Plate again into the RTCA DP analyzer at 37°C and 6% CO_2.

8. After 30 minutes incubation start the measurement (step 2). This incubation is important to allow the cells to settle to prevent background noise at the beginning of the experiment.

For more detailed information, read the RTCA DP Instrument Short Guide.

The manufacturer recommends using the E-Plates (≈40€ per plate) just once. However, it is possible to reuse the plates when cleaned properly.

1. Aspirate the medium from the wells.

2. Wash the wells 2-3x with PBS.

3. Add 200 µL 1x Trypsin/EDTA to the wells and incubate overnight at 37°C.

4. Aspirate the 1x Trypsin/EDTA and wash the wells 2-3 times with PBS.

5. Add 200 µL 70% ethanol to the wells and incubate for 2-4 hours.

6. Aspirate the ethanol and wash 2x with autoclaved H_2O. Aspirate the H_2O.

7. E-Plates are prepared for the next experiment.

One E-Plate can be used up to three times. But the sensitivity can suffer. Therefore, for critical experiments, for example with knockout VSMCs, it is recommended to use fresh E-Plates.
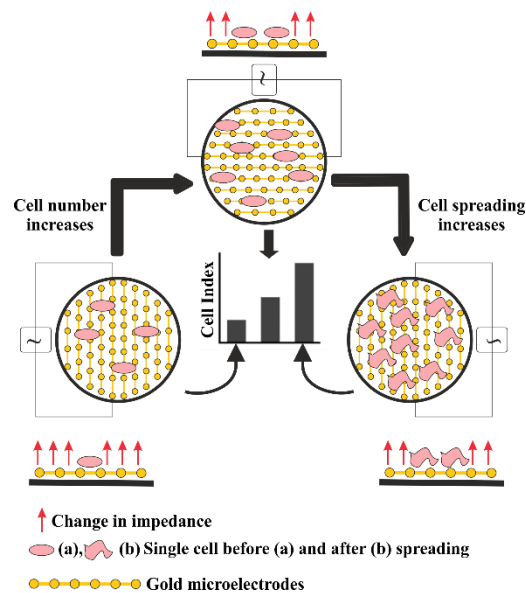
Figure 10. Schematic presentation of the xCELLigence working principle and different stages of cell growth

Processes of cell growth behavior like adhesion, proliferation, migration and death impede the electric current. Those changes are depicted by the cell index (CI). Modified from Limame et al. 2012 [159].

2.6 Live and dead staining of VSMCs

Another approach to investigate the impact of the cGMP signaling pathway on cell growth was the use of a live and dead staining Kit (Biotium). This Kit basically provides two fluorescent probes, which measure cell viability by detecting intercellular esterase activity. The non-fluorescent esterase substrate calcein-AM (acetoxymethyl) crosses the membrane of living cells. Subsequently, the acetomethoxy group is removed by intracellular esterases. This modification releases green fluorescence and traps the calcein molecule inside the cells (staining of viable cells). The membrane-impermeable, fluorescent dye, Ethidium homodimer III (EthD-III) interacts with the DNA of dead cells (cells with damaged plasma membrane) and stains them red **(Figure 11)**.

1. Isolate primary VSMCs and grow them for 3 days.
2. Aspirate the culture medium.
3. Prepare an appropriate volume of 2 µM calcein-AM (4 mM stock) and 4 µM EthD-III (2 mM stock) in Tyrode buffer **(Table 20)** and pipette it to the cells. It is important to pre-warm the Tyrode buffer to 37°C in a water bath.
4. Incubate the cells for 30-45 minutes at RT in the dark.
5. Take images of the fluorescent cells.

o Viability/Cytotoxicity Assay Kit for Animal Live & Dead Cells (Biotium)
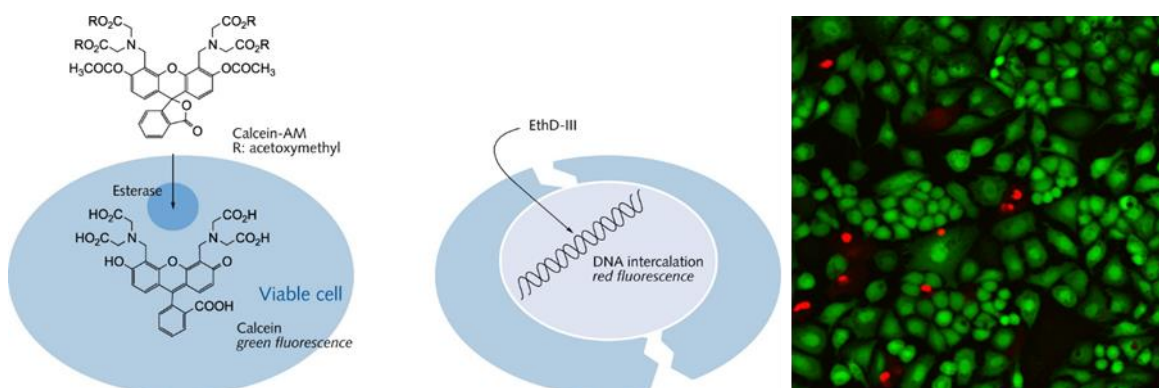
Figure 11. Schematic presentation of the live and dead staining assay

The live and dead staining kit uses two fluorescent probes to investigate the viability of cells. The esterase substrate calcein-AM stains viable cells green, whereas the membrane-impermeable dye EthD-III interacts with the DNA of dead cells and stains them red. Modified from www.takara-bio.co.jp.

2.7 Protein analysis

2.7.1 Protein extract generation

For the generation of protein extracts from VSMCs and tissues, SDS lysis buffer was directly added to the cells. Protein extraction from tissues was performed through homogenization within the FastPrep-24 instrument (MP Biomedicals).

Protein extraction from cells

1. Isolate primary VSMCs and grow them for a desired time at 37°C and 6% CO_2.
2. Aspirate culture medium and wash the cells 2x with PBS (RT).
3. Add the appropriate volume of SDS lysis buffer **(Table 10)** (for example, 1 well out of a 6 well plate can be lysed with 100 µL, but 2 wells can be pooled with 150 µL) and lyse the cells through scratching the culture dish with a pipette tip. If possible, pool the wells to increase protein concentration.
4. Tilt the culture dish and use a cell scratcher to pull the lysate to the bottom of the dish (this will increase the protein concentration). If several samples are collected, store them on ice.
5. Denature cell lysates at 95°C for 10 minutes.
6. Centrifuge for 5 min at 13,000 rpm and transfer the supernatant into a new tube.
7. Store the samples at -20°C.

Protein extraction from tissue

The amount of used SDS lysis buffer depends on the tissue **(Table 11)**.

1. Isolate the desired tissue and transfer it into an Eppendorf tube.
2. Shock freeze the samples in liquid nitrogen.
3. Start with the protein extraction or store the samples at -80°C.
4. Transfer tissues into prepared lysis cups with a ceramic ball and a spatula of sand.
5. Add SDS lysis buffer. The amount of lysis buffer used depends on the tissue **(Table 11)** but at the minimum 200 µL should be used.
6. Place the tubes in the FastPrep and run the device for 20 seconds at 6.5 m/s (speed).
7. Centrifuge the samples for 2 minutes at 10,000 rpm and check (by eye and pipetting) if they are lysed. If not add some additional lysis buffer and go back to step number six.
8. Denature the lysates at 95°C for 10 minutes.
9. Store at -20°C.

Table 10. SDS lysis buffer (prepare always fresh)

1 M Tris-Cl (pH 8.3)	21 µL
20% SDS	33.5 µL
100 mM PMSF	2 µL
H_2O	943.5 µL

Table 11. Recommended amount SDS lysis buffer per tissue

Tissue	SDS lysis buffer / mg tissue (min. 200 µL)
Brain, Liver, Colon	4 µL/mg
Lung	9 µL/mg
Heart, Spleen, Kidney	10 µL/mg

o PMSF: Prepare 100 mM phenylmethylsulfonylfluorid (Roth) in 100% ethanol, pipette into 1 mL aliquots and store at -20°C

o 20% (w/v) SDS: Weigh 20 g SDS (Roth) and adjust the volume to 100 mL with H_2O

o Tris-Cl (pH 8.3): Dissolve 121.14 g tris(hydroxymethyl)aminomethane (Roth) in 800 mL H_2O and add HCl until pH 8.3. Adjust the volume to 1 L with H_2O

2.7.2 Determination of protein concentration with Lowry assay

For the determination of protein concentration, the Total Protein Kit from Sigma was used. This assay is based on the Peterson modification of the Lowry method. In a first reaction step, alkaline copper tartrate forms complexes with protein peptide bonds (Biuret reaction). In the second colorimetric reaction step, Folin-Ciocalteau is reduced by copper, whereby a blue product is formed whose intensity correlates to the protein concentration. The Lowry assay is performed within a 96 well plate and the samples are quantified by the Thermo Multiskan EX plate reader. A concentration series of bovine serum albumin (BSA) is used for calibration.

1. Transfer 200 µL of each concentration from the BSA dilution series (see below) into a new Eppendorf tube. As reference use 200 µL H$_2$O.
2. Pipette 15 – 30 µL of the protein lysate into a new Eppendorf tube and fill up to 200 µL with H$_2$O. As reference use 15-30 µL lysis buffer filled to 200 µL with H$_2$O.
3. Add 200 µL Lowry Reagent Solution (total volume 400 µL), vortex the sample and incubate for 20 minutes at RT.
4. Add 100 µL Folin-Ciocalteau (total volume 500 µL), vortex the sample and incubate for 30 minutes at RT in the dark. At this step the colorimetric reaction is taking place.
5. Transfer 200 µL of this reaction into a 96 well plate. As the total volume is 500 µL, you can measure the optical density in duplicates per reaction. In case of air bubbles, take a needle, heat it with a lighter and puncture the bubbles.
6. Read absorption at 620 nm with the Thermo Multiskan EX plate reader.
7. Prepare a calibration curve of the BSA concentration series and use it to calculate the protein concentration of the samples.

o Total Protein Kit (Sigma): This Kit supplies the Lowry Reagent Solution and Folin-Ciocalteau
o Bovine serum albumin (BSA): Prepare a BSA (Roth) concentration series (200, 100, 50, 25, 12.5 µg/mL) with H$_2$O and store it at -20°C.

2.7.3 SDS-Page and Western blot

To investigate the samples for the presence of specific proteins, they were separated according to their molecular weight by SDS-Page (sodium dodecyl sulphate polyacrylamide gel electrophoresis). Subsequently, Western Blot analysis was performed. Thereby, the proteins separated by SDS-Page were transferred electrophoretically to a PVDF (poly-vinylidenfluoride) membrane. Specific primary antibodies were used to detect the proteins of

interest. HRP (horseradish peroxidase)-linked secondary antibodies were used to detect the bound primary antibodies on the PVDF membrane. For the detection of the secondary antibody, we used a commercially available ECL (enhanced chemiluminescense) reagent, which reacts with the HRP under light emission that was detected by a CCD camera.

SDS-Page

Depending on the molecular weight of the protein of interest SDS-gels with different acrylamide content were prepared (using the Mini Protean 3 system from BioRad). For bigger proteins (> 30 kDa), gels with lower acrylamide content (8%) were prepared **(Table 12)**, whereas for the separation of smaller proteins (< 30 kDa), gels with greater acrylamide content (12%) were used. Depending on the amount of protein loaded, it was possible to choose between 0.75 or 1.5 mm thick gels. The standard gel used was 1.5 mm thick and had an acrylamide content of 10%. Preferably, the 10 slot comb was used. This allowed for the loading of up to ≈30 µL protein sample.

Table 12. Composition of polyacrylamide gel

Components	Separating gel (1 gel 1.5 mm)			Stacking gel (max. 3 gels 1.5 mm)
	8%	10%	12%	4%
Rotiophorese®	2.7 mL	3.3 mL	4 mL	1.3 mL
4x Tris/SDS pH (8.8)	2.5mL	2.5 mL	2.5 mL	///
4x Tris/SDS pH (6.8)	///	///	///	2.5 mL
H_2O	4.7 mL	4.1 mL	3.4 mL	6.1 mL
TEMED	10 µL	10 µL	10 µL	20 µL
APS	50 µL	50 µL	50 µL	50 µL

For the preparation of 0.75 mm thick gels half the amount is used.

SDS gel preparation

1. Clean spacer and glass plates with soap and 70% ethanol.
2. Assemble the glass plates in the BioRad system.
3. Prepare the separating gel and pour it between the glass plates up to the lower edge of the green boarder. To get rid of bubbles overlay the gel with a thin ethanol layer. The polymerization reaction takes about 20-30 minutes.
4. Tilt the gel und use a paper towel to remove the ethanol.

5. Prepare the stacking gel and pour it up to the top edge of the glass plates.

6. Insert the comb and allow polymerization for about 20-30 minutes.

7. If the gel is not used immediately wrap it into wet paper towel, pack it with cling film and store at 4°C.

Table 13. 4x Tris-Cl/SDS pH 8.8 (store at 4°C)

Tris-Cl	1.5 M (182 g/L)
SDS	0.4% (4 g/L)
H_2O	to 1 L
pH 8.8	adjust with HCl

Table 14. 4x Tris-Cl/SDS pH 6.8 (store at 4°C)

Tris-Cl	0.5 M (60.04 g/L)
SDS	0.4% (4 g/L)
H_2O	to 1 L
pH 6.8	adjust with HCl

Table 15. 10x SDS running buffer

Tris-Cl	0.25 M (30.2 g/L)
Glycine	1.9 M (144 g/L)
SDS	0.1% (1 g/L)
H_2O	to 1 L

Table 16. 5x SDS loading dye (1 mL aliquots stored at -20°C)

Tris-Cl	3.2 mL/10 mL Tris-CL pH 6.8
Glycerol	40% (4 mL/10mL)
SDS	15% (1.5 g/10 mL)
2-mercaptoethanol	3.6 M (2.5 mL/10 mL)
Bromphenol blue	0.1% (10 mg/10 mL)
H_2O	to 10 mL

o 20% APS: Dissolve 2 g ammonium persulfate (APS) in 10 mL H_2O, prepare 1 mL aliquots and store at -20°C

SDS-Page and Western blot analysis

1. Pull out the comb from the SDS gel.

2. Carefully use deionized water to wash the gel pockets free of any remaining acrylamide.

3. Place the gel into the running chamber. The short side has to be faced inward.

4. Fill up the inner and outer part of the chamber with 1x SDS running buffer.

5. Denature the protein samples (lysate in 1x SDS loading dye) for 10 minutes at 95°C.

6. Load the samples and 3 μL protein marker (PageRuler^{TM} Plus Prestained Protein Ladder, Thermo scientific).

7. Run the gel with 100 V until the stacking gel is passed and then apply up to 150 V for the separating gel.

8. In the meantime, prepare the Whatman filter papers (16 per gel) and PVDF membrane for blotting.

9. Around 5 minutes before the SDS gel is ready immerse the Whatman papers in the proper buffers and rinse the PVDF membrane in methanol. This methanol procedure is crucial to "hydrate" the PVDF Otherwise, protein transfer and binding would be impaired (hydration with H_2O isn't possible due to the highly hydrophobic feature of PVDF).

10. Assemble the Whatman papers, PVDF membrane and SDS gel in the semi dry blotting device (Roth) **(Figure 12)**. After every layer of filter papers, use a plastic pipette and roll over the stack to remove potential air bubbles.
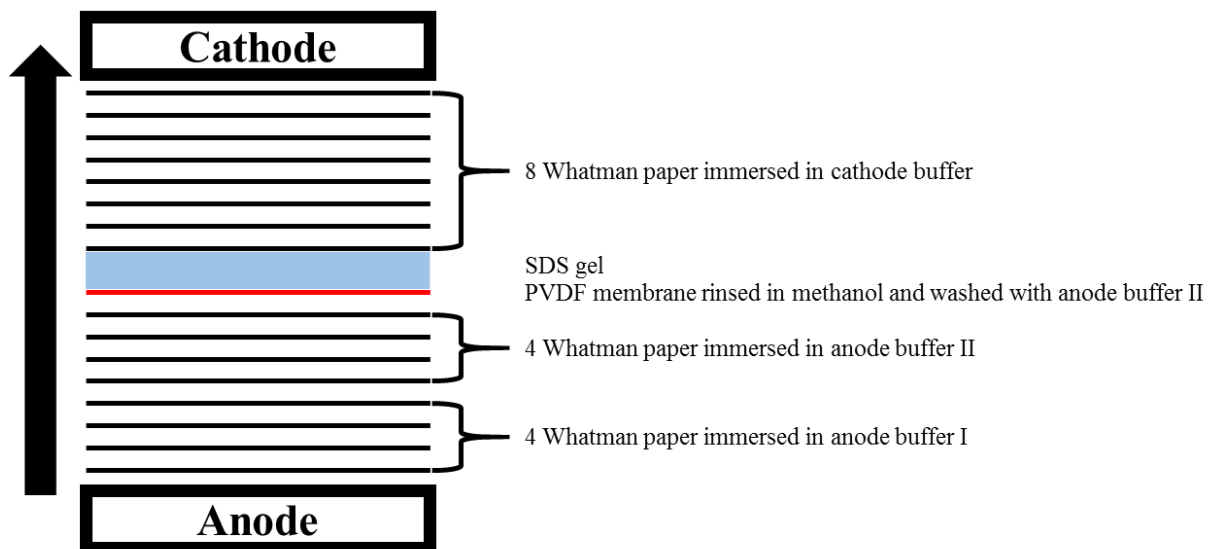
Figure 12. How to setup a Western blot with Whatman paper

11. Blot the membrane for 80 minutes with 55 mA per stack. In the meantime, prepare 5% and 1% milk powder in 1x TBS-T.

12. Cut the membrane and label it with a pencil. Especially highlight the marker bands for later analysis.

13. Block the membrane for 1 hour with 5% milk powder solution at RT.

14. Wash the membrane 2x 3 min with 1x TBS-T. Therefore put it into a bowl and place it on a shaker.

15. Put the membrane into the primary antibody and incubate it overnight at 4°C on a rolling shaker. Alternatively incubate for 2 hours at RT (This depends on the experience with the desired antibody).

16. Wash the membrane 3x 3 minutes with 1% milk powder solution. In the meantime prepare the HRP-linked secondary antibody (5 mL in a 50 mL Falcon tube are suitable).

17. Put the membrane into the secondary antibody and incubate it for at least 1 hour at RT on a rolling shaker.

It is recommended to seal the primary and secondary antibody tubes with Parafilm to prevent leaking.

18. Wash the membrane 1x 3 minutes in 1% milk powder and 2x 3 minutes in 1x TBS-T.

19. Prepare undiluted or diluted (1:2 up to 1:10) ECL reagent by mixing solution A and solution B. For the preparation of the dilution us 1x TBS-T. Pipette the ECL reagent on the membrane and acquire chemiluminescense images after appropriate acquisition times (3 seconds up to 10 minutes).

20. After developing the blot, also acquire a bright field image of the marker.

21. The Western Blot can be evaluated by ImageJ [160].

22.

Table 17. Anode buffer I (pH 10.4)

Tris-Cl	0.3 M (36.3 g/L)
Methanol	20% (200 mL/L)
H_2O	to 1 L

Table 18. Anode buffer II (pH 10.4)

Tris-Cl	0.025 M (3.03 g/L)
Methanol	20% (200 mL/L)
H_2O	to 1 L

Table 19. Cathode buffer (pH 7.6)

Aminocaproic acid	0.04 M (5.2 g/L)
Tris-Cl	0.025 M (3.03 g/L)
Methanol	20% (200 mL/L)
H_2O	to 1 L

o 1x TBS-T: 1x TBS (100 mL/L 10x TBS-T) with 0.1% Tween-20 (1 mL/L)

o Milk powder solution: Dissolve 5 g (5%) or 1 g (1%) milk powder in 100 mL TBS-T

o Primary antibody diluent: TBS-T with 5% BSA and 0.05% NaN_3. Primary antibodies are prepared in a 50 mL Falcon Tube (5-10 mL per antibody). The antibodies are stored at 4°C and used multiple times.

o Secondary antibody diluent: Secondary antibodies are prepared freshly in 1% milk powder solution.

2.8 VASP phosphorylation

The vasodilator-stimulated phosphoprotein VASP is associated with processes during cytoskeleton remodeling. VASP is phosphorylated at multiple sites. Ser157, Ser239 and Thr278 can be phosphorylated by cGK or cAK [161]. cAK phosphorylates VASP preferably at Ser157, and cGK at Ser239. More than twenty years ago, it was demonstrated that the migration of VASP in a SDS-Page is affected by the phosphorylation status. Unphosphorylated VASP migrates at 46 kDa, whereas after phosphorylation by cGK or cAK at Ser157 the protein migrates at 50 kDa [162]. For this reason, VASP is often used as a monitor for cAK and/or cGK activity.

1. Isolate primary VSMCs and grow them till 80-90% confluency.
2. Wash the cells 2x with PBS.
3. Serum starve the cells for 48 hours by incubating them in serum-free medium (see below).
4. Aspirate the serum-free medium and incubate the cells for additional 30 minutes in fresh serum-free medium containing the desired drugs (at 37°C and 6% CO_2).
5. Prepare protein lysates **(see chapter 2.7.1)**.

For the "short-term cGMP stimulation assays", it is recommended to prepare at least 1 well out of a 6 well plate per condition.

o VSMC serum-free medium: 500 mL DMEM medium -GlutaMAX^{TM} (Gibco) including 5 mL Pen/Strep, store at 4°C

2.9 Cell fixation and immunofluorescence

For several experiments it was important to perform immunofluorescence antibody stainings to detect a desired protein. In case of double staining of two target proteins it was necessary to check for potential cross-reactivity between the two primary and two secondary antibodies. If possible, the specificity of the primary antibody was verified with knockout samples of the desired protein. To distinguish between background staining of the secondary antibody and a specific antibody staining, every experiment contained a negative control, where the primary antibody was omitted.

1. Grow VSMCs on glass coverslips in the required culture format.
2. Wash the cells 2x with PBS.
3. Fix the cells for 10 min at RT with Immuno-Fix (3.7% formaldehyde in PBS).
4. Wash 2x with 2% BSA-PBS.
5. Continue with the staining or store the cells in 2% BSA-PBS at 4°C. Unless otherwise stated all following steps were performed at RT.
6. Incubate the cells for 10 min in Serum-PBS (+ 0.1% Triton X) and wash afterwards 1x with 0.5% BSA-PBS.
7. Prepare an appropriate amount of primary antibody and pipette it on parafilm. Put the glass slides with the cells downside on the antibody drop (For the common glass coverslip used within a 24 well plate, 75 µL of primary antibody were used).
8. Incubate the coverslip for 1 hour and make sure there are no air bubbles.
9. Put the coverslip back to the well plate (cells upside) and wash them 2x 3min with 0.5% BSA-PBS.
10. Prepare an appropriate volume of the secondary antibody (add 1:1000 Hoechst 33258, for nuclei staining). And repeat the same procedure as for the primary antibody. In case of a double staining do not add Hoechst to the 1st secondary antibody and continue at step 7 with the 2nd primary antibody.
11. Put the coverslip back into the well plate and wash 2x 3min with 0.5% BSA-PBS.
12. Dip the coverslip 3-4x into distilled water and embed it with a drop of mounting medium (cells downside). Store in the dark at 4°C.

- o Primary Antibody: Antibody diluted in 0.5% BSA-PBS supplemented with 0.1% TritonX-100
- o Secondary Antibody: Antibody diluted in 0.5% BSA supplemented with 1:1000 Hoechst 33258
- o Serum-PBS: 5% (500 µL/9.5 mL PBS) Normal Donkey Serum (NDS) in PBS supplemented with 0.1% TritonX-100.
- o 2% BSA-PBS: 2 g BSA dissolved in 10 mL PBS
- o 0.5% BSA-PBS: 0.25 g BSA dissolved in 50 mL PBS
- o Immuno-Fix (3.7% formaldehyde): 1 mL 37% formaldehyde (Chemsolute® Th. Geyer) diluted in 9 mL PBS
- o Normal Donkey Serum: Prepare 1 mL NDS (Millipore) Aliquots and store at 4°C
- o Mounting Medium: Shandon Immu-Mount (Thermo Scientific); store at RT
- o 1000x Hoechst 33528: Dissolve 1 mg/mL Hoechst 33528 (Sigma) in H_2O; prepare 1 mL aliquots and store at -20°C

2.10 In vitro FRET measurements

Primary transgenic VSMCs expressing the FRET-based cGMP biosensor cGi500 were used to analyze the cGMP signaling behavior of VSMCs under different conditions. For this purpose, an inverted Axiovert 200 microscope **(Figure 13)** with a 1.0/1.6x Optovar lens (Zeiss) and fluorescence grade objectives (Plan NeoFluar 10x/0.30, Carl Zeiss) was used. The microscope was equipped with a DualView beam splitter consisting out of a 516 nm dichroic mirror, and 480/50 nm and 535/40 nm emission filters (Dual View DV, DUAL-View, Photometrics). The beam splitter is responsible for the separation of CFP and YFP signals. The signals are generated by a computer controlled light source (Oligochrome, Till Photonics, Gräfeling, Germany) equipped with a 445/20 nm CFP excitation filter and electronic shutter. The CFP and YFP emission signals were recorded with a cooled electron multiplying charged coupled device (EM-CCD) camera (Retiga 2000R, QImaging). To examine cell samples by eye, an additional YFP filter set with 497/16 nm excitation filter, 516 nm dichroic mirror and 535/2 nm emission filter was used. This allowed to record YFP images without beam splitter in between. During the measurement, the cells were continuously superfused with Tyrode buffer
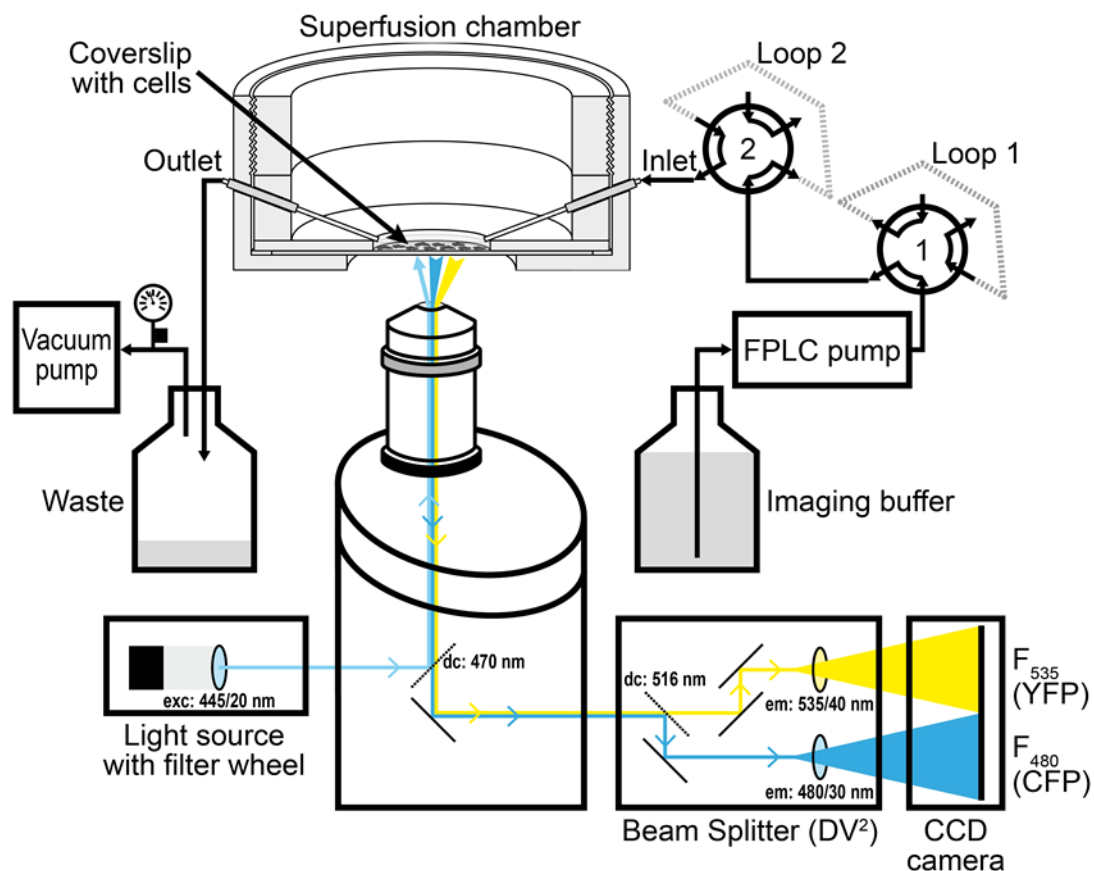
Figure 13. Schematic presentation of cGMP FRET imaging system

Taken from Thunemann et al. 2013 [149].

(Table 20).The custom-built superfusion system consisted of a FPLC pump (Pharmacia P-500, GE Healthcare), FPLC injection valves (Pharmacia V-7, GE Healthcare) and a superfusion chamber (RC.25/26, Warner instruments). To apply different drugs, the system also included sample loops of different sizes (2 and 7 mL). In general, the 2 mL loop was used for drug application. In addition, a vacuum pump (Laboport N86, KNF Neuberger) was connected to the system to remove buffer.

2.10.1 FRET-based cGMP measurements in VSMCs

For the FRET measurement of VSMCs, the 10x magnification objective was used.

1. Grow primary VSMCs on 12 mm glass coverslips.
2. Serum starve the cells for 12 hours by incubating them in serum-free medium, before measurement. This procedure should mimic the *in vivo,* situation where VSMCs are mitotically inactive.
3. Before measurement perform a solvent change (injection valves in load mode) with Tyrode buffer and check the beam splitter for CFP and YFP alignment. Also ensure that the appropriate sample loops are assembled and that all other materials needed for the measurement are prepared (drugs, drug application sheets, pipettes etc.).
4. Assemble the superfusion chamber with a coverslip: Use a paint brush to daub silicon on the chamber. But make sure that the border of the chamber where the coverslip is placed is free of silicon. Therefore, use a cotton stick. Otherwise the silicon may interrupt the measurement. Place the coverslip in the chamber and cover the cells with Tyrode buffer.
5. Clean the bottom side of the coverslip (where no cells should be) with ethanol.
6. Place the chamber on the microscope and connect it to the superfusion system.
7. Start the superfusion system with a rate of 60 mL/hour and place injection valves in the load mode. Make sure that the Tyrode buffer is correctly aspirated, so that it doesn't overflow. Also ensure that the chamber is not leaky.
8. Use the YFP filter set to identify a representative region of interest (ROI). Acquire a finely grained image of this region (1x1 binning and ≈2 sec exposure time). This image is required to ease the mapping process of your ROIs later during data evaluation.
9. Adjust the imaging settings: For cGMP imaging in VSMCs, use 4x4 binning, a cycle interval of 5 s and an exposure time of 300 ms.
10. Start the measurement and first record baseline for about 30 frames. This is important for the later baseline correction.

11. For drug application, prepare an appropriate concentration, diluting in Tyrode buffer and load it via a syringe into the simple loop through the injection valve. Release the drug to the cells through switching the injection valve into load mode. As NPs are quite stable, dilutions can be prepared at large scale. However, as NO donors like DEA-NO are only stable in alkaline stock solution **(see chapter 2.1.2)**, dilutions in Tyrode buffer should be prepared shortly before administration.

12. Observe FRET changes and wait till the drug is washed out and the baseline is reached before the next drug administration. After the baseline is reached, flush Tyrode buffer through the sample loop to remove potential drug residues, which could influence the next application.

13. After the measurement, clean the superfusion system by flushing it 2x with 20% ethanol (run solvent change, injection valves once in load mode and once in injection mode). Dissamble and clean the superfusion chamber and remove any remaining silicon.

Table 20. Tyrode buffer (pH 7.4)

NaCl	140 mM (8.18 g/L)
KCl	5 mM (0.372 g/L)
$MgCl_2$	1.2 mM (0.244 g/L)
$CaCl_2$	2 mM (0.222 g/L)
HEPES	5 mM (1.192 g/L)
H_2O	To 1 L

Add 4 mL 2.5 M D-Glucose to 1 L Tyrode buffer before use (final concentration 10 mM).

- o 2.5 M D-Glucose: Dissolve 9 g D-Glucose (Carl Roth) in 20 mL H_2O, sterilize by filtration, prepare 2 mL aliquots and store at RT.

2.10.2 Data analysis of FRET experiments

Live Acquisition software (TILL, Photonics) was used for image acquistion and online analysis of the measurement. For subsequent offline data analysis, ImageJ, Microsoft Excel (Microsoft Corp.), and Origin Pro 2016 (OriginLab Corp.) were used.

ImageJ:

ImageJ was used to generate the FRET traces of every single cell. The finely grained 1x1 binning picture recorded at the beginning of the experiment was used to draw the ROIs. In

addition, it is also necessary to draw a ROI for the background. Because the FRET measurement was performed with 4x4 binning, a Python script was used to downscale the ROIs drawn in the 1x1 binning image. The 4x4 ROIs where used to read out the mean fluoescence intensities for CFP (480 nm, F_{480}) and YFP (535 nm, F_{535}) from the time-lapse recording. These values were used for further analysis in Microsoft Excel.

Mircosoft Excel:

Microsoft Excel was used to calculate the normalized FRET responses. First, the background of F_{480} and F_{535} was substracted from the CFP and YFP intensitites, respectively. Subsequently, the background-corrected F_{480} and F_{535} values were used to calculate the F_{480}/F_{535} ratio R. $\Delta R/R$ values were calculated by normalization to the baseline recording before the first drug application.

Origin Pro:

The Peak Area/Height Analyzer of Origin Pro was used for $\Delta R/R$ peak height calculation. The peak borders were defined manually.

2.10.3 ANP/CNP response classification

The FRET experiments were mainly performed to investigate the link between the cGMP signaling pathway and the phenotypic modulation of VSMCs. In particular, it was investigated whether the phenotype of an individual VSMC (either contractile or synthetic) as determined by immunofluorescence staining of different marker proteins correlates with the ANP/CNP-preference of this cell. Primary VSMCs grown on grided coverslips (Bellco Biotechnology) were stimulated with two concentrations (50 nM / 250 nM) of ANP and CNP **(Figure 14)** and then fixed and stained for various marker proteins. The ANP/CNP-preference was classified by calculating the ratio between the $\Delta R/R$ peak heights induced by 50 nM or 250 nM of the respective peptide **(Table 21)**.
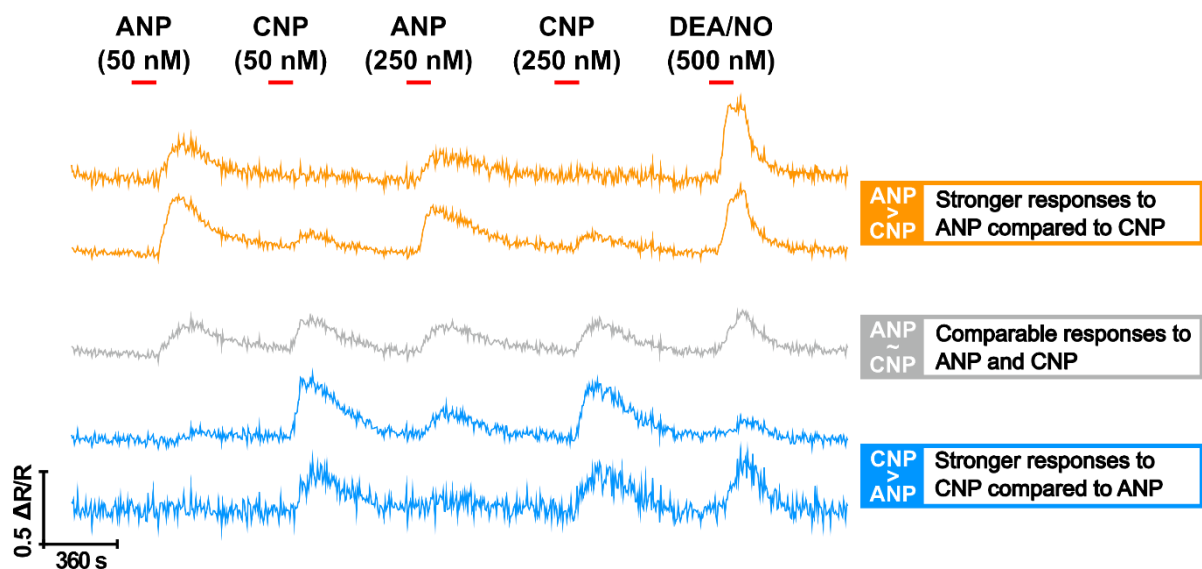
Figure 14. ANP/CNP-response classification in VSMCs

Primary VSMCs expressing the FRET-based cGMP sensor cGi500 where used for NP classification. Cells had been stimulated with altering concentrations of either ANP or CNP (50 nM or 250 nM). 500 nM DEA-NO stimulation at the end of the experiment was used as positive control. Figure provided by Moritz Lehners.

Table 21. NP-preference classification

Stimulation	ANP	ANP~CNP
	CNP	
ANP/CNP	≥1.5	0.67<1.5
50 nM	≤0.67	
ANP/CNP	≥1.5	0.67<1,5
250 nM	≤0.67	

ANP or CNP preferring cells:

ANP or CNP preferring cells were defined by a cGMP signal differential of ≥ 1.5 times (e.g. the cGMP signals induced by ANP were ≥ 1.5 times the cGMP signal induced by CNP, or vice versa). For the definition of the NP-preference, the cGMP signal differential of both stimuli (50 nM and 250 nM) had to be ≥ 1.5 times for either ANP or CNP.

ANP~CNP:

The ratio of cGMP signals induced via ANP or CNP was at least for one of the two concentrations applied between 0.67<1.5.

2.10.4 Correlation of NP-preference with marker protein expression

To correlate the NP-preference with marker protein expression, VSMCs were grown on gridded coverslips. This experiments were complex and took several steps.

1. Grow primary VSMCs expressing the cGi500 sensor on gridded coverslips.
2. Perform the FRET measurement described in section **2.10.1**.
3. Right after the FRET measurement fix the cells and stain them for the desired marker proteins described in section **2.9**.
4. Correlate the NP-preference with marker protein expression.

Note: Before the FRET measurement is started, take a bright field image of the grid. It is mandatory to analyze the same region of the gridded coverslip by immunostaining as during the FRET measurement (**Figure 15**).
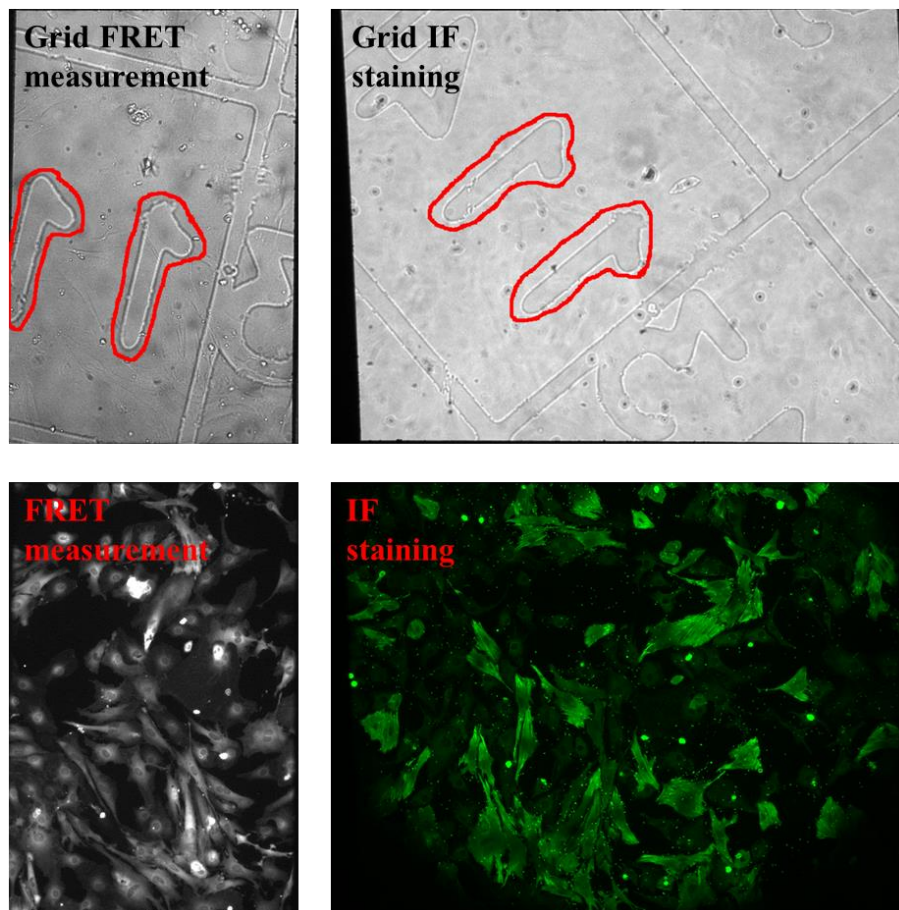
Figure 15. Images of the grid region during FRET measurement and after immunnostaining

For the image editing process the software ImageJ (Version 1.51d) was used.

1. Open the 1x1 binning grid image from the FRET measurement and the immunofluorescence staining in the software.

2. Adjust the brightness of both images so that they are comparable (Process → Enhance Contrast [☑ Normalize]). This is important for later stages, in which both images will be overlayed.

3. Use the Angle tool to adjust the orientation of the immunofluorescence image so that it fits to the grid of the FRET measurement **(Figure 16)**. It is important to adapt the immunofluorescent (IF) image to the FRET image. Otherwise the already drawn ROIs (which had been prepared for the FRET evaluation) can not be used. After the angles have been obtained, rotate the IF image to adjust the orientation (Image → Transform → Rotate [☑ Enlarge Image to Fit Result]). Note down the used angle.
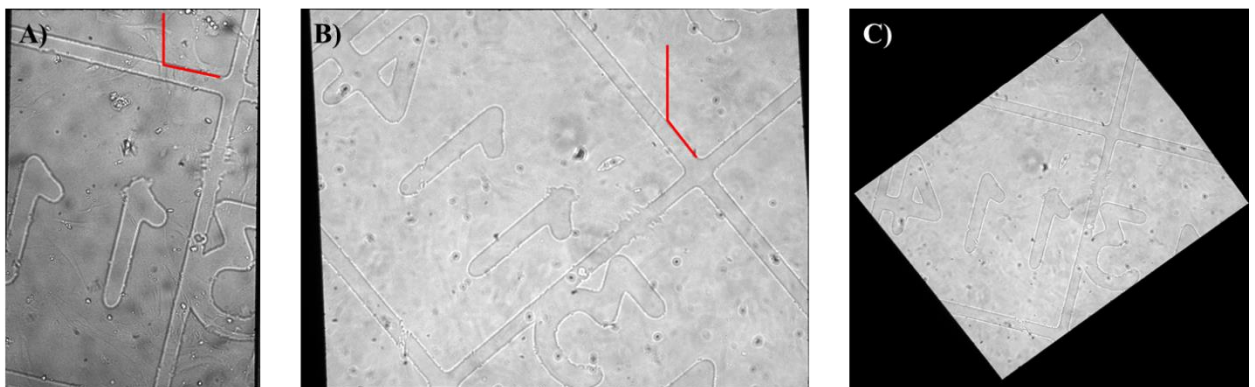
Figure 16. Example for adjusting the orientation

The red lines, display the angle, which is necessary to adjust the orientations of the IF and FRET image.

4. In the next step specify the region of the IF images so that it resembles the exact region that was recorded during the FRET measurement. Therefore select the FRET image (Strg A and Strg C) and paste (Strg V) it into the IF image. Rightclick → Paste Control → Blend.

5. Move the picture until both imgages overlie and specify the selection (Edit → Selection → Specify). Note down the coordinates.

6. Close all images and open the 1x1 snapshot (image of the cells) from the FRET measurement and the Hoechst image from the IF staining.

7. Repeat step 1-3 for these two images and use the settings obtained by the adjustment of the bright field grid images.

8. Paste the snapshot image into the Hoechst image (step 4). During the staining process it can happen that cells are slightly moved. Therefore, adjust both pictures until the cell nuclei fit into the cells and specify the new selection (Edit → Selection → Specify). Note down the updated coordinates.

9. Open all immunofluorescence images and repeat step 1-4 with the right angle and selection coordinates. After specifying the region crop the images (Strg- Umschalt – X) and save them.

The processed IF images can now be used to measure the mean fluoresscence intensity of the respective marker proteins.

1. Open the processed IF images in ImageJ and load the ROIs from the 1x1 FRET snapshot. The ROIs should exactly fit to the processed IF images.

2. Measure the fluoescence intensity (mean gray value).

3. Import these values into Microsoft Excel and substract the background mean fluorescence intensity (intensity from an ROI, of a cell free area).

4. As the ROIs for the FRET measurement and the IF staining are the same, the NP prefrence and marker protein expression of every single cell can easily be correlated.

5. For statistical analysis OriginLab was used.

2.11 Analysis of atherosclerosis

These experiments were performed to investigate whether SMC-specific depletion of Fn had an impact on the development of atherosclerotic plaques in mice. Since healthy mice under normal conditions do not develop atherosclerosis, we used mice with a $ApoE^{-/-}$ background. These mice have an impaired lipid metabolism [163] and are a commonly used model for atherosclerosis. To generate a SMC-specific depletion of Fn on an ApoE-deficient beckground (Fn-smko mice), mice expressing Cre recombinase under the control of the SM22 promoter [164] were crossbred with mice having a floxed Fn gene [165]. Mice were fed an atherogenic diet (20% fat, 1.5% cholesterol by weight, Altromin Germany) for 11 weeks. Litter-matched female and male KO and control mice were used for experiments. The experimental setup is summarized in (**Figure 17**).

Atherosclerosis experiment

⊢ Age of mice
🟩 Age of mice (wk)
🟦 Atherogenic diet
\# Oil Red O and IHC prepared
∗ Blood samples collected

11 wk

Start
(mice born)
16 wk
End #∗

Experimental animals

ctr n = 23
Fn-smko n = 12
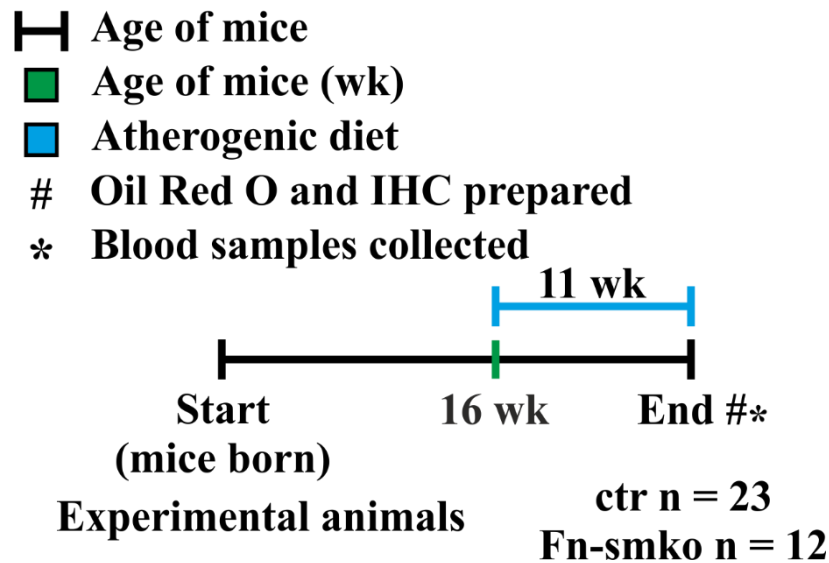
Figure 17. Atherosclerosis experimental setting

o Atherogenic diet: modified diet 1324 (20% fat and 1.5% cholesterol by weight) from Altromin (Altromin, Germany). The chow was delivered in vacuum sealed 5 kg packages. To enhance storage life, closed packages were stored at -20°C. Opened packages were stored at 4°C (for maximum 2 weeks). Note that it takes one night at 4°C to defrost the chow.

2.11.1 Preparation of mice fed with atherogenic diet

1. Mice are starved (chaw was removed) for 6-12 hours before sacrificing them.
2. Anesthetize mice via CO_2 inhalation. And open the thorax.
3. Use a thin heparinized cannula (Sterican®; G27 x ¾ inches 0.40 x 20 mm grey; Braun) to puncture the left ventricle of the heart and to collect the blood sample in a 1.5 mL Eppendorf tube.
4. To obtain the serum, let the blood coagulate for 2 hours at RT. Centrifuge it for 3 min at 3000g and distribute the supernatant into two Eppendorf tubes (1x 200 µL and 1x residual). Blast freeze in liquid nitrogen and store at -80°C.
5. Use a thin cannula (Sterican®; G27 x ¾ inches 0.40 x 20 mm grey; Braun) to perfuse the left ventricle of the heart with cold 10% formaldehyde (Chemsolute® Th. Geyer) until the heart brightens (2-3 mL).
6. Weigh the mice (Mettler PC 440), remove the desired organs (heart, spleen and kidney) and weigh them too.

7. Carefully isolate the aorta still attached to the heart. This step is critical to avoid damage to the aortic arch.

8. Perfuse the aorta with PBS (use a thin Sterican® cannula) to remove the remaining blood.

9. Use forceps to remove the surrounding tissue of the aorta and to dissect the aortic arch. Be very careful to not disrupt the brachiocephalic artery, left common carotid artery and left subclavian artery. Alternatively the preparation can also be done after fixation when the tissue is more stable. However, it may be easier to clean the aorta before fixation when the tissue is still soft.

10. Weigh the heart.

11. Fix the aorta for two hours at RT and afterwards over night at 4°C in 10% formaldehyde.

12. Wash the aorta 2x times with PBS and finish the cleaning process.

13. Store the aorta at 4°C in PBS. It is recommended to use 12 well plates with 3 mL PBS. Seal the well plate with parafilm.

o 20 U/mL Heparin: Dissolve 1 mg Heprain sodium salt ($\geq$180 I.U/mg; Roth) in 10 mL PBS; store at 4°C

o 10% Formaldehyde: 2.7 mL 37% formaldehyde (Chemsolute® Th. Geyer) diluted in 7.3 mL PBS

2.11.2 Blood sample analysis

The blood samples were analyzed in the "Zentrallabor des Universitätsklinikums Tübingen" by Prof. Dr. med. Andreas Peter. Standard lipid parameters like total cholesterol, LDL, HDL and triglyceride levels were determined. In addition, Prof. Peter investigated other blood parameters like uric acid (UA), Gamma-glutamyl transferase (GGT), non-esterified fatty acids (NEFA), etc.

2.11.3 Oil Red O staining of atherosclerotic plaques

For the analysis of atherosclerotic plaques, aortae **(see chapter 2.11.1)** were stained with Oil Red O (Sigma), which is a dye staining neutral fats and cholesteryl esters [166]. Oil Red O is commonly used to investigate plaque development during atherosclerosis.

1. Transfer the dissected aortae from PBS into a fresh 12 well plate containing 78% methanol and wash 5 min.

2. Aspirate the methanol and incubate the aortae for 90 min in Oil Red O staining solution.

3. Remove the staining solution and put the aortae for another 5 min into 78% methanol. This step will destain the less fatty tissue and enhance the contrast of atherosclerotic plaques.

4. Put the aortae back into PBS and remove the remaining surrounding tissue. Store the aortae at 4°C in PBS.

o 78% methanol: Dilute 78 mL technical methanol (Sigma) in 22 mL H_2O

o 1 M NaOH: Weight 40 g sodium hydroxide (Roth) and dilute in 1 L H_2O.

o 0.5% Oil Red O stock: Weigh 0.4 g Oil Red O (Sigma) and dilute it in 80 mL technical methanol. Protect the bottle from light with aluminum foil.

o Oil Red O staining solution: Mix 35 mL Oil Red O stock (0.5% in technical methanol) with 10 mL NaOH (1 M). Filter the solution (round filter, Macherey-Nagel). The staining solution has always to be prepared freshly before use.

2.11.4 Documentation of atherosclerotic plaques

To quantify the area of atherosclerotic lesions, Oil Red O-stained aortae were photographed (DSC-W17, Sony) under a Stemi microscope (Stemi 2000-CS, Zeiss). For documentation, a smaller magnification (0.65x Stemi + 1.7x digital zoom) and a greater magnification (1.65x Stemi + 1.7x digital zoom) were used. For better contrast, the aortae were placed on a black background. A 1 mm scale bar was photographed for calibration. Two different methods were applied for quantification of Oil Red O-stained lesions.

1. Intact aortae are mounted between two glass slides and photographed from both sides. It is important to put a drop of PBS between the slides.

2. Aortae are cut open longitudinally and pinned to Sylgard® 184 (Downcorning). Add a drop of PBS.

It is also important to use always the same settings of the camera.

Area of atherosclerotic plaques was quantified (relative plaque area in the aorta) with ImageJ and statistical analysis was performed with Origin Pro software.

2.**11.5 Preparation of paraffin sections**

For immunohistochemical analysis of the plaques, aortae were embedded into paraffin.

1. Dehydrate tissue with an increasing alcohol series:
   - ➔ 60% EtOH/H_2O for 1 hour at RT
   - ➔ 70% EtOH/H_2O for 1 hour at RT
   - ➔ 80% EtOH/H_2O for 1 hour at RT
   - ➔ 90% EtOH/H_2O for 1 hour at RT
   - ➔ 2x 100% EtOH/H_2O for 20 min at RT
   - ➔ 1x 100% toluene (Sigma) for 2 min at RT (proceed this step under a hood)

2. Pass tissue through 3 changes of liquid paraffin at 57°C. Each paraffin step should be at least overnight.

3. Embed tissue in clean liquid paraffin using an embedding system consisting of a metallic cassette and a plastic mold. To accelerate the stiffening process of paraffin place the embedded tissue at -20°C.

4. Store paraffin embedded tissue at RT until further processing.

5. A microtome (Micom HM 335 E) is used to prepare 10-µm tissue sections. Stretch the sections in a 37°C water bath and mount on polylysine slides (Thermo Scientific). Store sections at RT.

   o Paraffin: Fill Surgipath Paraplast X-tra grains (Leica) into a beaker and melt it overnight at 57°C

2.11.6 Immunohistochemistry of paraffin section

To analyze the composition of the plaques, the paraffin sections were investigated via immunohistochemistry for specific proteins (e.g. SMαA and Mac-2).

1. To prevent the tissue sections from detaching, the coverslips were incubated right before use overnight at 37°C.

2. Deparaffinize and rehydrate paraffin sections:
   - ➔ 2x 100% toluene for 2 min at RT (proceed this step under a hood)
   - ➔ 2x EtOH 100% for 2 min at RT
   - ➔ 1x EtOH 90% for 2 min at RT
   - ➔ 1x EtOH 80% for 2 min at RT
   - ➔ 1x EtOH 70% for 2 min at RT
   - ➔ 1x EtOH 60% for 2 min at RT

3. Wash slides in PBS for 5 min at RT.

4. Blocking of endogenous peroxidase:
    o Place coverslips in a damp chamber and incubate them in peroxidase blocking solution (≈1 mL per coverslip) for 20 min at RT.

5. Wash the coverslips 1x with PBS for 3 min.

6. Antigen unmasking:
    o Place the coverslips into a cuvette and incubate them in antigen retrieval solution for 15 min at RT.
    o Put the coverslips into a microwave and boil them carefully. This is a critical step, because the sections might detach.
    o Transfer the coverslips into a cuvette with 1x TBS-T and incubate them for 5 min at RT.

7. Blocking of unspecific binding sites:
    o Circle the sections with a pap pen, place them into a damp chamber and incubate them with blocking solution for 2-3 hours at RT (≈1 mL per coverslip).

8. Primary antibody:
    o Pipette the primary antibody on the sections (≈0.5 mL per coverslip) and incubate the coverslips in a damp chamber at 4°C overnight.
    o On the next day incubate the sections for another hour at RT.
    o Wash the sections 3x 10 min with 1x TBS-T in a cuvette.

9. Secondary antibody (biotinylated IgG):
    o Incubate the sections for 3 hours with the secondary antibody (≈0.5 mL per coverslip) in a damp chamber at RT.
    o To remove unspecifically bound antibodies, wash the sections 3x 10 min in 1x TBS-T in a cuvette. Meanwhile, prepare the ABC reagent for the next step (≈0.25 mL per coverslip) and incubate it for 30 min at RT in the dark.

10. Alkaline phosphatase reaction:
    o Place the coverslips again into the damp chamber, pipette the ABC reagent on the sections and incubate for 30 min at RT in the dark.
    o Wash the sections 3x 10 min with 1x TBS-T. During the last washing step, prepare the DAB staining solution (one DAB stock is sufficient for ≈6 coverslips).
    o Place the coverslips into the damp chamber and pipette the DAB staining solution on top.
    o Stop the reaction with H_2O when the sections are colored brown (after ≈1 min).

11. Mount the sections in Aquatex mounting medium (Merck).

To control for unspecific reactions, always prepare a negative control without primary antibody.

- o Peroxide blocking solution: 2.7 mL 30% H_2O_2 (Roth), 0.585 mL 20% methanol (in PBS), and 5.13 mL PBS
- o Blocking solution: 10% normal donkey serum in 1x TBS-T
- o Antigen retrieval solution: 10 mM tri-sodium citrate • $2H_2O$ (2.94 g dissolved in 1 L H_2O), adjust pH to 6.0 with HCl.
- o Primary antibody: Primary antibody is diluted in 5% NDS in 1x TBS-T. As negative control, prepare 10% NDS without primary antibody
- o Secondary antibody: Secondary antibody is diluted in 5% normal donkey serum in 1x TBS-T.
- o ABC-reagent: Mix 30 µL of Regent A and Reagent B (Vectastain alkaline phosphatase standard kit, Vector Laboratories) in 1.5 mL PBS
- o 0.1 % DAB stock solution: Dilute 40 mg (DAB) in 40mL PBS. Store at -20°C
- o DAB staining solution: Mix 800 µL of the DAB stock with 800 µL PBS.

Mice with a floxed fibronectin gene were kindly provided by Prof. Dr. Reinhard Fässler (Max Planck Institute for Biochemistry, Martinsried)

2.11.7 Documentation of immunohistochemically stained plaques

The stability of a plaque determines whether the atherosclerotic lesion ruptures and subsequent events like thrombosis, heart attack or stroke occur. To investigate the plaque stability, we determined the stability index of individual atherosclerotic lesions. This stability index was based on the relative amount of immunohistochemically stained **(see chapter 2.11.6)** SMαA and Mac-2 positive plaque area (in relation to the total area of the plaque).

Stability index = [%] SMαA positive plaque area / [%] Mac-2 positive plaque area

The relative SMαA and Mac-2 positive plaque areas were quantified with ImageJ and statistical analysis was performed with Origin Pro software. A higher stability index indicates a more robust plaque, protected against adverse effects.

2.12 Statistical analysis

Statistical analysis was performed using Origin Pro software. All data has been tested for normal distribution. For non-normally distributed data, we used the Mann-Whitney rank-sum test to compare between two groups. Statistical differences between more than two groups (normally distributed) were analyzed by one-way ANOVA, followed by Tukey post hoc test. Significance was determined at $*p \leq 0.05$; $**p \leq 0.01$; $***p \leq 0.001$.

3 Results

3.1 Effect of the NO-cGMP-cGKI axis on growth of VSMCs in culture

The NO-cGMP-cGKI axis in VSMCs has been intensively investigated over the last decades [11, 77-82]. However, it is still under debate whether this signaling pathway promotes or inhibits the growth of VSMCs. As already described in the introduction, there are several reasons for the seemingly contradicting results **(see chapter 1.5.1)**. In the last decade, the Feil laboratory has demonstrated that the growth-promoting effect of cGMP is cGKI-dependent [79, 101]. Most of the previous studies used conventional endpoint assays (WST, MTS) to characterize the cGMP-modulated growth behavior of VSMCs. One of the aims of the present work was to analyze dynamic effects of cGMP on different growth stages, especially on the initial adhesion phase. For this purpose, we used a device called xCELLigence, which allowed us to follow the growth of VSMCs in real-time and, thereby, analyze the impact of the cGMP signaling pathway at different stages.

3.1.1 Analysis of cGMP-promoted VSMC growth by endpoint assays

In previous studies, we demonstrated a growth-promoting effect of the membrane-permeable cGMP analogue 8-Br-cGMP (1 mM) in primary VSMCs [79, 101]. By comparing cGKI-expressing and cGKI-deficient VSMCs, we could also prove that this effect was mediated via cGKI [79, 101]. Furthermore, we could show that low (0.5 µM) concentrations of the NO-donor diethylenetriamine NONOate (DETA-NO) enhanced proliferation via a cGKI-dependent pathway, whereas high DETA-NO concentrations (100 µM) strongly reduced the growth of VSMCs, independent of cGKI [79]. This cGKI-independent anti-proliferative NO effect was also observed by other groups [80, 100]. Knowing the concentration-dependent effects of NO, we decided to determine which concentrations of 8-Br-cGMP and DETA-NO are suitable for further growth experiments. Therefore, primary VSMCs from wildtype mice were seeded into 96-well plates in the presence of increasing concentrations of 8-Br-cGMP and DETA-NO, and 72 hours later a conventional WST endpoint growth assay was performed **(Figure 18)**.
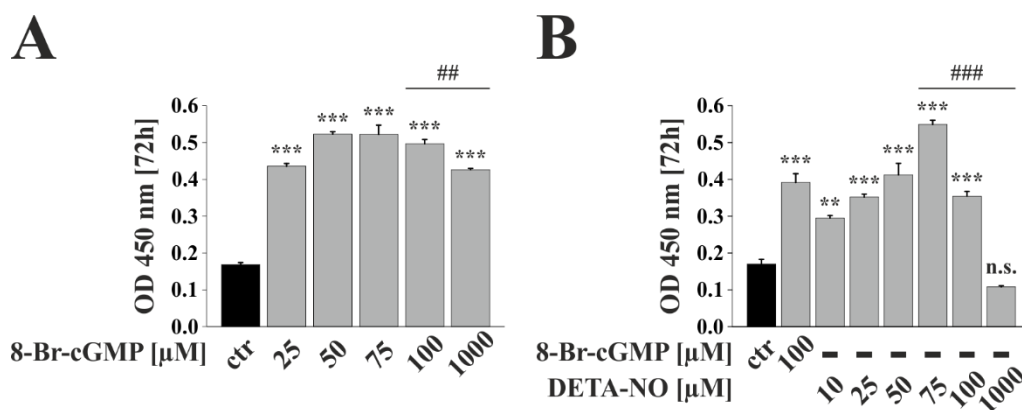
Figure 18. cGMP stimulation via 8-Br-cGMP and DETA-NO modulates growth of primary VSMCs

Primary VSMCs were seeded into a 96-well plate and grown in the absence (ctr) or presence of various concentrations of 8-Br-cGMP (25-1000 µM) or DETA-NO (10-1000 µM). The WST assay was used to determine VSMC growth 72 hours after seeding (OD 450 nm). **(A)** 8-Br-cGMP-induced growth (n= 4 wells per condition). **(B)** DETA-NO-induced growth. 100 µM 8-Br-cGMP was used as positive control (n= 4 wells per condition). All data are shown as mean ± SEM. * Asterisks indicate statistical significance vs. control condition (ctr); *$p \leq 0.05$; **$p \leq 0.01$; ***$p \leq 0.001$. # Hashes indicate statistical significance between the highlighted conditions; # $p \leq 0.05$; ## $p \leq 0.01$; ### $p \leq 0.001$.

Compared to unstimulated VSMCs (ctr), addition of 8-Br-cGMP clearly promoted the growth of our primary VSMCs (**Figure 18 A**). As expected from a previous study [79], DETA-NO showed a concentration-dependent biphasic effect. Low DETA-NO concentrations (10-100 µM) enhanced VSMC growth, whereas higher DETA-NO concentrations (100 µM, 1000 µM) appeared to mitigate the growth-promoting effect of lower concentrations (**Figure 18 B**).

Taken together, 8-Br-cGMP clearly promoted the growth of primary VSMCs, and DETA-NO showed dose-depend opposing effects. Low DETA-NO concentrations stimulated VSMC growth, while higher concentrations resulted, compared to lower concentrations, in growth reduction. Based on these data, for further experiments 100 µM 8-Br-cGMP and 75 µM DETA-NO were used to stimulate VSMC growth, and 1000 µM DETA-NO was used to induce potentially cGMP-independent effects.

3.1.2 Real-time measurement of NO-cGMP-modulated VSMC growth

To investigate the cGMP-mediated growth responses in more detail, we used a device called xCELLigence (**see chapter 2.5**). In comparison to conventional endpoint assays, the xCELLigence device allows to follow cell growth in real time and, therefore, to analyze different stages of the growth process within the same cell population and experiment.

To validate the functionality of the xCELLigence technology for cell growth monitoring, we tested if the results were comparable to the conventional growth assay (**Figure 19**). Both assays were performed in parallel with the same cell population. Primary VSMCs

from wildtype mice were grown in the absence (ctr) or presence of 8-Br-cGMP (100 µM) or DETA-NO (75 µM for growth promotion; 1000 µM for growth inhibition, see also **3.1.1**). Cells were seeded into a 96-well plate and analyzed after 72 hours using the WST assay, or they were seeded into an xCELLigence plate and their growth was monitored continuously by real-time impedance measurement.
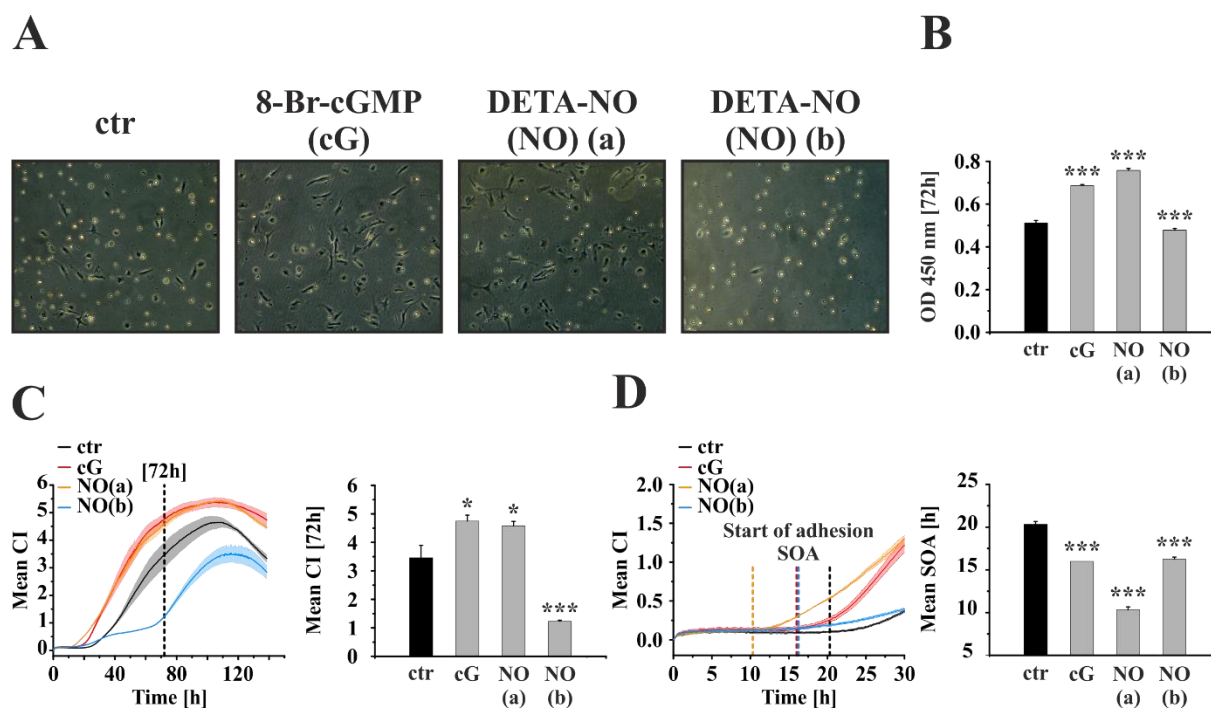
Figure 19. Impedance-based real-time measurements (xCELLigence) are suitable for growth behavior analysis of VSMCs

Primary VSMCs were grown in the absence (ctr) or presence of 8-Br-cGMP (100 µM; cG) or DETA-NO (75 µM (a) or 1000 µM (b); NO) and growth behavior was analyzed. **(A)** Representative photos of VSMCs 72 hours after seeding. **(B)** WST-1 growth assay 72 hours after seeding (OD 450 nm) (n= 4 wells per condition). One representative measurement of three biological replicates is shown. **(C)** Impedance-based (xCELLigence) real-time measurement of VSMC growth behavior (left) (n= 4 wells per condition). The vertical dashed line (black) highlights the mean cell index (CI) after 72 hours, which is also depicted as a separate bar graph (right). **(D)** Impedance-based (xCELLigence) real-time measurement of VSMCs during the early growth phase (left). Dashed lines are color-coded (ctr = black; cG = red; NO (a) = orange; NO (b) = blue) and highlight the time point at which the cells started to attach to the surface and to grow, designated "start of adhesion" (SOA); (n= 4 wells per condition). The SOA was defined as the time point at which the slope of the CI within one hour was greater than 0.0001. The mean SOA for every condition is depicted as a separate bar graph (right). One representative measurement of three biological replicates is shown. All data are represented as mean ± SEM. * Asterisks indicate statistical significance vs. control condition (ctr); $*p \leq 0.05$; $**p \leq 0.01$; $***p \leq 0.001$.

72 hours after the cells had been seeded, the growth of VSMC culture was also evaluated by light microscopy **(Figure 19 A)**. As shown by microscopic observation, 8-Br-cGMP (100 µM) and 75 µM DETA-NO enhanced the growth of elongated VSMCs. In contrast, 1000 µM DETA-NO inhibited cell growth and ≈90% of VSMCs still had a rounded morphology typical for VSMCs directly after isolation **(Figure 19 A)**. As in the previous experiment **(Figure 18)**,

the conventional WST assay showed that 8-Br-cGMP (100 µM) or 75 µM DETA-NO stimulated VSMC growth, whereas 1000 µM DETA-NO reduced growth **(Figure 19 B)**.

In contrast to the WST assay, the xCELLigence measurement allowed us to follow the whole growth process, from adhesion to putative cell death, in real-time **(Figure 19 C and D)**. From these data, it seems that depending on the experimental conditions (± NO/cGMP stimulation) VSMCs started to attach and grow approx. 10-20 hours after seeding and reaching maximum confluency at approx. 100 hours **(Figure 19 C, left)**. From this time onwards the growth curves dropped, most likely as a result of increased cell death.

For better comparability with the WST assay, the mean cell index (CI) after 72 hours was determined to describe the effect of cGMP on VSMC growth behavior **(Figure 19 C, right)**. In both assays, stimulation with 8-Br-cGMP (100 µM) and the low concentration of DETA-NO (75 µM) enhanced growth, while the high concentration of DETA-NO (1000 µM) had a growth-inhibiting effect. The inhibiting effect was much stronger in the xCELLigence assay compared to the WST assay **(Figure 19 B vs. C, right)**.

As already mentioned, depending on the condition (± NO/cGMP) the cells started to attach and grow at different time points after plating. To characterize the time when VSMCs started to grow, we determined the "start of adhesion" (SOA), which we defined as the time at which the slope of the CI within one hour was greater than 0.0001 (CI/h). The SOAs are indicated by dashed lines in the growth curves **(Figure 19 D, left)** (color matches the corresponding condition) and the respective values are given in a bar graph **(Figure 19 D, right)**. As compared to control conditions, addition of 100 µM 8-Br-cGMP, 75 µM DETA-NO as well as 1000 µM DETA-NO significantly reduced the SOA (ctr at ≈ 20 hours; 100 µM 8-Br-cGMP at ≈ 16 hours; 75 µM DETA-NO at ≈ 10 hours; 1000 µM DETA-NO at ≈ 16 hours) **(Figure 19 D, right)**. Interestingly, the high DETA-NO concentration (1000 µM) had opposing effects on VSMC growth. Similar to 8-Br-cGMP and the low concentration of DETA-NO (75 µM) it promoted cell adhesion and start of growth (SOA ≈ 16 hours) **(Figure 19 D),** but in contrast to 8-Br-cGMP and the low DETA-NO concentration, it clearly reduced VSMC growth after 72 hours **(Figure 19 C)**. The biphasic growth effect of 1000 µM DETA-NO is nicely documented **(Figure 19 C)** (blue growth curve).

Taken together, the results from the WST and xCELLigence assay showed comparable results 72 hours after seeding. In addition, the xCELLigence measurements showed that stimulation of the NO/cGMP signaling pathway led to earlier cell attachment and growth. Furthermore, it was also possible to demonstrate that the growth-inhibiting effect of a high DETA-NO concentration (1000 µM) observed at 72 h after plating is not caused by inhibition

of the initial growth phase, but rather depends on adverse effects on later growth stages, presumably via cGMP-independent actions of NO.

3.1.3 NO-induced growth promotion is mediated through activation of NO-GC

To clarify whether the promotion of VSMC growth by low concentrations of NO is indeed mediated by cGMP, we investigated the effects of NO in VSMCs isolated from NO-GCβ1 knockout mice. The knockout VSMCs and respective NO-GC β1 expressing wildtype cells (isolated from litter-matched wildtype mice) were seeded into xCELLigence plates and their growth was compared in the absence (ctr) or presence of DETA-NO (75 µM) or 8-Br-cGMP (100 µM) (**Figure 20**).
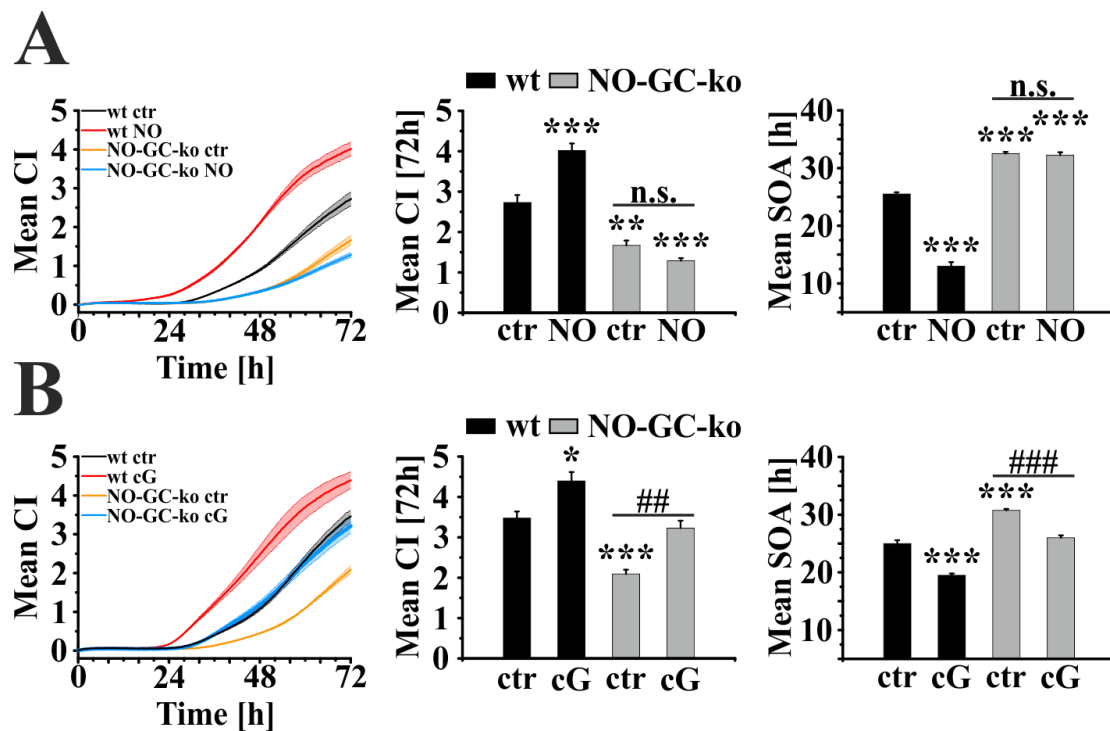
Figure 20. The NO-induced growth stimulation is mediated via activation of NO-GC

Primary VSMCs isolated from NO-GC β1 knockout mice (NO-GC-ko, L1/L1) and their respective wildtype (wt) controls were seeded in the absence (ctr) or presence of DETA-NO (75 µM; NO) or 8-Br-cGMP (100 µM; cG). Impedance-based (xCELLigence) real-time measurement was used to investigate the growth behavior (A-B; left panel = xCELLigence growth curve; middle panel = mean cell index (CI) after 72 hours; right panel = mean start of adhesion (SOA)). (**A**) Growth behavior of wildtype or NO-GC β1 knockout VSMCs in the absence (ctr) or presence of DETA-NO (75 µM; NO) (n= 4 wells per condition). (**B**) Growth behavior of wildtype or NO-GC β1 knockout VSMCs in the absence (ctr) or presence of 8-Br-cGMP (100 µM; cG) (n= 4 wells per condition). All data are represented as mean ± SEM. * Asterisks indicate statistical significance vs. control condition (wt ctr); *$p \leq 0.05$; **$p \leq 0.01$; ***$p \leq 0.001$. # Hashes indicate statistical significance between the conditions indicated by a horizontal line; # $p \leq 0.05$; ## $p \leq 0.01$; ### $p \leq 0.001$; n.s. = not significant. NO-GC β1 knockout mice were kindly provided by Prof. Andreas Friebe.

Interestingly, NO-GC β1-deficient VSMCs showed already in the unstimulated control condition (ctr) an impaired growth behavior as compared to the wildtype cells **(Figure 20)**. Knockout cells had a postponed SOA ($\approx$ 30 hours) compared to the wildtype cells ($\approx$ 25 hours) and the mean CI 72 hours after seeding was significantly reduced. Compared to the respective control (ctr) condition, DETA-NO (75 µM) clearly stimulated the growth of wildtype cells, reflected by an earlier SOA and an increased mean CI after 72 hours, while the same concentration of DETA-NO was ineffective in NO-GC β1 knockout cells **(Figure 20 A)**. As expected, stimulation by 8-Br-cGMP (100 µM) had a growth-promoting effect in both wildtype and NO-GC-deficient VSMCs **(Figure 20 B)**.

Taken together, this experiment demonstrated that NO-GC might be already active under basal conditions and that the NO-induced growth stimulation is mediated through the activation of NO-GC. The finding that 8-Br-cGMP had a normal growth-promoting effect in NO-GC-deficient VSMCs is in line with the notion that cGMP acts downstream of NO-GC and, in addition, indicates that the growth-promoting pathway downstream of cGMP is not altered in the absence of NO-GC.

3.1.4 cGMP-induced growth promotion is mediated through activation of cGKI

To investigate the growth-promoting pathway downstream of NO-GC and cGMP, we assessed the growth behavior of VSMCs from cGKI-deficient mice. Wildtype and cGKI knockout (L1/L1) VSMCs were isolated, seeded into a xCELLigence plate and grown for several days in the absence (ctr) or presence of DETA-NO (75 µM) or 8-Br-cGMP (100 µM) **(Figure 21)**. Similar to the NO-GC knockout VSMCs **(see chapter 3.1.3)**, the cGKI-deficient VSMCs showed an impaired growth behavior under basal conditions (ctr) in comparison to the wildtype cells **(Figure 21)**. Both drugs, 8-Br-cGMP and DETA-NO, clearly promoted the growth of wildtype VSMCs, as shown by the increased mean CI after 72 hours and the earlier SOA as compared to control conditions **(Figure 21 A and B)**. In contrast to the wildtype cells, the growth-promoting effects of both NO and cGMP were absent in the cGKI knockout cells **(Figure 21 A and B)**. Interestingly, in all experiments **(see chapters 3.1.2-4)** wildtype VSMCs stimulated by DETA-NO started to adhere/grow at an earlier time point than the cells treated with 8-Br-cGMP, while the mean CI at 72 hours was comparable between both conditions.

Taken together, the NO-induced growth-promoting effect was clearly mediated through the activation of NO-GC and cGKI. Furthermore, with the xCELLigence device it was possible

to show that the NO-cGMP-cGKI signaling pathway enhances already the initial stage of VSMC growth as visualized by the altered SOA in the respective experiments.
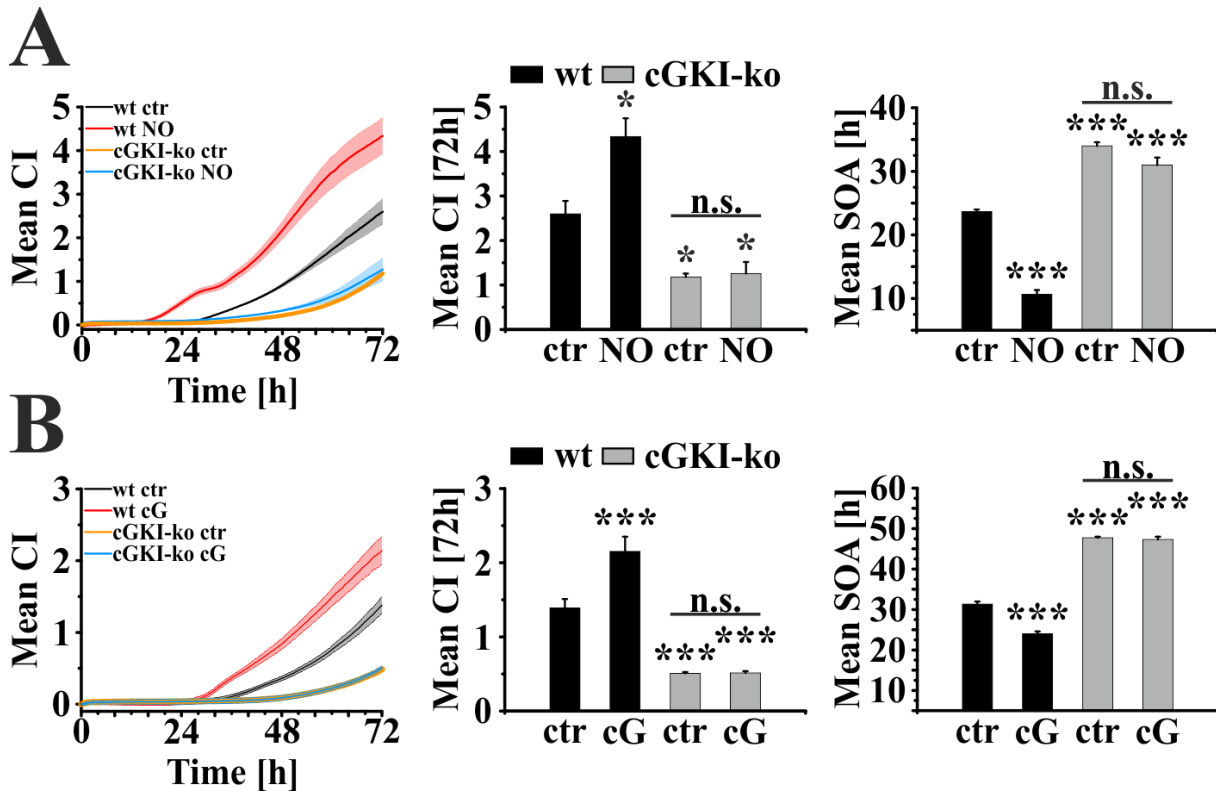
Figure 21. NO/cGMP-induced growth promotion is mediated via activation of cGKI

Primary VSMCs isolated from cGKI knockout mice (cGKI-ko, L1/L1) and their respective wildtype (wt) controls were seeded in the absence (ctr) or presence of DETA-NO (75 µM; NO) or 8-Br-cGMP (100 µM; cG). Impedance-based (xCELLigence) real-time measurement was used to investigate the growth behavior (A-B; left panel = xCELLigence growth curve; middle panel = mean cell index (CI) after 72 hours; right panel = mean start of adhesion (SOA)). **(A)** Growth behavior of wildtype or cGKI knockout VSMCs in the absence (ctr) or presence of DETA-NO (75 µM; NO) (n= 4 wells per condition). **(B)** Growth behavior of wildtype or cGKI knockout VSMCs in the absence (ctr) or presence of 8-Br-cGMP (100 µM; cG) (n= 4 wells per condition). All data are represented as mean ± SEM. * Asterisks indicate statistical significance vs. control condition (wt ctr); *$p \leq 0.05$; **$p \leq 0.01$; ***$p \leq 0.001$; n.s. = not significant.

3.1.5 Influence of natriuretic peptides on VSMC growth

As shown in the previous experiments, NO-GC stimulation through NO-releasing drugs or direct activation of cGKI via the cGMP analogue 8-Br-cGMP clearly enhanced the growth of primary VSMCs. These stimuli might increase cGMP in a spatiotemporal profile that differs from cGMP signals induced by NPs like ANP and CNP. To test whether the NP-stimulated cGMP has different growth effects compared to DETA-NO or 8-Br-cGMP, primary VSMCs were grown in the presence of ANP (0.5 µM) or CNP (0.5 µM). As positive control for cGMP-promoted growth, 8-Br-cGMP (100 µM) was applied **(Figure 22)**.

In comparison to 8-Br-cGMP, treatment of VSMCs with ANP only resulted in a moderate growth promotion. Stimulation with CNP showed a tendency towards stronger growth that was, however, not significant compared to the unstimulated control (ctr) **(Figure 22)**. None of the NPs induced an earlier SOA.

In conclusion, stimulation of the transmembrane guanylyl cyclase GC-A (ANP receptor) but not GC-B (CNP receptor) promoted the growth of primary VSMCs. The extent as well as the growth phase influenced by ANP appeared to differ from NO-induced growth stimulation.
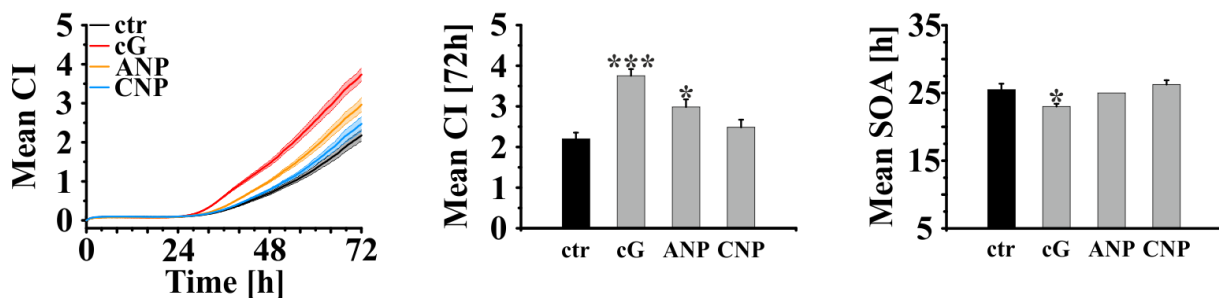
Figure 22. Effect of ANP and CNP on the growth behavior of VSMCs

Primary VSMCs were seeded in the absence (ctr) or presence of 8-Br-cGMP (100 µM; cG), ANP (0.5 µM), or CNP (0.5 µM). Impedance-based (xCELLigence) real-time measurement was used to investigate the growth behavior .Left panel = xCELLigence growth curve; middle panel = mean cell index (CI) after 72 hours; right panel = mean start of adhesion (SOA) (n= 4 wells per condition). All data are presented as mean ± SEM. * Asterisks indicate statistical significance vs. control condition (ctr); *$p \leq 0.05$; **$p \leq 0.01$; ***$p \leq 0.001$.

3.1.6 Impact of the cGMP signaling pathway on VSMC viability

As shown by the xCELLigence measurements, activation of the cGMP signaling cascade promotes VSMC cell growth. To further dissect this process, we analyzed the impact of the signaling cascade on the viability of VSMCs. For this purpose, primary VSMCs were grown for 72 hours in the absence (ctr) or presence of various cGMP-elevating agents. Subsequently, cell viability was assessed by a live and dead staining method **(Figure 23)**. This staining works through detection of intracellular esterase activity **(see chapter 2.6)**. The esterase substrate calcein-AM stains living (viable) cells green (fluorescence), while the membrane-impermeable dye Ethidium homodimer III (EthD-III) interacts with the DNA of dead cells and stains them red (fluorescence) **(Figure 23 A)**.

The impact on cell viability differed strongly between the cGMP-elevating compounds tested **(Figure 23 B)**. In line with the xCELLigence measurements, treatment with 8-Br-cGMP (100 µM; cG) clearly enhanced the amount of viable cells as compared to the control condition (ctr) **(Figure 23 B and C)**. Interestingly, DETA-NO (75 µM; NO) or ANP (0.5 µM) had unexpected effects on viability. In the xCELLigence growth monitoring experiments,

DETA-NO strongly enhanced VSMC growth comparable to 8-Br-cGMP **(Figure 19)**, and the pro-growth effect of ANP was relatively moderate **(Figure 22)**. In the cell viability experiment, however, DETA-NO had no significant effect, and ANP strongly enhanced VSMCs viability similar to 8-Br-cGMP **(Figure 23 B)**. Similar to the xCELLigence growth data **(Figure 22)**, CNP did also not affect cell viability **(Figure 23 B)**.

It is well known that NO also exerts effects independent of the cGMP signaling cascade, which could oppose and, thus, mask potential pro-survival effects on NO-induced cGMP. To test this possibility, we sought to shift the NO-induced effect into a more cGMP-dependent direction via enhancement of the NO-induced cGMP level by addition of the PDE 5 inhibitor sildenafil **(Figure 23 C)**. As expected, application of sildenafil (30 µM; Sil) or DETA-NO (75 µM; NO) alone did not influence the fraction of viable cells. However, the combination of both drugs strongly promoted cell viability **(Figure 23 C)**.
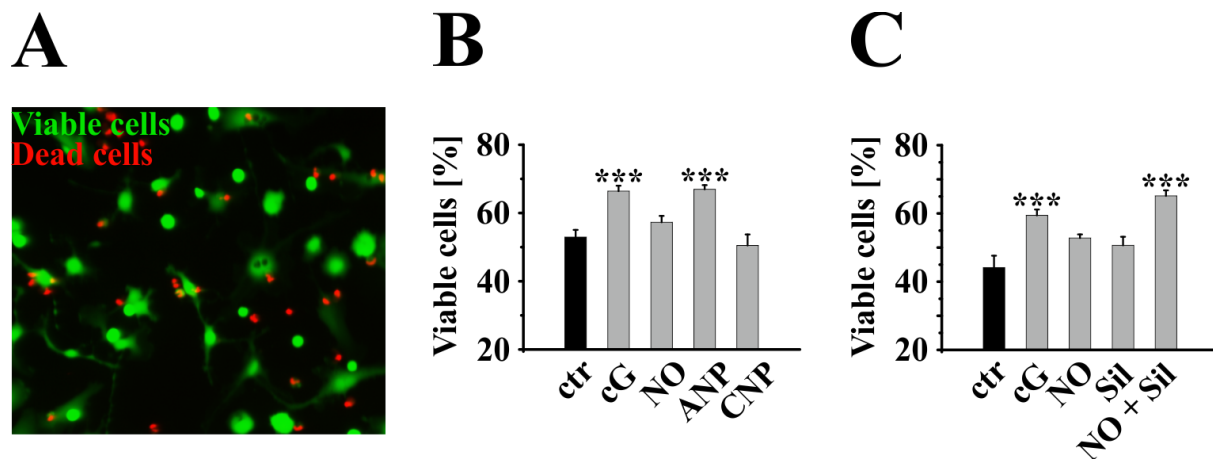
Figure 23. Activation of the cGMP signaling cascade enhances the viability of VSMCs

Primary VSMCs were seeded into an Ibidi µ-slide and grown for three days in the absence (ctr) or presence of various cGMP- modulating drugs. Cell viability was assessed via live and dead staining. **(A)** Fluorescent images of VSMCs stained for viable (green) and dead (red) cells. **(B)** Fraction of viable VSMCs three days after treatment with 8-Br-cGMP (100 µM; cG), DETA-NO (75 µM; NO), ANP (0.5 µM), or CNP (0.5 µM). **(C)** Fraction of viable VSMCs three days after treatment with 8-Br-cGMP (100 µM; cG), DETA-NO (75 µM; NO), sildenafil (30 µM; Sil), or DETA-NO (75 µM) and sildefanil (30 µM) (NO + Sil). All data are represented as mean ± SEM. * Asterisks indicate statistical significance vs. control condition (ctr); $*p \leq 0.05$; $**p \leq 0.01$; $***p \leq 0.001$.

To test if the pro-survival effect of cGMP was mediated by activation of cGKI, we compared the viability of VSMCs from wildtype and cGKI knockout mice in the absence (ctr) and presence of 8-Br-cGMP (100 µM; cG) **(Figure 24)**. 8-Br-cGMP clearly promoted the viability of wildtype cells, whereas this effect was absent in cGKI-deficient VSMCs **(Figure 24)**. Furthermore, in line with the xCELLigence experiments that indicated an impaired growth behavior of cGKI-deficient cells already under basal conditions (ctr) **(Figure 21)**, cGKI knockout VSMCs showed a decreased viability compared to wildtype cells **(Figure 24)**.

In conclusion, activation of the cGMP-cGKI signaling cascade promotes cell viability. This pro-survival effect likely contributes to the growth-promoting effect of cGMP on VSMCs as measured by xCELLigence technology.
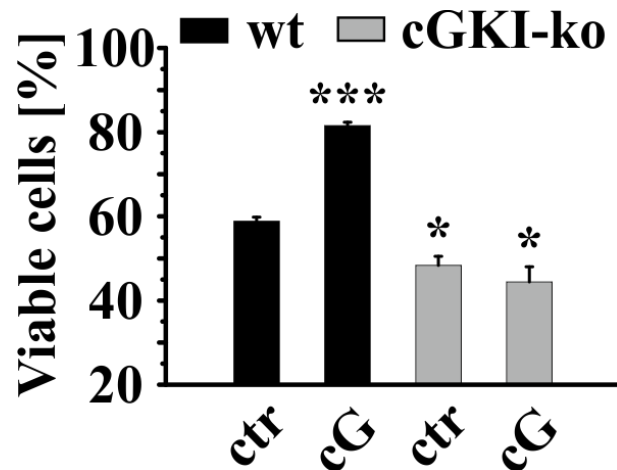
Figure 24. cGMP-promoted cell viability is mediated by cGKI

Primary VSMCs isolated from cGKI knockout mice (cGKI-ko) and their respective wildtype (wt) controls were seeded into an Ibidi µ-slide and grown for three days in the absence (ctr) or presence of 8-Br-cGMP (100 µM; cG). Fraction of viable cells was assessed via live and dead staining. All data are represented as mean ± SEM. * Asterisks indicate statistical significance vs. control condition (ctr); $*p \leq 0.05$; $**p \leq 0.01$; $***p \leq 0.001$.

3.1.7 Modulation of VSMC growth by stimulating the cGMP signaling cascade at different time points during cell isolation and growth

As shown in the previous sections, the growth of VSMCs is clearly stimulated, if 8-Br-cGMP is added during the seeding process and then maintained during cell attachment and growth for three days. Next, we investigated whether the effect of cGMP on VSMC growth, varies depending on the time point at which the signaling axis was stimulated. To this end, we isolated primary VSMCs and added 8-Br-cGMP (100 µM; cG) at different time points and/or for varying durations.

First, we tested whether a short cGMP pulse only during the VSMC isolation process (duration ≈ 1 hour and 12 minutes; [lys] cG) is sufficient to promote VSMC growth **(Figure 25)**. The standard condition (addition of 100 µM 8-Br-cGMP directly during the seeding process; cG) clearly promoted the growth of VSMCs **(Figure 25)**. In contrast, addition of 100 µM 8-Br-cGMP only during the VSMC isolation process ([lys] cG) had no growth-promoting effect **(Figure 25)**.
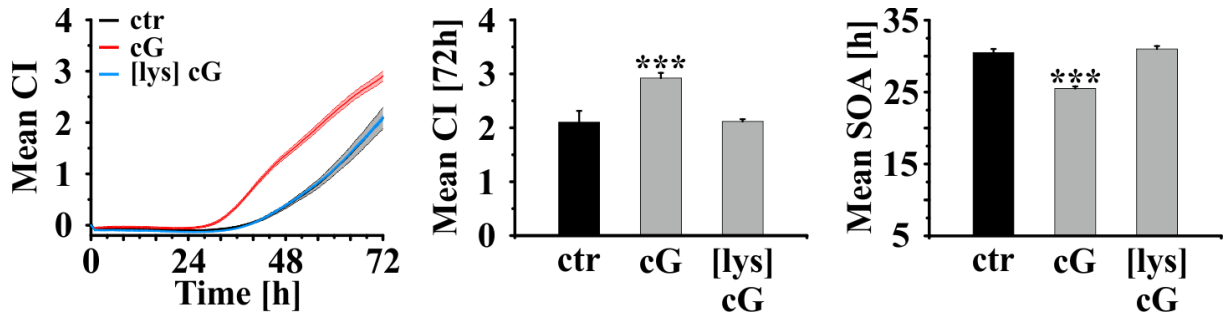
Figure 25. A short cGMP pulse during the VSMC isolation process is not sufficient to promote cell growth

Primary VSMCs were seeded in the absence (ctr) or presence of 8-Br-cGMP (100 µM; cG) or after a short (~ 1 hour and 15 minutes) 8-Br-cGMP pulse during the VSMC isolation process (100 µM; [lys] cG). Impedance-based (xCELLigence) real-time measurement was used to investigate the growth behavior .Left panel = xCELLigence growth curve; middle panel = mean cell index (CI) at 72 hours; right panel = mean start of adhesion (SOA) (n= 4 wells per condition). All data are represented as mean ± SEM. * Asterisks indicate statistical significance vs. control condition (ctr); *$p \leq 0.05$; **$p \leq 0.01$; ***$p \leq 0.001$.

In addition, we analyzed whether 8-Br-cGMP (100 µM; cG) would also promote cell growth when it is added 1-24 hours after the seeding process **(Figure 26)**. The standard condition (8-Br-cGMP directly during seeding; cG) clearly promoted VSMC cell growth and the effect of 8-Br-cGMP was comparable if it was added 1 hour after cell plating. However, growth stimulation did not reach statistical significance if 8-Br-cGMP was added 3 hours after seeding, and it vanished further if 8-Br-cGMP was added 5, 7, 10, or 24 hours after cell plating **(Figure 26)**.
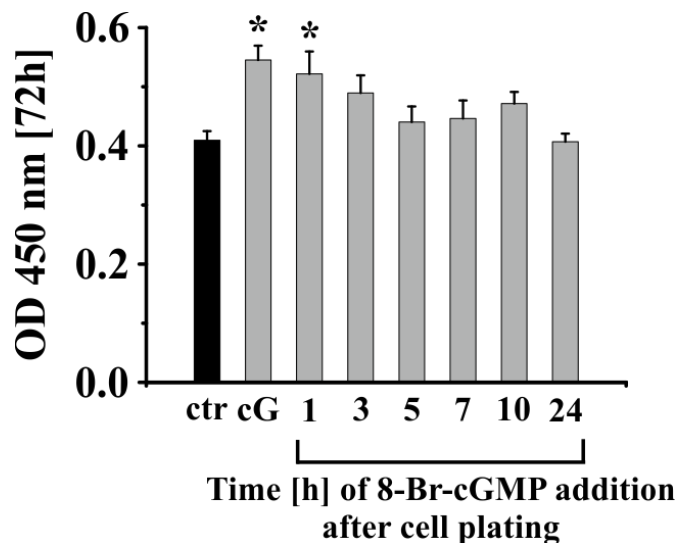
Figure 26. The 8-Br-cGMP-induced growth effect on VSMCs decreases with the time of its addition after cell plating

Primary VSMCs were seeded into a 96-well plate and grown in the absence (ctr) or presence of 8-Br-cGMP (100 µM; cG). Additionally we investigated the temporal influence of 8-Br-cGMP addition (1-24 hours after cell seeding). The WST proliferation assay was used to determine cell growth 72 hours after seeding (OD 450 nm). All data are represented as mean ± SEM. * Asterisks indicate statistical significance vs. control condition (ctr); *$p \leq 0.05$; **$p \leq 0.01$; ***$p \leq 0.001$.

In another experimental setting, we investigated whether pre-incubation of VSMCs with 8-Br-cGMP before plating is sufficient to promote VSMC growth. For this purpose, primary VSMCs were isolated and the cell suspension kept in a falcon tube with serum-containing medium in the absence (ctr) or presence of 8-Br-cGMP (100 µM; cG) with occasional resuspension (1-2x per hour). After 10 or 24 hours of pre-incubation, the medium was exchanged and 8-Br-cGMP was added to some of the cell aliquots as illustrated in **Figure 27**. Then, the cells were seeded and growth behavior was analyzed **(Figure 28)**.

In total, we had one control condition (ctr) where cells had not been stimulated with 8-Br-cGMP at all, and three condtions where cells had been stimulated at distinct time points. In the first condtion, cG (a), VSMCs had been stimulated over the complete experiment. In the second condition, cG (b), VSMCs had only been stimulated during the pre-incubation step (10 or 24 hours). And in the last condition, cG (c), VSMCs had not been stimulated during the pre-incubation period, but 8-Br-cGMP was added directly before seeding, which represents the standard condition **(Figure 27)**.
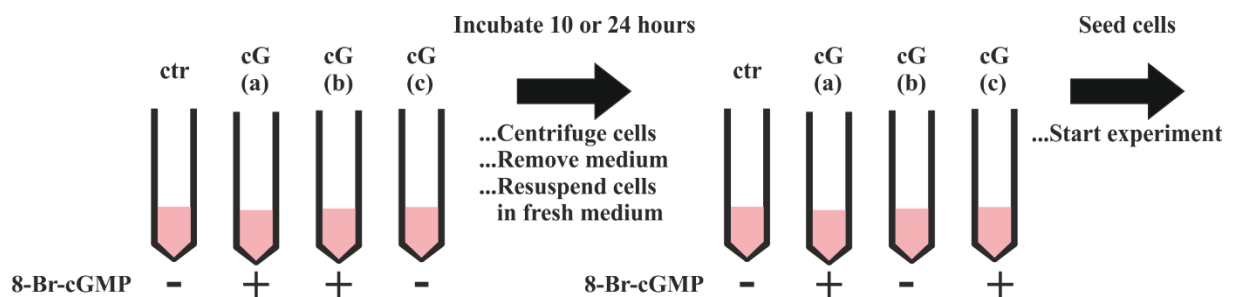
Figure 27. Experimental setup for 8-Br-cGMP pre-incubation experiment shown in Figure. 28

In both pre-incubation experiments **(Figure 28 A and B),** the presence of 8-Br-cGMP during the complete experiment (cG (a)) promoted the growth of VSMCs as compared to the control condition without cGMP (ctr). Interestingly, pre-incubation over 10 hours did not induce a significant growth effect **(Figure 28 A; cG (b))**, whereas there was a clear growth-promoting effect after 24 hours of pre-incubation **(Figure 28 B; cG (b))**. VSMCs that were pre-incubated in the absence of cGMP and then simulated with 8-Br-cGMP during plating and subsequent growth, reached after 72 hours a similar mean CI as cells that were exposed to cGMP for the entire experiment **(Figure 28 B, cG (c) vs. cG (a))**. It was noted, however, that cells under condition cG (c) had a decelerated growth behavior compared to the cG (a) condition **(Figure 28 B, left panel)**. This finding might be due to a weakened cell viability under cG (c) conditions arising from the absence of cGMP during the pre-incubation phase. Overall, it appeared that the growth behavior of primary VSMCs was very similar if 8-Br-cGMP was

present already during 10 or 24 hours pre-incubation or if it was added later during plating **(Figure 28 A and B)**.
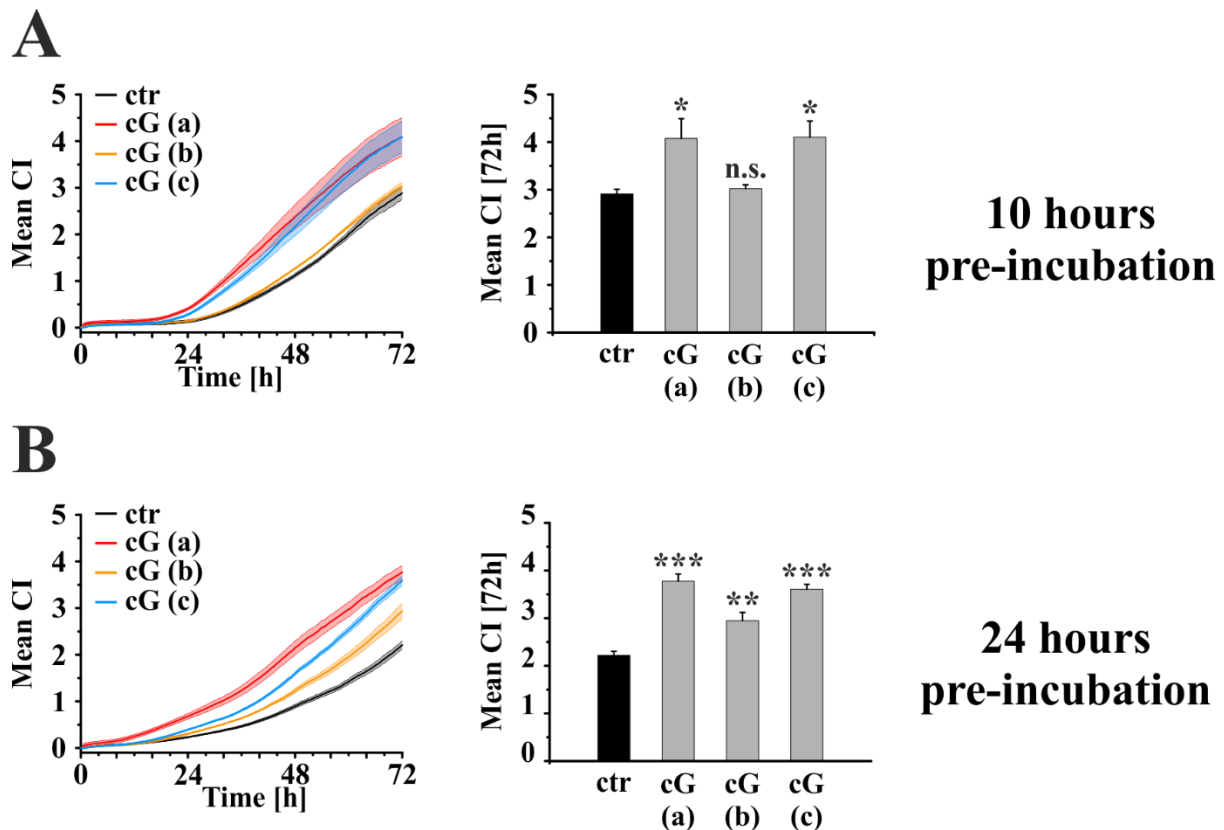
Figure 28. Pre-incubation with 8-Br-cGMP before cell plating has only a weak effect on VSMC growth

Primary VSMCs were isolated and pre-incubated in a falcon tube ± 8-Br-cGMP (100 µM; cG) for 10 or 24 hours (cells had been mixed by inverting the falcon tube occasionally, ≈ 1-2x per hour). After the pre-incubation time, medium was exchanged and 8-Br-cGMP was added depending on the condition (for experimental design, see **Figure 27**). This experiment was performed to obtain a detailed view on the time-dependent impact of cGMP simulation on VSMC growth. cG (a)= cGMP stimulation during pre-incubation and seeding. cG (b)= cGMP stimulation only during pre-incubation. cG (c)= cGMP stimulation only after pre-incubation (standard stimulation). Impedance-based (xCELLigence) real-time measurement was used to investigate the growth behavior .Left panel = xCELLigence growth curve; middle panel = mean cell index (CI) at 72 hours.. All data are represented as mean ± SEM. * Asterisks indicate statistical significance vs. control condition (ctr); *$p \le 0.05$; **$p \le 0.01$; ***$p \le 0.001$.

In conclusion, the cGMP-mediated growth effect appeared to be strongest when the VSMCs were stimulated directly during the seeding process. A short cGMP pulse (≈ 1 hour) only during the VSMC isolation process is not sufficient to stimulate their growth **(Figure 25)**, and the growth-promoting effect is decreasing with the time that passes between cell plating and addition of 8-Br-cGMP **(Figure 26)**. Moreover, cGMP pre-incubation of VSMCs in suspension for 10 hours (without further cGMP stimulation during plating and adherent cell growth) does not promote cell growth **(Figure 28 A)**. Longer cGMP pre-incubation for 24 hours slightly promoted subsequent adherent VSMC growth **(Figure 28 B)**, likely due to an impact on the viability of the cells in suspension. The combined results of these experiments

support the notion that the major mechanism behind the cGMP-promoted growth of primary VSMCs is increased adhesion and survival of cells during the seeding period.

3.2 Phenotypic plasticity of VSMCs

It is already well described that contractile VSMCs in healthy blood vessels are responsible for the regulation of blood flow and that activation of the NO-cGMP-cGKI axis leads to vasodilation [11]. However, VSMCs are also involved in vascular remodeling during diseases such as atherosclerosis and restenosis [17]. Under pathological conditions, contractile VSMCs undergo phenotypic modulation into synthetic smooth muscle cells **(see chapters 1.5.1-3)**. In contrast to contractile VSMCs, which are characterized by their low proliferation rate and abundant expression of contractile proteins, synthetic VSMCs are highly proliferative, have low contractility and produce large amounts of ECM [76]. Especially Fn, a component of the ECM, is generated under pathological conditions [136]. Moreover, it has been shown that (coating of cell culture wells with) Fn induces the switch from a contractile into a synthetic VSMC [145]. Although phenotypic plasticity of VSMCs has been under investigation for many years, a potential interaction of Fn with the cGMP signaling axis and its impact on VSMC phenotype has not been studied to date.

3.2.1 Impact of fibronectin on the cGMP signaling axis in VSMCs

The experiments described in this section are based on previous work done in our laboratory with primary VSMCs expressing the FRET-based cGMP biosensor cGi500 [167]. These data demonstrated that individual cells of a given VSMC population show heterogeneous cGMP responses upon stimulation with ANP, CNP or DEA-NO.

Interestingly, the different cGMP response patterns were associated with different VSMC phenotypes. Contractile VSMCs (identified by strong expression of smooth muscle α-actin (SMαA) and transgelin (SM22α)) responded stronger to ANP than to CNP (ANP preference), while synthetic VSMCs (identified by weak expression of SMαA and SM22α) responded stronger to CNP than to ANP (CNP preference). As already mentioned, Fn induces the phenotypic modulation from contractile to synthetic cells. Our aim was to investigate how this ECM component impacts the cGMP signaling axis in VSMCs.

First, we investigated the growth behavior of primary VSMCs seeded on Fn coated wells (Fn, 50 µg/mL overnight at RT) compared to cells grown on uncoated wells (uc). In addition, cells were stimulated ± 8-Br-cGMP (100 µM) to analyze if Fn can potentiate the cGMP-induced growth effect **(Figure 29 A)**. As compared to growth on uncoated wells (uc), Fn coating did

not induce a significantly different mean CI after 72 hours in the absence (ctr Fn) or presence of 8-Br-cGMP (cG Fn) **(Figure 29 A)**. However, cells growing on Fn showed a significantly earlier SOA as compared to cells grown on uncoated wells (ctr Fn = 27 hours vs. ctr uc = 32 hours) **(Figure 29 A)**.

Next, we analyzed whether Fn influences the ANP/CNP preference of VSMCs. We isolated VSMCs from transgenic mice expressing the cGi500 biosensor ubiquitously and let the cells grow on uncoated or Fn-coated wells. After four days, the medium was exchanged and cells were serum-starved overnight before FRET/cGMP measurements **(Figure 29 B)**. VSMCs were stimulated by alternating concentrations of ANP or CNP (50 and 250 nM). At the end of each measurement, DEA-NO (500 nM) stimulation was used as a positive control. Based on the response of every individual cell, VSMCs were classified as ANP-preferring (ANP > CNP, orange), CNP-preferring (CNP > ANP, blue) or as cells with no clear preference (ANP ~ CNP, green) **(Figure 29 B upper left; see chapter 2.10.3 for detailed explanation)**. Compared to the control condition (uncoated), Fn coating clearly promoted the phenotypic modulation into CNP-preferring cells **(Figure 29 B upper right)**. In the uncoated condition, the ratio of ANP-preferring over CNP-preferring cells was ≈3 (64 % vs. 21%), whereas for the Fn condition the ratio ANP/CNP-preferring cells was only ≈0.6 (33% vs. 60%) **(Figure 29 B lower left)**.

Finally, we verified whether the ANP-preferring VSMCs had indeed a contractile phenotype and, therefore, expressed higher amounts of SMαA. For this purpose, the VSMCs used for cGMP measurements had been grown on gridded coverslips, which allowed us to map, overlay and correlate the cGMP response with marker expression in every individual cell **(Figure 29 C, left)**. Thereby, we confirmed that ANP- and CNP-preferring cells indeed express high and low amounts of contractile marker protein, respectively. Looking at the intensity (SMαA expression) of every individual cell **(Figure 29 C, right)**, once again the impact of Fn on promoting the CNP-preferring phenotype is convincingly shown.

Taken together, Fn coating had no effect on overall growth of primary VSMCs after 72 hours, but induced a significantly earlier SOA in the absence and presence of 8-Br-cGMP **(Figure 29 A, right)**. Interestingly, as shown by correlative analysis of cGMP responses and marker expression in individual cells, Fn coating clearly shifted VSMCs towards a CNP-preferring "synthetic" phenotype with weaker expression of the contractile marker protein SMαA **(Figure 29 B and C)**.
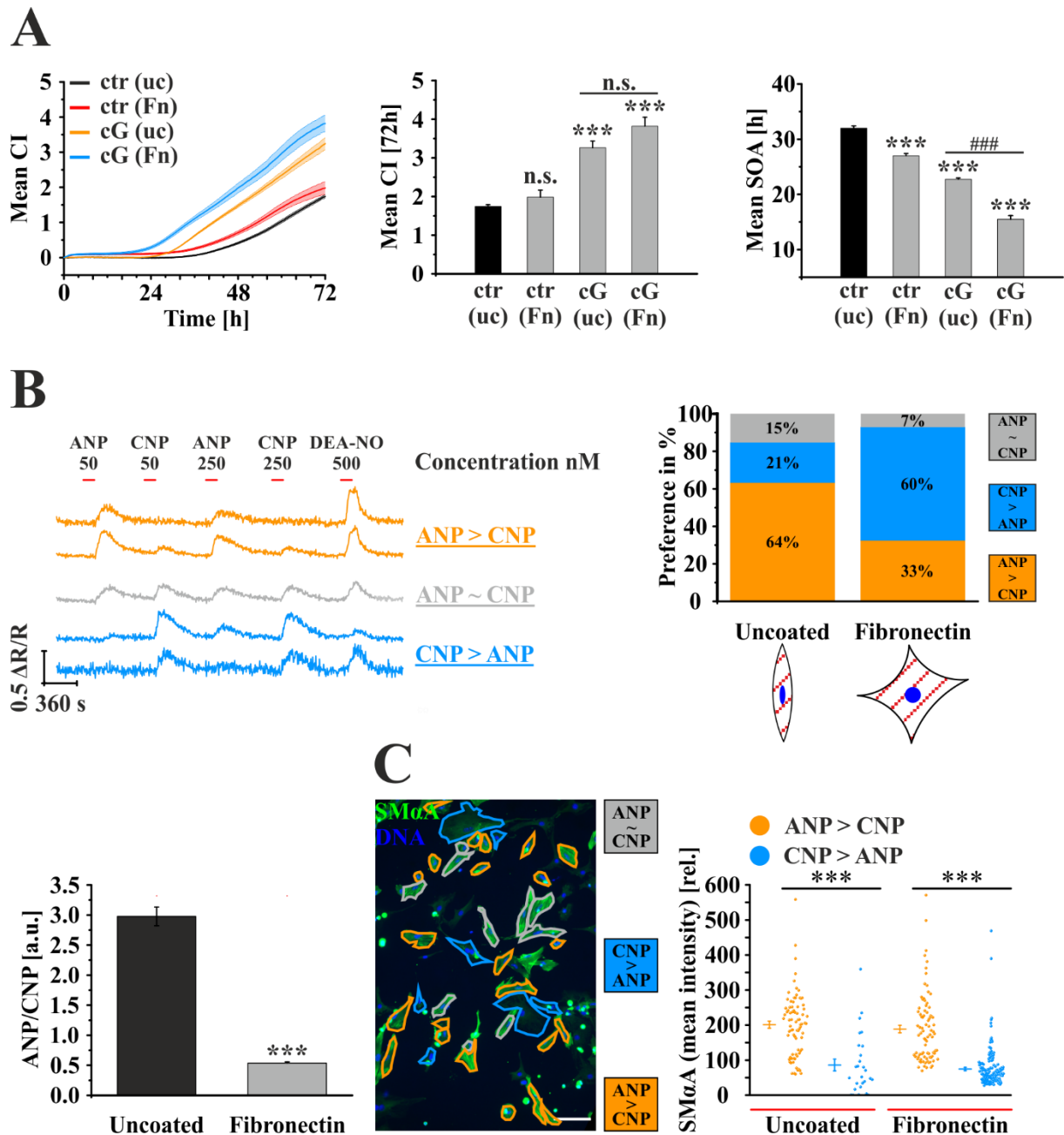
Figure 29. Fibronectin stimulates the early adhesion phase of primary VSMCs and promotes the synthetic phenotype

Primary VSMCs were either isolated from wildtype mice (A) or transgenic mice expressing the FRET-based cGMP biosensor cGi500 ubiquitously (B and C) and then seeded into uncoated or Fn-coated wells to analyze the impact of Fn coating on growth behavior and the cGMP signaling cascade. **(A)** Impedance-based (xCELLigence) real-time measurement was used to investigate the growth behavior of wildtype VSMCs seeded on uncoated (uc) or Fn-coated wells ± 8-Br-cGMP (100 µM; cG). Left panel = xCELLigence growth curve; middle panel = mean cell index (CI) at 72 hours; right panel = mean start of adhesion (SOA) (n= 4 wells per condition). **(B)** FRET measurements (ΔR/R) of cGi500-expressing VSMCs seeded on ± Fn-coated gridded coverslips. Left panel depicts the classification scheme of VSMCs depending on the NP-preference. Right panel shows the percentage of VSMCs with a certain NP-preference. Lower left panel highlights the ratio of ANP-and CNP-preferring cells (uncoated n = 178 cells from three individual coverslips; Fibronectin n = 357 cells from three individual coverslips). **(C)** Immunofluorescence analysis of SMαA expression in ANP-and CNP-preferring cells. Left panel = Representative immunofluorescence picture of cGi500 expressing VSMCs after FRET-based NP classification, stained for SMαA (green) and DNA (blue). Right panel = Evaluation of SMαA expression from ANP-and CNP-preferring cells (uncoated n = 109 cells from three individual coverslips; Fibronectin n = 231 cells from three individual coverslips). All data are represented as mean ± SEM. * Asterisks indicate statistical significance vs. control condition (ctr); *$p \leq 0.05$; **$p \leq 0.01$; ***$p \leq 0.001$. # Hashes indicate statistical significance between the conditions indicated by horizontal lines; # $p \leq 0.05$; ## $p \leq 0.01$; ### $p \leq 0.001$; n.s. = not significant. Experiments were performed in collaboration with Moritz Lehners.

3.3 Impact of smooth muscle-derived fibronectin on atherosclerosis

The secretion of high amounts of ECM is one characteristic of synthetic VSMCs. The group of Reinhard Fässler showed previously that ApoE-deficient mice lacking plasma-derived Fn from hepatocytes, develop significantly smaller and fewer atherosclerotic plaques than control mice with a normal level of hepatocyte-derived, plasma Fn [136]. Atherosclerotic lesions from these mice lacked SMCs and were unable to develop a fibrous cap. This study suggested that the role of SMCs in the progression of atherosclerosis is linked to the deposition of Fn derived from blood [136]. In the previous section **(see chapter 3.2.1)**, we showed that Fn interferes with the growth behavior of primary VSMCs, in that it promotes an earlier SOA and the phenotypic modulation into a CNP-preferring synthetic phenotype. In the next step, we investigated which impact a SMC-specific deletion of Fn would have on the development of atherosclerosis. For conditional ablation of Fn in SMCs, we used the Cre/loxP recombination system. Specifically, we crossed the SM22-Cre transgenic mouse line, which expresses the Cre recombinase selectively in SMCs [164], with mice carrying a loxP-flanked ("floxed") Fn gene [165]. As mice do not develop atherosclerosis under normal conditions, all experimental animals were generated on an ApoE-deficient background [163] (ctr: (1) ApoE$^{-/-}$ x SM22Cre$^{tg/+}$ x Fn$^{+/+}$; (2) ApoE$^{-/-}$ x SM22Cre$^{+/+}$ x Fn$^{L2/L2}$; Fn-smko: ApoE$^{-/-}$ x SM22Cre$^{tg/+}$ x Fn$^{L2/L2}$). For *in vivo* experiments, control mice (ctr) and SMC-specific Fn knockout mice (Fn-smko) were fed a high fat diet **(see chapter 2.11)** for 11 weeks.

3.3.1 Impact of SM22Cre-induced fibronectin ablation on the behavior of primary VSMC

Before starting the atherosclerosis experiments, we analyzed whether Fn expression was indeed abolished in VSMCs isolated from our Fn-smko mice. For this purpose, we compared Fn expression in primary VSMCs isolated from Fn-smko mice and litter-matched controls by Western blot analysis **(Figure 30)**. The cells were grown for five days and then serum-starved for additional two days before protein samples were collected.
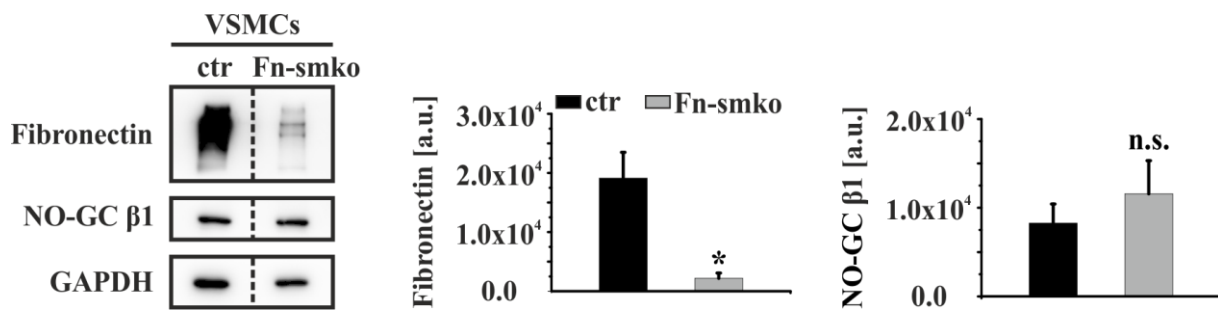
Figure 30. SM22Cre-induced Fn knockout VSMCs have significantly reduced Fn expression compared to ctr VSMCs

Protein lysates of primary VSMCs isolated from Fn-expressing control mice (ctr = (1) ApoE$^{-/-}$ x SM22Cre$^{tg/+}$ x Fnflox$^{+/+}$; (2) ApoE$^{-/-}$ x SM22Cre$^{+/+}$ x Fnflox$^{L2/L2}$) and SMC-specific Fn knockout mice (Fn-smko = ApoE$^{-/-}$ x SM22Cre$^{tg/+}$ x Fnflox$^{L2/L2}$) were analyzed via Western blot with the indicated antibodies (left). GAPDH was used as loading control. Densitometric analysis of Fn and NO-GC β1 expression (right). Representative data from one of three independent experiments are shown. All data are presented as mean ± SEM. * Asterisks indicate statistical significance vs. control condition (ctr); *$p \leq 0.05$; **$p \leq 0.01$; ***$p \leq 0.001$; n.s. = not significant.

The Western blot demonstrated that our SMC-specific Fn knockout significantly reduced the expression of Fn in cultured primary VSMCs **(Figure 30)**. In addition, we tested whether the expression of the NO-GC β1 subunit was altered by our knockout. The control (ctr) and the Fn-smko VSMCs expressed similar levels of NO-GC β1 **(Figure 30)**.

In the previous section **(see chapter 3.2.1)**, we showed that VSMCs grown on Fn-coated wells have a significantly earlier SOA **(Figure 29 A, right)**. Therefore, we investigated whether the growth behavior of Fn-smko VSMCs was altered **(Figure 31)**. We stimulated our cells with DETA-NO to induce the cGMP signaling pathway and to study whether the Fn ablation had an effect on cGMP-promoted VSMC growth **(Figure 31)**. Surprisingly, we observed that Fn-smko VSMCs were growing significantly better under basal conditions than the Fn-expressing control cells (ctr) **(Figure 31)**. Fn-smko cells showed an increased mean CI after 72 hours and an earlier SOA than ctr cells (27 hours vs. 32 hours) **(Figure 31)**. Addition of DETA-NO (75 µM) further amplified the growth of Fn knockout VSMCs (Fn-smko NO vs. Fn-smko ctr) resulting in an increased mean CI after 72 hours compared to the stimulated control cells (Fn-smko NO vs. ctr NO) **(Figure 31)**. These results indicated that, although the Fn-smko cells did not have altered NO-GC expression **(Figure 30)**, they may may be more sensitive to growth stimulation by NO **(Figure 31)**.
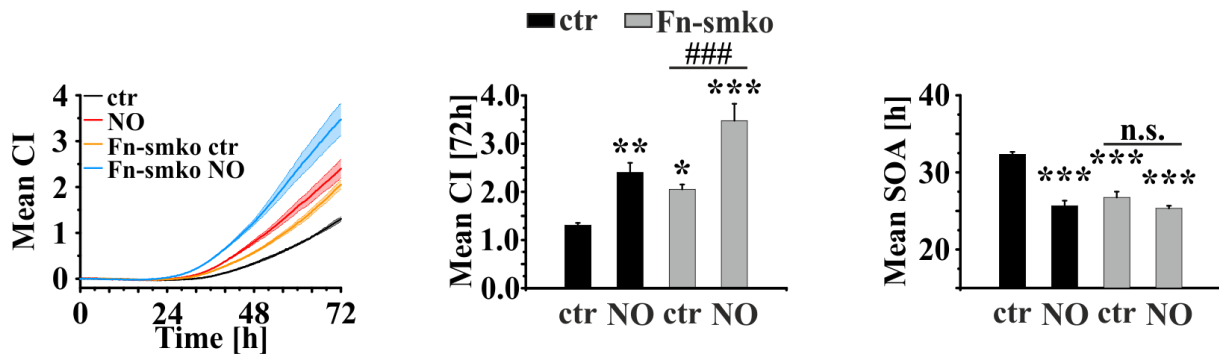
Figure 31. Fn-smko VSMCs show increased basal and DETA-NO-stimulated growth

Impedance-based (xCELLigence) real-time measurement of primary VSMCs isolated from control (ctr = ApoE$^{-/-}$ x SM22Cre$^{+/+}$ x Fnflox$^{L2/L2}$) and SMC-specific Fn knockout (Fn-smko = ApoE$^{-/-}$ x SM22Cre$^{tg/+}$ x Fnflox$^{L2/L2}$) mice in the absence (ctr) or presence of DETA-NO (75 µM; NO). Left panel = xCELLigence growth curve; middle panel = mean cell index (CI) at 72 hours; right panel = mean start of adhesion (SOA) (n= 4 wells per condition). All data are presented as mean ± SEM. * Asterisks indicate statistical significance vs. control condition (ctr); *$p \leq 0.05$; **$p \leq 0.01$; ***$p \leq 0.001$. # Hashes indicate statistical significance between the conditions indicated by horizontal lines; # $p \leq 0.05$; ## $p \leq 0.01$; ### $p \leq 0.001$; n.s. = not significant.

In order to test this hypothesis, we assessed acute cGMP responses to increasing concentrations of the NO-releasing compound DEA-NO (1-250 nM) in real-time by a FRET-based approach. Primary VSMCs expressing the cGMP biosensor cGi500 were isolated from Fn-smko mice (ApoE$^{-/-}$ x SM22Cre$^{tg/+}$ x Fn$^{L2/L2}$ x cGi500$^{L1/+}$) and litter-matched control mice (ApoE$^{-/-}$ x SM22Cre$^{+/+}$ x Fn$^{L2/L2}$ x cGi500$^{L1/+}$). Four days after seeding they were serum-starved for 12-24 hours and cGMP/FRET measurements were performed **(Figure 32)**. Indeed, cGMP responses of Fn-smko VSMCs were more sensitive to DEA-NO than cGMP responses of Fn-expressing control cells (ctr), with an EC$_{50}$ of 21 nM and 38 nM, respectively **(Figure 32)**.
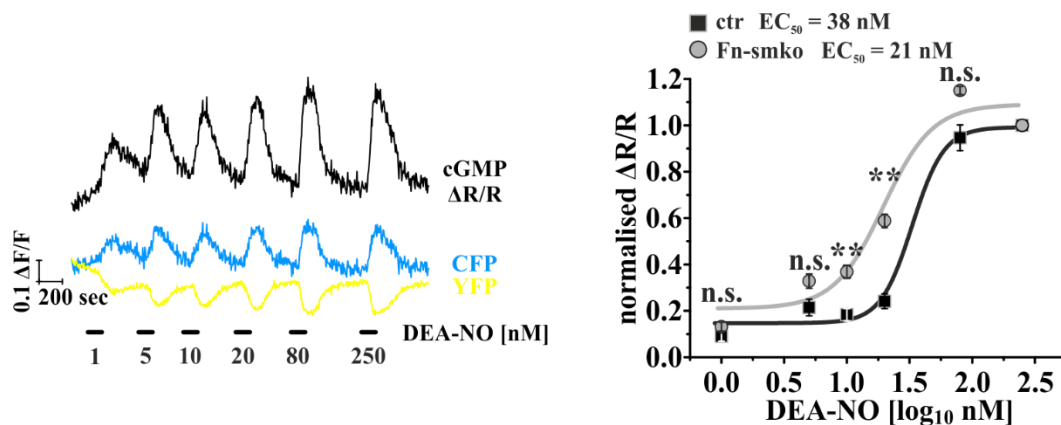
Figure 32. cGMP responses in Fn-smko VSMCs are more sensitive to stimulation with DEA-NO than cGMP responses in Fn-expressing cells

cGMP responses to increasing concentrations of DEA-NO (1-250 nM) in primary VSMCs isolated from control mice (ctr = ApoE$^{-/-}$ x SM22Cre$^{+/+}$ x Fnflox$^{L2/L2}$ cGi500$^{L1/+}$) and Fn knockout mice (Fn-smko = ApoE$^{-/-}$ x SM22Cre$^{tg/+}$ x Fnflox$^{L2/L2}$ x cGi500$^{L1/+}$) expressing the cGMP biosensor cGi500 ubiquitously. A representative measurement in one single Fn-smko VSMC is shown (left). DEA-NO concentration-response analysis is shown (right). Control VSMCs (ctr = 69 individual cells from four coverslips); Fn-smko VSMCs (n = 98 individual cells from four coverslips). All data are represented as mean ± SEM. * Asterisks indicate statistical significance vs. control condition (ctr); *$p \leq 0.05$; **$p \leq 0.01$; ***$p \leq 0.001$; n.s. = not significant.

To obtain further biochemical proof that Fn-smko VSMCs have a "sensitized" NO-cGMP-cGKI signaling cascade, we monitored the activity of cGKI via detection of VASP phosphorylation in Western blots **(Figure 33)**. Primary VSMCs were grown for five days and serum-starved for additional two days. Then, VSMCs were stimulated with DETA-NO (75 µM) for 30 minutes **(see chapter 2.8)** before the reaction was stopped by addition of SDS lysis buffer. For detection of phosphorylated VASP we used a phospho-specific antibody, which specifically detects VASP when it is phosphorylated at Ser239, the preferential target site of cGKI. Indeed, the Fn-smko VSMCs responded to DETA-NO stimulation with a significantly stronger VASP phosphorylation than control cells (ctr) **(Figure 33)**.
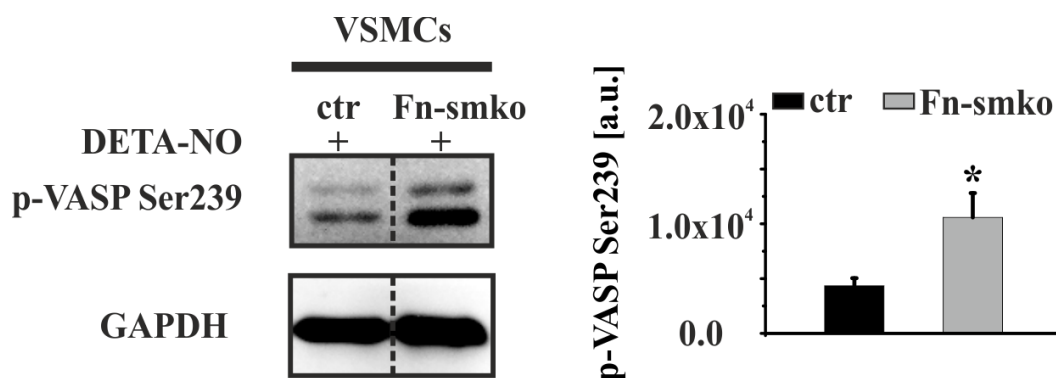
Figure 33. Fn-smko VSMCs show stronger NO-induced VASP phosphorylation than control cells

Protein lysates of primary VSMCs isolated from control mice (ctr = (1) ApoE$^{-/-}$ x SM22Cre$^{tg/+}$ x Fnflox$^{+/+}$; (2) ApoE$^{-/-}$ x SM22Cre$^{+/+}$ x Fnflox$^{L2/L2}$) and SMC-specific Fn knockout mice (Fn-smko = ApoE$^{-/-}$ x SM22Cre$^{tg/+}$ x Fnflox$^{L2/L2}$) stimulated with DETA-NO (75 µM) for 30 minutes had been analyzed via Western blot for p-VASP Ser239 (left). GAPDH was used as loading control. Densitometric analysis of p-VASP Ser239 (right). Representative data from one of four independent experiments are shown. All data are represented as mean ± SEM. * Asterisks indicate statistical significance vs. control condition (ctr); *$p \leq 0.05$; **$p \leq 0.01$; ***$p \leq 0.001$.

In summary, Western blot analysis confirmed the successful knockout of Fn in primary VSMCs of Fn-smko mice **(Figure 30)**. The deletion of Fn in VSMCs (Fn-smko) was associated with enhanced growth in the absence and presence of the NO-donor DETA-NO **(Figure 31)**. Interestingly, concentration-response analysis of NO-induced cGMP signals by FRET imaging **(Figure 32)** and monitoring of cGKI activity by detection of VASP phosphorylation **(Figure 33)** suggested that Fn-smko VSMCs have a "sensitized" NO-cGMP-cGKI growth-promoting pathway, although the expression level of NO-GC β1 is not altered **(Figure 30)**. These findings imply an interaction of Fn with the NO-cGMP-cGKI signaling axis via a yet unknown mechanism.

3.3.2 Impact of smooth muscle-specific fibronectin ablation on atherosclerosis

After demonstrating that Fn expression was abolished in primary VSMCs isolated from our Fn-smko mice **(Figure 30)**, we analyzed Fn expression in the intact aorta pre and post atherosclerosis development. To induce atherosclerosis, Fn-smko mice and their litter-matched controls were fed an atherogenic diet (20% fat, 1.5% cholesterol by weight, Altromin Germany) for 11 weeks **(see chapter 2.11)**. Whole aortae were isolated and Fn expression was analyzed via Western blot **(Figure 34)**. As "healthy" control, aortae of littermates fed a normal chow were used. The expression of Fn was almost completely abolished in aortae from Fn-smko mice with and without atherosclerosis **(Figure 34)**.
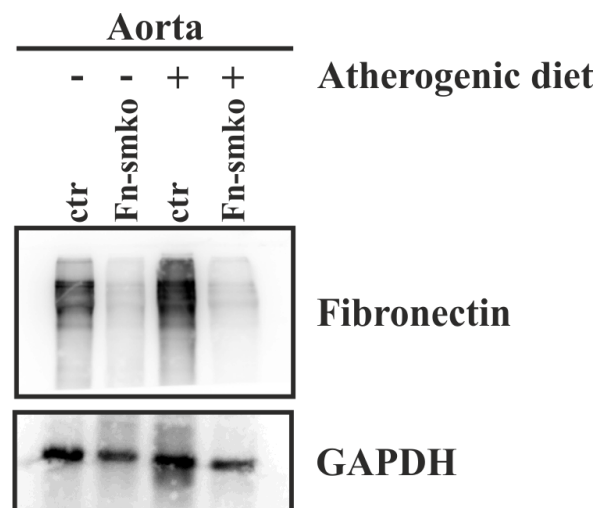
Figure 34. Fibronectin expression is almost abolished in aortae from Fn-smko mice fed normal chow or an atherogenic diet

Fn-expressing control mice (ctr = ApoE$^{-/-}$ x SM22Cre$^{tg/+}$ x Fnflox$^{+/+}$) and SMC-specific Fn knockout mice (Fn-smko = ApoE$^{-/-}$ x SM22Cre$^{tg/+}$ x Fnflox$^{L2/L2}$) fed with normal chow or atherogenic diet. Fn expression was analyzed in protein lysates of isolated aortae via Western blot. GAPDH was used as loading control. Data obtained from one aorta respectively.

It also seemed that Fn expression in the aorta of the control mouse (ctr) fed an atherogenic diet was higher in comparison to the control mouse fed a normal chow ("healthy control"),but as the data was obtained only from one aorta respectively, this observation will be checked in future experiments. However, aorta from Fn-smko mice didn't seem to have an increased Fn expression after atherogenic diet **(Figure 34)**. Those results also indicate that during the development of atherosclerosis, VSMCs are likely the major source of Fn in the aorta.

To exclude that Fn ablation affected physiological parameters, (e.g. plasma lipid levels, body weight, heart-to-body weight or kidney-to-body weight), which might also influence the

progression of atherosclerosis, we measured these parameters and found that they were similar in ctr and Fn-smko mice **(Table 22)**.

Table 22. Physiological parameters of mice after atherogenic diet

Parameter	ctr	Fn-smko
	(n=17)	(n=13)
Total cholestrol [mg/dl]	1178.7 ± 149.7	1417.5 ± 176.7
Triglyceride [mg/dl]	151.9 ± 16.9	132.2 ± 17.0
HDL [mg/dl]	11.5 ± 1.8	12.8 ± 2.7
LDL [mg/dl]	244.2 ± 45.1	311.6 ± 58.1
	(n=17)	(n=13)
Body weight [g]	33.9 ± 1.2	33.4 ± 1.5
Heart to body weight [mg/g]	0.5 ± 0.02	0.6 ± 0.03
Kidney to body weight [mg/g]	1.5 ± 0.05	1.41 ± 0.04

HDL, high-density lipoprotein; LDL, low-density lipoprotein. All data are represented as mean ± SEM. The blood samples were analyzed in the "Zentrallabor des Universitätsklinikums Tübingen" by Prof. Dr. med. Andreas Peter.

To investigate the influence of SMC-specific Fn ablation on the development of atherosclerosis, the aortae of Fn-smko and control mice were isolated after 11 weeks on atherogenic diet and plaque lesions were analyzed. To visualize the plaque area, aortae were fixed overnight and subsequently stained with Oil Red O **(see chapter 2.11.3) (Figure 35 and 36)**. The lesion area was quantified by two different methods **(see chapter 2.11.4)**. In the first method, intact aortae were mounted between two glass slides and photographed from both sides. In the second method, aortae were cut open longitudinally and pinned to Sylgard® 184 before being photographed. There was no statistical difference between data obtained with these methods. The lesion area was either quantified in the aortic arch alone **(Figure 35, first method)** or in the total aorta including the abdominal region **(Figure 36, second method)**. As already evident from visual inspection of the pictures of aortic arches **(Figure 35 A)**, Fn-smko mice had clearly more and bigger plaques after 11 weeks on atherogenic diet than control mice. This observation was confirmed by statistical analysis of the relative plaque area covering the aortic arch **(Figure 35 B, left)**.
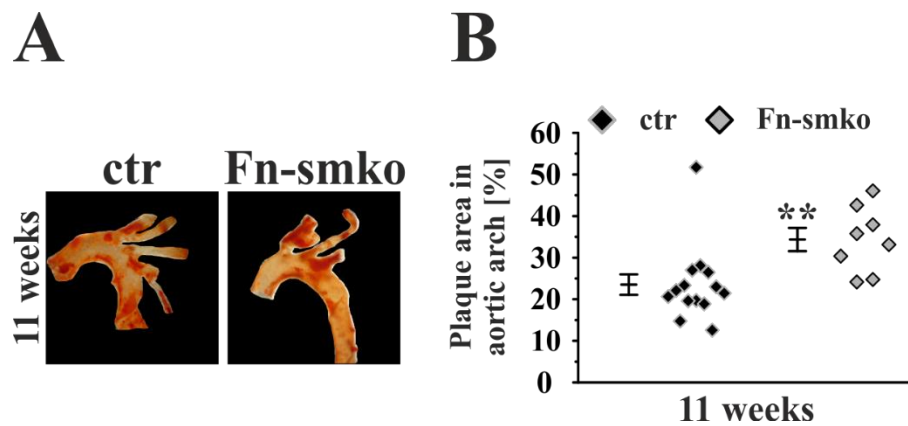
Figure 35. SMC-specific ablation of fibronectin accelerates development of atherosclerosis in the aortic arch as analyzed by method 1 (see chapter 2.11.4)

Fn-expressing control mice (ctr = (1) ApoE$^{-/-}$ x SM22Cre$^{tg/+}$ x Fnflox$^{+/+}$; (2) ApoE$^{-/-}$ x SM22Cre$^{+/+}$ x Fnflox$^{L2/L2}$) and SMC-specific Fn knockout mice (Fn-smko = ApoE$^{-/-}$x SM22Cre$^{tg/+}$ x Fnflox$^{L2/L2}$) were fed an atherogenic diet for 11 weeks and then the progression of atherosclerosis was investigated. **(A)** Representative images of Oil Red O-stained atherosclerotic lesions in the aortic arch of control and knockout mice after 11 weeks on atherogenic diet. **(B)** Lesion areas in the aortic arch of control and knockout mice after 11 weeks on atherogenic diet. Horizontal lines indicate the corresponding mean lesion area for each group of animals (11 weeks: ctr = (1) 7 animals; (2) 7 animals; Fn-smko = 8 animals). All data are presented as mean ± SEM. * Asterisks indicate statistical significance vs. control condition (ctr); *$p \leq 0.05$; **$p \leq 0.01$; ***$p \leq 0.001$; n.s. = not significant.

Similar results were obtained when the total aorta was analyzed **(Figure 36)**. Aortae of Fn-smko mice fed an atherogenic diet for 11 weeks developed a significantly greater relative lesion area than control mice **(Figure 36 B, left)**. Based on the results obtained from evaluation of the aortic arch **(Figure 35)** and total aorta **(Figure 36)**, we concluded that Fn-smko mice show enhanced atherosclerosis after 11 weeks on atherogenic diet, implying that Fn from VSMCs normally acts to attenuate early atherogenesis in mice.
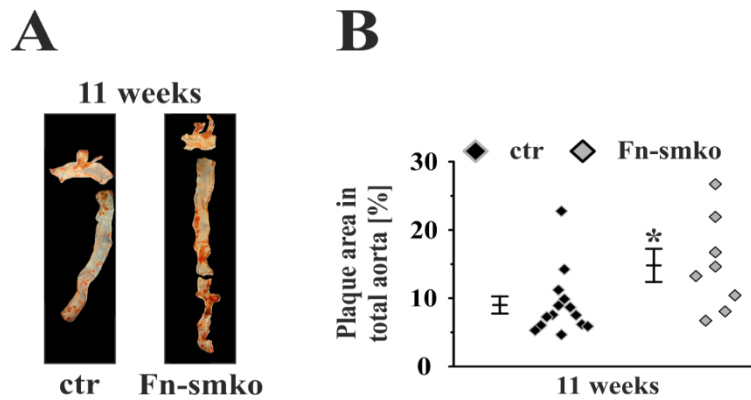
Figure 36. SMC-specific ablation of fibronectin accelerates development of atherosclerosis in the total aorta as analyzed by method 2 (see chapter 2.11.4)

Fn-expressing control mice (ctr = (1) ApoE$^{-/-}$ x SM22Cre$^{tg/+}$ x Fnflox$^{+/+}$; (2) ApoE$^{-/-}$ x SM22Cre$^{+/+}$ x Fnflox$^{L2/L2}$) and SMC-specific Fn knockout mice (Fn-smko = ApoE$^{-/-}$ x SM22Cre$^{tg/+}$ x Fnflox$^{L2/L2}$) were fed an atherogenic diet for 11 weeks and then the progression of atherosclerosis was investigated. **(A)** Representative images of Oil Red O-stained atherosclerotic lesions in total aorta of control and knockout mice after 11 weeks on atherogenic diet. **(B)** Lesion areas in the total aorta from control and knockout mice after 11 weeks on atherogenic diet. Horizontal lines indicate the corresponding mean lesion area for each group of animals (11 weeks: ctr = (1) 7 animals; (2) 7 animals; Fn-smko = 8 animals). All data are presented as mean ± SEM. * Asterisks indicate statistical significance vs. control condition (ctr); *$p \leq 0.05$; **$p \leq 0.01$; ***$p \leq 0.001$; n.s. = not

Finally, we investigated whether the increased plaque area in Fn-smko mice after 11 weeks on atherogenic diet might be linked to changes in the cellular composition of the plaques. It is known that during atherosclerosis VSMCs can switch into macrophage-like cells [115].We prepared paraffin sections (10 µm) of atherosclerotic aortae and analyzed them by immunohistochemistry with antibodies against SMαA (marker for VSMCs) and Mac-2 (marker for macrophages and/or macrophage-like cells). Plaque stability was determined by calculating the stability index (ratio of SMαA-positive area over Mac-2-positive area) **(see chapter 2.11.7)**. A higher stability index indicates a higher plaque stability against adverse events such as plaque rupture and subsequent thrombosis. Plaques from aortic arches of Fn-smko mice had a higher stability index than plaques from control mice **(Figure 37)**. This finding indicated that plaques from knockout mice might be more stable than plaques from the respective control mice.
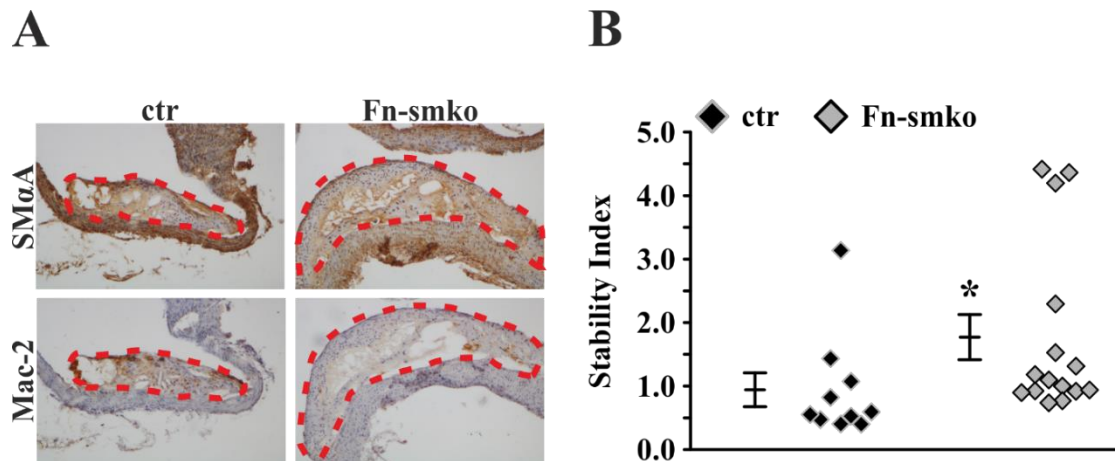
Figure 37. SMC-specific fibronectin ablation increases plaque stability

Sections (10 µm) of the aortic arch region of atherosclerotic mice fed an atherogenic diet for 11 weeks were prepared. Plaque stability was analyzed in control mice (ctr = (1) ApoE$^{-/-}$ x SM22Cre$^{tg/+}$ x Fnflox$^{+/+}$; (2) ApoE$^{-/-}$ x SM22Cre$^{+/+}$ x Fnflox$^{L2/L2}$) and SMC-specific Fn knockout mice (Fn-smko = ApoE$^{-/-}$ x SM22Cre$^{tg/+}$ x Fnflox$^{L2/L2}$). **(A)** Representative images of immunostainings for SMαA to detect SMCs (top) and Mac-2 to detect macrophages / macrophages-like cells (bottom). **(B)** Plaque stability index calculated by the (% SMαA positive plaque area) divided by the (% of Mac-2 positive plaque area). Each data point represents an individual plaque (ctr = 10 plaques from three individual mice; Fn-smko = 15 plaques from three individual mice). All data are presented as mean ± SEM. * Asterisks indicate statistical significance vs. control condition (ctr); *$p \leq 0.05$; **$p \leq 0.01$; ***$p \leq 0.001$; n.s. = not significant.

Taken together, Western blot analysis showed efficient deletion of Fn in the aorta of Fn-smko mice **(Figure 34)**. Fn ablation in VSMCs did not influence plasma lipid profiles in the experimental atherosclerotic mice **(Table 22)**, which otherwise might affect the development of atherosclerosis. In line with the increased *in vitro* growth of primary VSMCs from Fn-smko mice **(Figure 31)**, Fn-smko mice developed significantly more/bigger plaques than the respective Fn-expressing control mice after 11 weeks on atherogenic diet **(Figure 35 and 36)**. In addition, immunohistochemical analysis of plaque sections indicated that SMC-specific Fn ablation promotes the development of lesions with increased smooth muscle cell content and, therefore, enhanced stability **(Figure 37)**.

4 Discussion

4.1 Impact of the cGMP signaling cascade on VSMC growth & survival

VSMCs are implicated in a process called "vascular remodeling" which takes place during pathological conditions such as atherosclerosis and restenosis **(see chapter 1.5)**. Despite numerous studies published on this topic over the last years, the influence of the cGMP signaling cascade on phenotypic modulation of VSMCs is still controversially discussed. The common view was that NO-cGMP inhibits proliferation and promotes the contractile VSMC phenotype [78]. Interestingly, most *in vitro* studies reporting an anti-proliferative effect of NO-cGMP were based on data from subcultured/passaged VSMCs **(see chapter 1.5.1)**. Recently, we and others demonstrated that NO-cGMP promotes growth and survival of primary murine VSMCs [17]. The differing results obtained with primary vs passaged cells indicate that the cGMP signaling cascade might change depending on the VSMC phenotype (primary contractile VSMCs vs. passaged synthetic VSMCs) as already discussed in the introduction **(see chapter 1.5.1)**.

In previous studies, VSMC growth behavior was analyzed by conventional endpoint assays (e.g. WST, MTS), which only capture a single time point, while growth is a continuous process. Because of the limitations of classical growth assays, our aim was to investigate NO-cGMP-induced growth behavior as a dynamic process rather than at a single endpoint. Therefore, we sought to establish an impedance-based assay measuring VSMC growth in real-time (xCELLigence assay) **(see chapter 2.5)**. Before comparing the WST and xCELLigence assay we determined suitable concentrations of 8-Br-cGMP and DETA-NO for subsequent experiments in primary VSMCs **(see chapter 3.1.1)**.

8-Br-cGMP promoted the growth of VSMCs for all tested concentrations (25-1000 µM), with the strongest effect was induced in a concentration range between 50 µM and 100 µM **(Figure 18 A)**. Interestingly, the effect of 1000 µM 8-Br-cGMP was weaker compared to 100 µM 8-Br-cGMP **(Figure 18 A)**. One explanation for this observation could be that high concentrations of 8-Br-cGMP ($\geq$ 1000 µM) might induce the anti-proliferative cAMP pathway, either directly via cross-activation of cAK [168] or indirectly by inhibiting cAMP- hydrolyzing PDEs, such as PDE3 [16].

Similar to 8-Br-cGMP **(Figure 18 A)**, the effect of DETA-NO on VSMC growth was concentration-dependent as well **(Figure 18 B)**. For low concentrations of DETA-NO

(10-75 µM), the growth promotion was positively correlated with increasing concentrations, whereas high concentrations (100 µM) exerted weaker growth-promoting effects. Furthermore, the highest concentration of DETA-NO (1000 µM) showed a tendency to inhibit growth **(Figure 18 B)**. These results are in line with data obtained by Wolfsgruber et al. [79], where low concentrations of DETA-NO (0.5 µM) promoted VSMC growth, whereas high concentrations of DETA-NO (100 µM) had the opposite effect [79].

In the present study, the growth-promoting and-inhibiting effects of DETA-NO were observed at higher DETA-NO concentrations. One explanation for this concentration difference might be, that compounds from varying batches can differ in their potency. Therefore it is possible that the DETA-NO used by Wolfsgruber released higher amounts of NO than the DETA-NO in the present study. Another reason for the concentration discrepancy between both studies might be, the different assay conditions used. In the Wolfsgruber study [79] the proliferative effect of 0.5 µM DETA-NO and anti-proliferative, growth-inhibiting effect of 100 µM DETA-NO were assessed either by a 3H-thymidine incorporation assay (proliferation) in the presence of PDGF-BB or by cell counting (growth) at day 0, day 2 and day 4 (under serum-containing conditions). Whereas in the present study, we used the WST assay (under serum-containing conditions), which depicts the growth behavior by measuring cell viability.

After we determined suitable concentrations of 8-Br-cGMP and DETA-NO, we validated the xCELLigence method **(see chapter 3.1.2)** by comparing VSMC growth after 72 hours between the new method and the well-established WST assay **(Figure 19)**. The results obtained with the xCELLigence measurement were comparable in regard to the growth-promoting effect of 8-Br-cGMP (100 µM) or DETA-NO (75 µM) after 72 hours **(Figure 19 C and D)**. Remarkably, in contrast to the relatively small inhibiting effect of DETA-NO (1000 µM) in the WST assay **(Figure 19 B)**, the xCELLigence assay demonstrated strong growth inhibition **(Figure 19 C and D)**. This observation might be explained by the different working principle of both methods. In contrast to the WST assay (metabolic activity of cells), the xCELLigence assay detects growth behavior via impedance changes reflected by the CI, measuring the area of the well that is covered by cells. Cell spreading and proliferation will increase the CI, while cell death leads to detachment of cells and, thus, decreases the CI.

Morphological analysis of the cultured VSMCs 72 hours after seeding **(Figure 19 A)** supports the hypothesis that the different extent of growth inhibition by DETA-NO (1000 µM) detected by the WST and xCELLigence method is related to the different ways how these assays detect cell growth. 8-Br-cGMP (100 µM) and DETA-NO (75 µM) promoted the development of elongated VSMCs (leading to a high CI) **(Figure 19 A)**, whereas ≈90% of VSMCs stimulated

by high DETA-NO (1000 µM) concentrations were still round, similar to the morphology of VSMCs directly after isolation (leading to a small CI) **(Figure 19 A)**.

Interestingly as shown by the xCELLigence measurements, primary VSMCs treated with 1000 µM DETA-NO started to show normal growth behavior after ≈60 hours, reaching its maximum after ≈100 hours **(Figure 19 C)**. This observation suggest that high DETA-NO concentrations (1000 µM) do not reduce the viability of VSMCs (leading to cell death), but rather induce adverse effects on VSMC growth behavior. This hypothesis can be supported by the WST assay **(Figure 19 B)** where the growth-inhibiting effect of 1000 µM DETA-NO was relatively small, indicating a negligible impact on the viability of VSMCs.

One possible explanation for the retarded VSMC growth by treatment with high 1000 µM DETA-NO could be the half-life of the drug (≈24 hours at 37°C). A relatively high concentration of NO (released by DETA-NO) at the beginning of the experiment, might inhibit the VSMC growth process (more VSMCs with round morphology). However, due to decomposition of DETA-NO the NO concentration decreases gradually with time, unlocking the VSMC growth process and allowing normal growth behavior after a while (more VSMCs with elongated morphology).

Having successfully validated the xCELLigence assay, we analyzed the xCELLigence data in more detail **(Figures 19 C and D)**. Our real-time measurements correlated well with the different phases of VSMC growth: (1) adhesion and development of protrusions (cell spreading); (2) growth & proliferation; and (3) cell death (apoptosis). All three phases are visible in the growth curves provided by the xCELLigence measurements: The SOA (first phase) indicates that VSMCs started to attach, spread and grow ≈10-20 hours after they had been seeded. The following growth & proliferation phase (fast increase of the CI) ended after roughly 100 hours. Subsequently, the last phase (apoptosis / cell death) was visualized by the subsequent drop / fall down of the growth curves. The apoptotic phase was likely caused by the lack of nutrients and an insufficient clearance of harmful metabolites as the medium was not exchanged during the measurement.

By comparing the xCELLigence growth curves recorded under different conditions and with knockout VSMCs, we obtained a more differentiated picture on the actions of NO/cGMP during VSMC growth. Activation of the cGMP signaling cascade by 8-Br-cGMP (100 µM) significantly reduced the SOA of VSMCs and this effect was even stronger in VSMCs stimulated with DETA-NO (75 µM) **(Figure 19 D)**. One could argue that the effect of DETA-NO could be mediated by cGMP-cGKI-independent effects. However, DETA-NO did not induce an earlier SOA in NO-GC knockout **(Figure 20)** or cGKI knockout VSMCs

(Figure 21). These findings demonstrate that the strong acceleration of the SOA by DETA-NO was solely mediated by cGMP and cGKI. At first glance, this observation is inexplicable. As 8-Br-cGMP is a direct stimulator of cGKI, we would expect an earlier SOA compared to stimulation with DETA-NO. However, it isn't unlikely that the effective concentration of DETA-NO, in VSMCs, is higher compared to 8-Br-cGMP. Therefore the enhanced effect of DETA-NO on the SOA of VSMCs, might be explained by an earlier/stronger activation of the cGMP-cGKI signaling pathway. One simple experiment to test this hypothesis would be to analyze the phosphorylation of VASP (monitor for cGKI activity) upon stimulation of VSMCs with either 100 µM 8-Br-cGMP or 75 µM DETA-NO. Moreover, similar to 75 µM DETA-NO, high DETA-NO (1000 µM) also promoted the SOA of VSMCs **(Figure 19 D)**. Regarding the inhibiting effect of DETA-NO (1000 µM) on the mean CI of VSMCs after 72 hours **(Figure 19 C),** this observation is proving the ambivalent role of NO on VSMC growth (pro/anti-proliferative), likely independent of cGMP which has been already demonstrated by ourselves [79] and others as well [80, 100].

In addition, we used this real-time analysis to investigate growth behavior of VSMCs lacking functional NO-GC **(3.1.3; Figure 20)** or cGKI **(3.1.4; Figure 21)**. Compared to wildtype cells, it was not possible to promote growth (SOA and mean CI after 72 hours) of NO-GC or cGKI-deficient VSMCs upon stimulation with DETA-NO (75 µM) **(Figures 20 A and 21 A)**. In contrast, 8-Br-cGMP (100 µM) clearly promoted the growth of NO-GC knockout VSMCs **(Figure 20 B)**. As expected from previous studies from our lab [79, 101], the growth-promoting effects of both DETA-NO and 8-Br-cGMP were absent in cGKI-deficient VSMCs **(Figure 21 B)**. Thus, we conclude that the NO-induced growth enhancement of primary VSMCs is mediated via cGMP-cGKI signaling and not by cGMP-independent actions of NO.

Interestingly, the growth behavior (SOA and mean CI after 72 hours) of NO-GC- or cGKI-deficient VSMCs was already impaired under control conditions (ctr) in the absence of added drugs **(Figures 20 A and B; Figures 21 A and B)**. These observations indicate that the endogenous NO-cGMP-cGKI signaling cascade in primary VSMCs displays a certain level of basal activity that enhances their growth already under physiological conditions in the absence of pharmacological agents that increase cGMP.

Since in all previous experiments cGMP-elevating or cGKI-stimulating drugs were added directly after VSMCs had been seeded **(3.1.1-5)**, we decided to investigate whether the time point of cGMP stimulation might influence its effect on VSMC growth **(see chapter 3.1.7)**. To test this, we performed three types of experiments. (1) A short pulse of

cGMP only during the VSMC isolation process (≈ 1 hour 15 minutes) did not promote VSMC growth **(Figure 25)**. (2) We observed that 8-Br-cGMP (100 µM) promoted VSMC growth significantly only when it was added within a one hour after seeding of the cells **(Figure 26)**. (3) In a more complex experiment **(Figure 27),** we investigated whether pre-incubation of VSMCs with 8-Br-cGMP alters VSMC growth. We observed that 10 hours pre-incubation of VSMCs with 8-Br-cGMP (100 µM) did not affect cell growth **(Figure 28 A, cG (b))**, whereas longer pre-incubation (24 hours) clearly enhanced cell growth **(Figure 28 B, cG (b))**. However, 24 hours pre-incubation was not as effective as growth promotion by adding 8-Br-cGMP to the medium directly after seeding the cells (with cG(a) and without pre-incubation cG(c)) **(Figure 28 B)**. The observations that pre-incubation of VSMCs with 8-Br-cGMP for 24 hours **(Figure 28 B, cG (b))** does not promote VSMC growth as strong as adding 8-Br-cGMP to the cells during seeding, indicates that the effect induced by pre-incubation is rather mediated by influencing the viability of cells (in suspension) and this in turn promotes growth after seeding. Furthermore, in line with this hypothesis, 8-Br-cGMP addition after seeding without prior pre-incubation (24 hours) did promote VSMC growth less efficiently than with 8-Br-cGMP present during pre-incubation as well as after seeding **(Figure 28 B, cG(c) and cG (a))**. Collectively, these three experiments showed that cGMP promotes VSMC growth most efficiently, when the signaling cascade is stimulated shortly after cell seeding **(Figure 25-28)**, indicating that cGMP is modulating the early phase of cell adhesion and growth.

Up to now we got a detailed insight into the cGMP-mediated growth behavior of VSMCs triggered by NO. Next, we investigated the impact of NP-generated cGMP on VSMC growth and survival. As there is the hypothesis of distinct cGMP pools, i.e. the global NO-induced and the local NP-stimulated pool, we also sought to analyze whether cGMP's growth effects might differ depending on their stimulation with NO or NPs. In our xCELLigence measurements we observed a significantly increased mean CI (at 72 hours) upon stimulation with ANP (0.5 µM) but not CNP (0.5 µM) **(Figure 22)**. In contrast to the growth-promoting effects of 8-Br-cGMP (100 µM) and DETA-NO **(Figure 19)**, the ANP-induced effect was relatively small and, interestingly, exclusively influencing the mean CI after 72 hours but not the SOA **(Figure 22)**. In several independent experiments, ANP did always promote the growth of VSMCs, whereas CNP effect was inconsistent (→"data not shown"). In addition to xCELLigence-based growth monitoring, we performed a live and dead staining to investigate the impact of various "global" and "local" cGMP stimulators (DETA-NO, 8-Br-cGMP, ANP and CNP) on cell-viability **(see chapter 3.1.6) (Figure 23)**. 8-Br-cGMP clearly enhanced the viability of VSMCs **(Figures 23 B and C)**. Surprisingly,

although ANP (0.5 µM) had only a small growth-promoting effect (**Figure 22**), it strongly enhanced cell viability similar to 8-Br-cGMP (**Figure 23 B**). Another unexpected finding was that, while DETA-NO (75 µM) clearly promoted VSMC growth in previous experiments (**e.g. Figure 20**), it did not promote VSMC viability (**Figure 23 B and C**). Since it is known that NO can also induce effects independent of the cGMP signaling cascade (potentially interfering with the viability of VSMCs), we shifted the NO-induced effect into a more cGMP dependent direction. Indeed, simultaneous stimulation with the PDE5 inhibitor sildenafil (30 µM) and DETA-NO (75 µM) enhanced the viability of VSMCs (**Figure 23 C**), whereas this effect was absent by stimulation with DETA-NO or sildenafil alone. These findings indicate that NO and ANP trigger cGMP signals in VSMCs in different compartments, presumably global and local cGMP pools, respectively, which might indeed induce differential functional effects on VSMCs growth and survival.

Experiments with cGKI-deficient VSMCs confirmed that the cGMP-induced effect on cell viability was exclusively mediated via cGKI (**Figure 24**). Furthermore, as already shown in the growth experiments (**3.1.4; Figure 21**) deletion of cGKI impaired the viability of cells already under control conditions (no stimulation). This indicates that basal endogenous cGMP-cGKI activity promotes the viability/survival of primary VSMCs. A summary of all effects on VSMC growth and survival mediated by the different drugs is shown in **Table 23**.

Table 23. Effects of the different drugs on growth and survival of VSMCs

Drug	Mean CI [72h]	SOA	Viability
8-Br-cGMP (100 µM)	+++	++	+++
DETA-NO (75 µM)	+++	+++	no effect
DETA-NO (1000 µM)	---	++	not tested
ANP (0.5 µM)	+	no effect	+++
CNP (0.5 µM)	no effect	no effect	no effect

(+) = promoting effect compared to control condition. (-) = inhibitory effect compared to control condition.

Supporting the hypothesis of distinct cGMP pools, Castro et al. demonstrated in cardiomyocytes that stimulation of pGCs was more effective in activating CNG channels than stimulation of NO-GC [169]. These authors also showed the NO-induced cGMP was mainly regulated via PDE5, whereas the NP-induced cGMP was regulated via PDE2 [169]. In line with the hypothesis of separate cGMP compartments, Piggott et al. reported similar results in cardiomyocytes and also observed in VSMCs differential CNG channel activity upon stimulation of cGMP signals with NP and NO [170].

In summary, our data strongly implicate the NO-cGMP-cGKI signaling cascade in early processes that improve growth and survival of primary VSMCs, whereas the ANP-stimulated VSMC growth is most likely related to its positive effect on cell viability. Therefore, future experiments with cGKI-deficient VSMCs need to proof, whether the NP-induced effects are mediated by the cGMP-cGKI signaling cascade as well.

Interactions of the NO-cGMP cascade with other signaling pathways regulating VSMC growth have already been described. For example, Wolfsgruber et al. [79] showed that activation of cGMP signaling results in upregulated expression of vascular cell adhesion molecule 1 (VCAM-1), peroxisome proliferator-activated receptor γ (PPAR-γ) and increased PI3K/Akt signaling. Conversely, plasminogen activator inhibitor-1 (PAI-1) mRNA level was decreased [79]. These changes were reported to be pro-proliferative and pro-atherogenic. Moreover, Weinmeister et al. [101] demonstrated that VSMC growth was mainly affected by cGMP via increased adhesion efficiency, whereas effects on proliferation and apoptosis played a minor role. For example, these authors investigated the role of the small GTPase RhoA, which is involved in cell adhesion and a known substrate of cGKI [171, 172]. Phosphorylation by cGKI stabilizes RhoA in a cytosolic inactive RhoA-GTP/GDI complex [73, 173]. Activation of the cGMP-cGKI signaling cascade upon stimulation with 8-Br-cGMP led to suppression of the RhoA/Rho kinase signaling, resulting in activation of β1 and β3 integrins and, subsequently, enhanced adhesion of primary VSMCs. Both integrins have also been reported as binding partners of the ECM protein fibronectin [174].

4.2 Impact of the ECM protein fibronectin on phenotypic plasticity in VSMCs

Phenotypic plasticity is a major feature of VSMCs. In a healthy environment, VSMCs with a contractile phenotype regulate blood flow, but upon pathological changes VSMCs can switch into a synthetic phenotype. This phenotype is characterized by reduced expression of contractile marker proteins and increased proliferation and migration. The influence of the NO-cGMP-cGKI cascade on this process and on the development of atherosclerosis is still a matter of debate (see chapter 1.5.3).

More than 15years ago, Wolfsgruber et al. [79] showed by using a SMC-specific cGKI knockout model that the cGMP-cGKI signaling cascade in VSMCs promotes the development of atherosclerotic lesions. Interestingly, cGKI-deficient VSMCs were mainly located in the media but not in the plaque core, whereas VSMCs from cGKI wildtype mice contributed not only to the fibrous cap of the plaque but to the core as well [79]. These findings led us to the

hypothesis that during vascular remodeling the cGMP signaling cascade might be involved phenotypic modulation of VSMCs. In 2014, the Feil lab used lineage tracing experiments and co-staining of VSMC-derived plaque cells to clearly demonstrate that medial VSMCs can undergo clonal expansion and switch into macrophage-like cells that lose expression of smooth muscle markers, but gain markers for macrophages [115]. Other groups used similar approaches and confirmed the model of smooth-muscle-to-macrophage transdifferention [118-121]. Together, we and others could provide strong evidence that VSMC plasticity plays a major role in vascular diseases such as atherosclerosis. Moreover, *in vitro* **(see chapter 1.5.1)** and *in vivo* **(see chapter 1.5.3)** studies suggested that alterations of the cGMP signaling cascade are associated with phenotypic modulation of VSMCs.

However, it is not clear how VSMC phenotype influences cGMP signaling and *vice versa*. For example, it is not known whether contractile and synthetic VSMCs display differences in their cGMP signaling cascades. In the present study, we have addressed this question **(see chapter 3.2.1)**.

The ECM component Fn is mainly generated under pathological conditions [136] and on Fn coated surfaces it was already shown that this protein induces phenotypic modulation of VSMC into a synthetic phenotype [144]. First, we investigated whether the Fn-induced phenotypic modulation of VSMCs is associated with changes in growth behavior. As shown by our xCELLigence measurements, Fn coating of wells did not induce a significant change of the mean CI after 72 hours **(Figure 29 A; middle)**, but significantly promoted cell adhesion reflected by an earlier SOA **(Figure 29 A; right)**. The same effect on SOA could be observed when VSMCs grown on Fn, were stimulated with 8-Br-cGMP (100 μM) **(Figure 29 A; right)**. Furthermore, in collaboration with Moritz Lehners from the Feil lab, who developed a method for classification of VSMC populations at the single-cell level **(see chapter 2.10.3 and 2.10.4)** [167], we investigated how Fn affects VSMC phenotype and whether changes in phenotype are associated with differences in the cGMP signaling cascade **(3.2.1; Figure 29)**. As shown by FRET-based cGMP measurements in cGi500-expressing primary VSMCs, there was a much greater population of CNP-preferring cells when grown on Fn **(Figure 29 B)**, whereas most of the VSMCs grown on uncoated coverslips were ANP-preferring **(Figure 29 B)**. As shown by immunofluorescence analysis of individual cells, ANP-preferring VSMCs expressed higher levels of the contractile marker SMαA than CNP-preferring cells **(Figure 29 C)**.

These results indicate that phenotypic modulation of VSMCs is clearly associated with alterations of the cGMP signaling cascade. Indeed, phenotype-dependent cGMP signaling was previously suggested as a possible reason for the different effects of cGMP in primary vs.

subcultured VSMCs **(see chapter 1.5.1)**. Supporting this hypothesis further, Moritz Lehners was able to demonstrate that already after the first passage (passaging is a well-accepted maneuver to promote the synthetic phenotype of VSMCs), VSMCs were mostly preferring CNP over ANP (unpublished data, Moritz Lehners). Furthermore, and more related to the *in vivo* situation, healthy aortae expressing the cGi500 biosensor responded to ANP and DEA-NO stimulation, but did not show cGMP signals upon CNP stimulation (Moritz Lehners, unpublished data). Therefore, we suggest that contractile VSMCs are characterized by an ANP-preferring cGMP pathway, whereas modulation towards a synthetic VSMC phenotype is characterized by a CNP-preferring cGMP pathway. In line with this hypothesis, ANP was shown to have a greater impact on the relaxation of aortic rings and regulation of blood pressure than CNP [175]. Our model of phenotype-dependent cGMP signaling might also explain why in contrast to ANP, CNP failed to promote VSMC growth and survival in our experiments **(Figure 22-23)**. Namely, at the time point where we stimulate growth of primary VSMCs the CNP receptor GC-B is probably not expressed at all, or only in a very small amount of VSMCs. As we could demonstrate that Fn promotes the development of CNP-preferring VSMCs *in vitro*, our aim was to investigate the influence of SMC-derived Fn on the phenotypic modulation *in vivo*, during the development of atherosclerosis.

4.3 Impact of smooth muscle derived fibronectin on development of atherosclerosis

Development of vasculature depends on the secretion of ECM [112]. The basement membrane of healthy vasculature mainly consists of collagen type IV and laminin [135, 136], whereas pathologically remodeled vessels are characterized by the expression of Fn [135, 136]. VSMCs respond to the surrounding ECM via activation of integrins. In this work, we already showed that Fn coating of wells promotes the synthetic phenotype of VSMCs *in vitro* and, thereby, alters the NP-stimulated cGMP signaling pathway **(3.2.1; Figure 29)**. However, a potential interaction of Fn with the NO-cGMP-cGKI pathway and the *in vivo* relevance of Fn-cGMP crosstalk in VSMCs and vascular diseases remains unclear.

The group of Reinhard Fässler showed that transgenic mice lacking plasma-derived Fn have significantly smaller and fewer atherosclerotic plaques than control mice that have normal levels of plasma Fn [136]. Remarkably, atherosclerotic lesions from these mouse mutants lacked SMCs and were, thus, unable to develop a fibrous cap. This phenotype indicates that the contribution of SMCs to the progression of atherosclerosis is somehow linked to the deposition of plasma-derived Fn, to atherosclerotic-prone sites [136]. Based on this study and the effect of

Fn coating on the phenotype of VSMCs in our *in vitro* experiments (**3.2.1; Figure 29**), we investigated the development of atherosclerosis and potentially associated alterations of the cGMP signaling cascade in Fn-smko mice with a SMC-specific ablation of Fn (**see chapter 3.3**). The SMC-specific ablation of Fn was achieved by crossing mice that express the Cre recombinase under control of the SM22α promoter [164] with mice carrying a floxed Fn gene [165]. For the investigation of atherosclerosis, all mice had an ApoE-deficient background.

Western blot analysis of primary VSMCs isolated from Fn-smko mice and the respective Fn-expressing control mice were performed to prove the efficacy of the knockout. The expression of Fn was almost completely abolished in primary VSMCs (**Figure 30**). Primary VSMC cultures can contain small amounts of non-SMCs (e.g. fibroblasts) which could be responsible for the remaining Fn expression. In addition, the Cre recombinase might not be expressed/active in all VSMCs, therefore some cells might still secrete Fn.

Surprisingly, Fn deficiency resulted in improved growth behavior of primary VSMCs in culture (**Figure 31**). This phenotype was somewhat unexpected, because growth of wildtype VSMCs on Fn-coated surfaces promoted the synthetic VSMC phenotype, which is known for its enhanced growth behavior (**Figure 29 A**). Our initial hypothesis was that ablation of Fn would lead to reduced growth of VSMCs due to maintaining the slowly proliferating contractile phenotype. Instead, Fn deletion in VSMCs resulted in a significantly earlier SOA and increased mean CI after 72 hours compared to Fn-expressing control cells (**Figure 31**). In contrast, growing VSMCs on Fn coated surfaces (**Figure 29 A**), did only induce an earlier SOA. Therefore it is likely that Fn secreted by VSMCs itself might be connected to other intracellular signaling pathways, influencing growth and survival of VSMCs, as well. From our previous FRET-based cGMP measurements (**3.2.1; Figure 29**) we knew that Fn coating affects the cGMP signaling cascade by promoting the CNP-preferring phenotype (**Figure 29 B**). Based on these results, we investigated whether SMC-specific ablation of Fn also led to alterations in cGMP signaling. As revealed by Western blot analysis, Fn deletion did not alter the expression of the NO-GC β1 subunit (**Figure 30**) in primary VSMCs.

Interestingly, Western blot analysis of phosphorylation of the well-known cGKI target VASP showed, that Fn-smko VSMCs were more sensitive to VASP phosphorylation induced by short (30 min) incubation with DETA-NO than Fn-expressing control VSMCs (**Figure 33**). The increased NO sensitivity was revealed by a significantly stronger phosphorylation of VASP at Ser239 in Fn-smko than in control cells (**Figure 33**). Ser239 is known to be the preferential cGKI phosphorylation site of VASP [161]. Nevertheless, additional phosphorylation of VASP

at Ser157 (preferential phosphorylation site of cAK) results in a bandshift in SDS-Page (46 kDa → 50 kDa), explaining why the phosphospecific Ser239 VASP-antibody detects two bands at 46 kDa (VASP only phosphorylated at Ser239 ± Thr278) and 50 kDa (VASP phosphorylated at Ser239 and Ser157 ± Thr278). Together, these Western blot experiments indicated that Fn-smko VSMCs display an increased activity of the cGMP-cGKI axis in response to a given NO concentration (NO-induced VASP phosphorylation), which is, however, not caused by increased expression of NO-GC (**Figure 30**).

Next, we tested whether Fn-smko VSMCs are more sensitive to NO-induced cGMP elevation, presumably because their NO-GC is more active than NO-GC of Fn-expressing control VSMCs.

We crossed our Fn-smko animals (ApoE$^{-/-}$ x SM22Cre$^{tg/+}$ x Fn$^{L2/L2}$) with mice expressing the cGMP biosensor cGi500 ubiquitously, which resulted in Fn-smko mice expressing cGi500 (ApoE$^{-/-}$ x SM22Cre$^{tg/+}$ x Fn$^{L2/L2}$ x cGi500$^{L1/+}$). To investigate whether Fn-smko VSMCs had an increased sensitivity to NO-induced cGMP elevations, we isolated primary VSMCs from cGi500-expressing control and Fn-smko mice and determined concentration-response curves for NO-induced cGMP increases by FRET/cGMP imaging. Indeed, Fn-smko VSMCs were significantly more sensitive to DEA-NO stimulation than the respective Fn-expressing control VSMCs (EC$_{50}$= 21 nM vs. 38 nM) (**Figure 32**). In summary, our data indicate that Fn deficiency in VSMCs leads to an enhanced NO sensitivity of NO-GC and increased activity of the growth-promoting NO-cGMP-cGKI pathway in primary VSMCs.

Encouraged by our *in vitro* studies (**see chapter 3.3.1**), we investigated the role of SMC-derived Fn in the development of atherosclerosis. For this purpose, mice were fed with atherogenic diet (20% fat, 1.5% cholesterol by weight) for 11 weeks (**see chapter 3.3.2**).

To assess the efficiency of SMC-specific Fn ablation *in vivo* in "healthy" and atherosclerotic vessels, Fn expression in aortae of Fn-smko and control mice (+/- 11 weeks atherogenic diet) was compared by Western blot analysis (**Figure 34**). The expression of Fn was almost completely abolished in "healthy" (normal chow) as well as atherosclerotic (atherogenic diet) aortae of Fn-smko mice (**Figure 34**). Interestingly, the Western blot also indicated that Fn-expressing control mice fed an atherogenic diet had a greater amount of Fn in their aorta than control mouse fed with normal (non-atherogenic) chow (**Figure 34**). However, it should be noted that this Western blot analysis was only performed once as a proof-of-principle. Therefore, it is not possible to corroborate these observations by statistical calculations. Nevertheless, these findings suggest that in our ApoE-deficient mouse model the

concentration of Fn in the aorta increases during development of atherosclerosis and that VSMCs are the major source of Fn in both the healthy as well as atherosclerotic aorta.

By quantification of the Oil Red O-positive plaque area, we found that Fn-smko mice (11 weeks on atherogenic diet) had a significantly greater lesion area in the aorta than respective control mice **(Figures 35 and 36)**. In general, the total percental plaque area in the aortic arch **(Figure 35)** was greater than the percental plaque area in the total aorta **(Figure 36)**. This observation was expected as it was already known that lesions develop preferentially at sites exposed to turbulent blood flow, for example, at curvatures and branching points [176]. Fn-smko mice showed normal body weight, heart-to-kidney weight and kidney-to-body-weight, and their plasma lipid profile (e.g. HDL and LDL) was also not different from control mice **(Table 22)**. Thus, it is highly unlikely that Fn ablation in SMCs resulted in systemic phenotypes (e.g. altered plasma lipids) that could be confounding factors influencing the progression of atherosclerosis.

In summary, our results from the *in vitro* experiments, in which Fn-smko VSMCs showed enhanced growth already under basal conditions **(Figure 31),** and *in vivo* experiments, in which SMC-specific Fn ablation accelerated the progression of atherosclerosis **(Figures 35 and 36)**, are consistent with each other. Considering the *in vivo* study of the Fässler group (showing that Fn from the plasma promotes the development of atherosclerosis) [136] and our own *in vitro* data (showing that extracellular Fn present on the surface of a plastic well promotes the synthetic VSMC phenotype), the phenotype of increased atherosclerosis in Fn-smko mice was unexpected.

To understand these seemingly contradicting effects of Fn, we investigated whether SMC-specific Fn ablation interferes with the general composition of atherosclerotic lesions. Plaque composition and stability was analyzed by immunohistochemical staining of sections of atherosclerotic lesions with antibodies against SMαA (marker of contractile VSMCs) and Mac-2 (marker of macrophages and macrophage-like cells) **(Figure 37)**. Results from these stainings indicated that plaques from Fn-smko mice are more stable (stability index = SMαA-positive area / Mac-2-positive area) than plaques from respective control mice **(Figure 37)**. In support of our hypothesis that SMC-specific Fn ablation improves plaque stability Doddapattar et al. [135] demonstrated that plaques from Fn deficient mice were characterized by small necrotic cores, thick fibrous caps containing high amounts of VSMCs and collagen, and decreased apoptosis of macrophages and VSMCs [135].

As discussed above, our results regarding the effect of SMC-specific Fn ablation on VSMC behavior *in vitro* (enhanced growth) and the development of atherosclerosis *in vivo*

(larger lesions with a higher VSMC content and stability) were surprising, but consistent with each other. How could Fn deficiency in VSMCs lead to enhanced cell growth? A possible explanation could be that Fn ablation interferes with mechanotransduction in VSMCs. In the present study, we demonstrated by Western blot analysis **(Figure 33)** and cGMP measurements **(Figure 32)** that the growth-promoting NO-cGMP-cGKI signaling cascade was enhanced in Fn-smko VSMCs. The higher activity of the cGMP pathway cannot be explained by increased NO-GC expression **(Figure 30)**, but might be due to an increased NO sensitivity of NO-GC in VSMCs in the absence of Fn (**Figure 32**). Indeed, Wen et al. [45] recently identified a shear-dependent NO-cGMP-cGKI cascade in platelets that inhibits thrombosis *in vitro* and *in vivo*. In platelets, it appears that mechanical stress sensitizes NO-GC to activation by NO, thus, generating much higher cGMP concentrations in the presence of NO and shear-stress than in the presence of NO alone. Interestingly, Wen and colleagues show also data suggesting that VSMCs might have a similar mechanosensitive NO-cGMP pathway [45]. Thus, it is tempting to speculate that ablation of Fn in VSMCs changes mechanotransduction, so that the activity of NO-GC is enhanced and growth and survival of VSMC is increased *in vitro* and *in vivo*. Furthermore, the ablation of Fn is likely to interfere with the tension of VSMCs in general and this might lead to alteration of NO-GC activity under unstimulated conditions (without shear-stress). This assumption would explain why Fn-smko VSMCs show increased growth behavior (without shear stress) compared to Fn-expressing cells, in our growth experiments **(Figure 31)**. Both hypotheses ((1) Fn ablation interferes with the shear-dependent NO-cGMP-cGKI cascade (2) Fn ablation alters the tension of VSMCs, interfering with the NO-cGMP-cGKI cascade (independent of shear-stress) need to be investigated by extensive research in the future.

Wolfsgruber et al. [79] and Segura-Puimedon et al. [80] already showed that components of the NO-cGMP signaling cascade (NO-GC and cGKI) have a pro-atherosclerotic effect. However, it is important to note that cGMP-mediated plaque growth is not necessarily an unfavorable process. In fact, cGMP-cGKI signaling in VSMCs is associated with altered plaque composition [79, 80], which may or may not stabilize the plaque [17]. In the future, we need to investigate whether the accelerated development of atherosclerosis in Fn-smko mice is indeed associated with alterations in the cGMP signaling cascade *in vivo* like it has been indicated by our *in vitro* studies **(see chapter 3.3.1)**.

5 Summary & Outlook

In summary we made several new findings regarding the effect of the NO-cGMP-cGKI signaling cascade on growth and survival in VSMCs. For instance, we showed that stimulation of VSMCs with either 8-Br-cGMP, DETA-NO or the NPs, ANP and CNP, induces different effects in VSMCs. Namely, direct stimulation of cGKI with 8-Br-cGMP strongly promoted cell growth and survival of VSMCs, whereas DETA-NO only promoted their growth. ANP's effect on viability was similar to 8-Br-cGMP but the effect on the growth of VSMCs was relatively small (CNP had no effect at all) **(Figure 38)**. Those results indicate that stimulation of distinct cGMP pools, "global" NO-cGMP-cGKI signaling cascade, and "local", NP-stimulated cGMP pathway might have different functions in VSMCs (possibly independent of cGKI). Furthermore, we were able to show that SMC-specific ablation of Fn leads to accelerated development of atherosclerosis. At first, this finding was surprising. However, we were able to demonstrate that the cGMP pathway of Fn-smko VSMCs is pronounced, probably due to changes in mechanotransduction which are likely to increase NO sensitivity of VSMCs **(see chapter 4.3) (Figure 38)**.
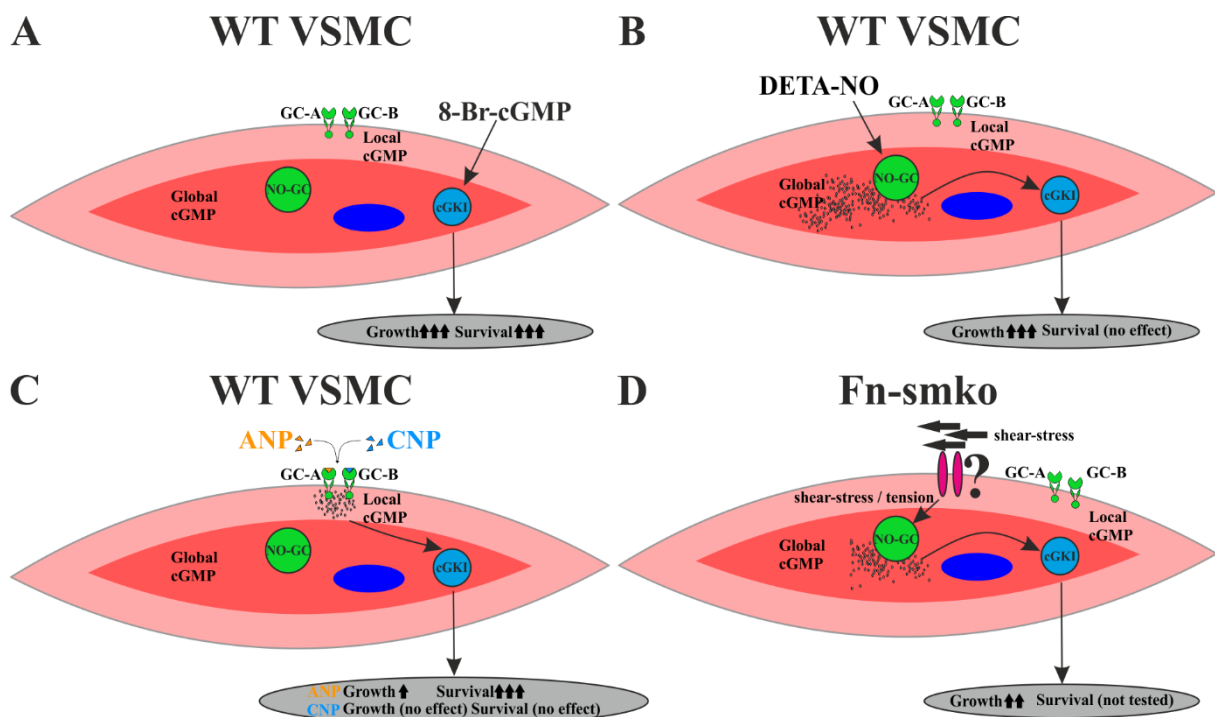
Figure 38. Summary of the different effects of cGMP and SMC-specific ablation of Fn on VSMC growth and survival

Effect of different cGMP enhancing drugs and SMC-specific ablation of Fn on growth and survival in primary VSMCs. **(A)** Direct stimulation of cGKI with 8-Br-cGMP. **(B)** Stimulation of the "global" cGMP pool with DETA-NO. **(C)** Stimulation of the "local" cGMP pool with either ANP or CNP. **(D)** Effect of SMC-specific Fn ablation on the shear-stress/-tension-dependent activity of NO-cGMP-cGKI signaling cascade. For details see text.

Despite those numerous findings, there is plenty of work left. For example, (1) it is necessary to increase the n-numbers for the Western blot analysis of atherosclerotic aortae **(Figure 34)**. (2) The growth behavior of primary Fn-smko VSMCs in response to ODQ treatment should be analyzed to confirm the hypothesis of increased basal NO-GC activity. (3) cGMP-FRET analysis with subsequent staining for contractile and synthetic marker proteins should be performed to analyze whether SMC-specific deletion of Fn interferes with the process of phenotypic modulation of VSMCs (ANP vs. CNP-preference). (4) The different effects mediated by stimulation of "global" and "local" cGMP pools should be further investigated.

6 Appendix

6.1 Polymerase chain reaction

Table 24. PCR primer

Primer	Sequence (5´ → 3´)
BB01	CTCTGCTGCCTCCTGGCTTCT
BB02	CGAGGCGGATCACAAGCAATA
BB03	TCAATGGGCGGGGGTCGTT
BB31	GTACTGTCCCATATAAGCCTCTG
BB32	CTGAGCATCTTGAGTGGATGGGA
BB19	AAGATGCTGAAGGGAAGGATGC
BB20	CAGCCCAAAGAAACAAGAAGAAAG
BB21	GATGTGGGATTGTTTCTGAGGA
RF115	GCCTAGCCGAGGGAGAGCCG
RF117	GCCGCCCCGACTGCATCT
RF151	AGTTCTTGTGTGACTTGGGAG
Cre800	GCTGCCACGACCAAGTGACAGCAATG
Cre1200	GTAGTTATTCGGATCATCAGCTACAC
RF53	CCTGGCTGTGATTTCACTCCA
RF118	AAATTATAACTTGTCAAATTCTTG
RF125	GTCAAGTGACCACTATG

Table 25. PCR programs

PCR (mouse line / allele)	Primer	Product size	PCR program	
SM22-Cre	Cre800 Cre1200	tg 402 bp wt none	95°C → 5 min	
			95°C → 10 sec 58°C → 30 sec 72°C → 30 sec	35x
			72°C → 5 min	
ApoE	RF115 RF117 RF151	ko 245 bp wt 163 bp	95°C → 5 min	
			95°C → 10 sec 65°C → 30 sec 72°C → 30 sec	35x
			72°C → 5 min	
Fibronectin flox	BB31 BB32	L2 300 bp wt 250 bp	95°C → 5 min	
			95°C → 30 sec 62°C → 30 sec 72°C → 30 sec	35x
			72°C → 5 min	
cGi500 (L1)	BB01 BB02 BB03	L1 250 bp wt 300 bp	95°C → 5 min	
			95°C → 10 sec 61°C → 30 sec 72°C → 30 sec	35x
			72°C → 5 min	
NO-GC β1 ko / flox (L2)	BB19 BB20 BB21	ko 830 bp L2 720 bp wt 680 bp	95°C → 3 min	
			95°C → 60 sec 60°C → 45 sec 72°C → 60 sec	30x
			72°C → 7 min	
cGKI ko / flox (L2)	RF53 RF118 RF125	ko 250 bp L2 338 bp wt 284 bp	95°C → 5 min	
			95°C → 10 sec 50°C → 30 sec 72°C → 30 sec	35x
			72°C → 5 min	

7 References

1.   *Glyceryl trinitrate and angina*, in *Br Med J*. 1969. p. 252.
2.   Murrell, W., *Nitroglycerine as a remedy for angina pectoris.* The Lancet, 1879.
3.   Katsuki, S., et al., *Stimulation of guanylate cyclase by sodium nitroprusside, nitroglycerin and nitric oxide in various tissue preparations and comparison to the effects of sodium azide and hydroxylamine.* J Cyclic Nucleotide Res, 1977. **3**(1): p. 23-35.
4.   Furchgott, R.F. and J.V. Zawadzki, *The obligatory role of endothelial cells in the relaxation of arterial smooth muscle by acetylcholine.* Nature, 1980. **288**(5789): p. 373-6.
5.   Ignarro, L.J., et al., *Endothelium-derived relaxing factor from pulmonary artery and vein possesses pharmacologic and chemical properties identical to those of nitric oxide radical.* Circ Res, 1987. **61**(6): p. 866-79.
6.   Palmer, R.M., A.G. Ferrige, and S. Moncada, *Nitric oxide release accounts for the biological activity of endothelium-derived relaxing factor.* Nature, 1987. **327**(6122): p. 524-6.
7.   Ashman, D.F., et al., *Isolation of adenosine 3', 5'-monophosphate and guanosine 3', 5'-monophosphate from rat urine.* Biochem Biophys Res Commun, 1963. **11**: p. 330-4.
8.   Beavo, J.A. and L.L. Brunton, *Cyclic nucleotide research -- still expanding after half a century.* Nat Rev Mol Cell Biol, 2002. **3**(9): p. 710-8.
9.   Kemp-Harper, B. and R. Feil, *Meeting report: cGMP matters.* Sci Signal, 2008. **1**(9): p. pe12.
10.   Hofmann, F., et al., *Function of cGMP-dependent protein kinases as revealed by gene deletion.* Physiol Rev, 2006. **86**(1): p. 1-23.
11.   Feil, R., et al., *Cyclic GMP-dependent protein kinases and the cardiovascular system: insights from genetically modified mice.* Circ Res, 2003. **93**(10): p. 907-16.
12.   Biel, M. and S. Michalakis, *Cyclic nucleotide-gated channels.* Handb Exp Pharmacol, 2009(191): p. 111-36.
13.   Francis, S.H., M.A. Blount, and J.D. Corbin, *Mammalian cyclic nucleotide phosphodiesterases: molecular mechanisms and physiological functions.* Physiol Rev, 2011. **91**(2): p. 651-90.
14.   Mullershausen, F., et al., *Direct activation of PDE5 by cGMP: long-term effects within NO/cGMP signaling.* J Cell Biol, 2003. **160**(5): p. 719-27.
15.   Sonnenburg, W.K. and J.A. Beavo, *Cyclic GMP and regulation of cyclic nucleotide hydrolysis.* Adv Pharmacol, 1994. **26**: p. 87-114.
16.   Aizawa, T., et al., *Role of phosphodiesterase 3 in NO/cGMP-mediated antiinflammatory effects in vascular smooth muscle cells.* Circ Res, 2003. **93**(5): p. 406-13.
17.   Lehners, M., et al., *cGMP signaling and vascular smooth muscle cell plasticity.* J Cardiovasc Dev Dis, 2018. **5**(2).
18.   Forstermann, U. and W.C. Sessa, *Nitric oxide synthases: regulation and function.* Eur Heart J, 2012. **33**(7): p. 829-37, 837a-837d.
19.   Kuhn, M., *Molecular physiology of membrane guanylyl cyclase receptors.* Physiol Rev, 2016. **96**(2): p. 751-804.
20.   Loscalzo, J. and G. Welch, *Nitric oxide and its role in the cardiovascular system.* Prog Cardiovasc Dis, 1995. **38**(2): p. 87-104.
21.   Knowles, R.G. and S. Moncada, *Nitric oxide synthases in mammals.* Biochem J, 1994. **298 (Pt 2)**: p. 249-58.
22.   Alderton, W.K., C.E. Cooper, and R.G. Knowles, *Nitric oxide synthases: structure, function and inhibition.* Biochem J, 2001. **357**(Pt 3): p. 593-615.

23. Garthwaite, J., *Concepts of neural nitric oxide-mediated transmission.* Eur J Neurosci, 2008. **27**(11): p. 2783-802.

24. Brenman, J.E., et al., *Interaction of nitric oxide synthase with the postsynaptic density protein PSD-95 and alpha1-syntrophin mediated by PDZ domains.* Cell, 1996. **84**(5): p. 757-67.

25. Christopherson, K.S., et al., *PSD-95 assembles a ternary complex with the N-methyl-D-aspartic acid receptor and a bivalent neuronal NO synthase PDZ domain.* J Biol Chem, 1999. **274**(39): p. 27467-73.

26. Friebe, A. and D. Koesling, *The function of NO-sensitive guanylyl cyclase: what we can learn from genetic mouse models.* Nitric Oxide, 2009. **21**(3-4): p. 149-56.

27. Yuen, P.S., L.R. Potter, and D.L. Garbers, *A new form of guanylyl cyclase is preferentially expressed in rat kidney.* Biochemistry, 1990. **29**(49): p. 10872-8.

28. Derbyshire, E.R. and M.A. Marletta, *Biochemistry of soluble guanylate cyclase.* Handb Exp Pharmacol, 2009(191): p. 17-31.

29. Russwurm, M., et al., *Functional properties of a naturally occurring isoform of soluble guanylyl cyclase.* Biochem J, 1998. **335 (Pt 1**): p. 125-30.

30. Hanafy, K.A., J.S. Krumenacker, and F. Murad, *NO, nitrotyrosine, and cyclic GMP in signal transduction.* Med Sci Monit, 2001. **7**(4): p. 801-19.

31. Wilson, E.M. and M. Chinkers, *Identification of sequences mediating guanylyl cyclase dimerization.* Biochemistry, 1995. **34**(14): p. 4696-701.

32. Chinkers, M. and D.L. Garbers, *The protein kinase domain of the ANP receptor is required for signaling.* Science, 1989. **245**(4924): p. 1392-4.

33. Kuhn, M., *Function and dysfunction of mammalian membrane guanylyl cyclase receptors: lessons from genetic mouse models and implications for human diseases.* Handb Exp Pharmacol, 2009(191): p. 47-69.

34. Matsukawa, N., et al., *The natriuretic peptide clearance receptor locally modulates the physiological effects of the natriuretic peptide system.* Proc Natl Acad Sci U S A, 1999. **96**(13): p. 7403-8.

35. Orstavik, S., et al., *Characterization of the human gene encoding the type I alpha and type I beta cGMP-dependent protein kinase (PRKG1).* Genomics, 1997. **42**(2): p. 311-8.

36. Pfeifer, A., et al., *Defective smooth muscle regulation in cGMP kinase I-deficient mice.* EMBO J, 1998. **17**(11): p. 3045-51.

37. Hofmann, F., A. Ammendola, and J. Schlossmann, *Rising behind NO: cGMP-dependent protein kinases.* J Cell Sci, 2000. **113**(10): p. 1671-1676.

38. Ruth, P., et al., *Identification of the amino acid sequences responsible for high affinity activation of cGMP kinase Ialpha.* J Biol Chem, 1997. **272**(16): p. 10522-8.

39. Hofmann, F., et al., *cGMP regulated protein kinases (cGK).* Handb Exp Pharmacol, 2009(191): p. 137-62.

40. Lohmann, S.M., et al., *Distinct and specific functions of cGMP-dependent protein kinases.* Trends Biochem Sci, 1997. **22**(8): p. 307-12.

41. Werner, C., et al., *Importance of NO/cGMP signalling via cGMP-dependent protein kinase II for controlling emotionality and neurobehavioural effects of alcohol.* Eur J Neurosci, 2004. **20**(12): p. 3498-506.

42. Collado-Alsina, A., et al., *Altered Synaptic Membrane Retrieval after Strong Stimulation of Cerebellar Granule Neurons in Cyclic GMP-Dependent Protein Kinase II (cGKII) Knockout Mice.* Int J Mol Sci, 2017. **18**(11).

43. Kawasaki, Y., et al., *Phosphorylation of GSK-3beta by cGMP-dependent protein kinase II promotes hypertrophic differentiation of murine chondrocytes.* J Clin Invest, 2008. **118**(7): p. 2506-15.

44. Pfeifer, A., et al., *Intestinal secretory defects and dwarfism in mice lacking cGMP-dependent protein kinase II.* Science, 1996. **274**(5295): p. 2082-6.

45. Wen, L., et al., *A shear-dependent NO-cGMP-cGKI cascade in platelets acts as an auto-regulatory brake of thrombosis.* Nat Commun, 2018. **9**(1): p. 4301.

46. Massberg, S., et al., *Increased adhesion and aggregation of platelets lacking cyclic guanosine 3',5'-monophosphate kinase I.* J Exp Med, 1999. **189**(8): p. 1255-64.

47. Wegener, J.W., et al., *cGMP-dependent protein kinase I mediates the negative inotropic effect of cGMP in the murine myocardium.* Circ Res, 2002. **90**(1): p. 18-20.

48. Aicher, A., et al., *cGMP-dependent protein kinase I is crucial for angiogenesis and postnatal vasculogenesis.* PLoS One, 2009. **4**(3): p. e4879.

49. Yamahara, K., et al., *Significance and therapeutic potential of the natriuretic peptides/cGMP/cGMP-dependent protein kinase pathway in vascular regeneration.* Proc Natl Acad Sci U S A, 2003. **100**(6): p. 3404-9.

50. Senthilkumar, A., et al., *Sildenafil promotes ischemia-induced angiogenesis through a PKG-dependent pathway.* Arterioscler Thromb Vasc Biol, 2007. **27**(9): p. 1947-54.

51. Sausbier, M., et al., *Mechanisms of NO/cGMP-dependent vasorelaxation.* Circ Res, 2000. **87**(9): p. 825-30.

52. Koeppen, M., et al., *cGMP-dependent protein kinase mediates NO- but not acetylcholine-induced dilations in resistance vessels in vivo.* Hypertension, 2004. **44**(6): p. 952-5.

53. Feil, S., et al., *Distribution of cGMP-dependent protein kinase type I and its isoforms in the mouse brain and retina.* Neuroscience, 2005. **135**(3): p. 863-8.

54. Kleppisch, T., et al., *Hippocampal cGMP-dependent protein kinase I supports an age- and protein synthesis-dependent component of long-term potentiation but is not essential for spatial reference and contextual memory.* J Neurosci, 2003. **23**(14): p. 6005-12.

55. Dhayade, S., et al., *Sildenafil potentiates a cGMP-dependent pathway to promote melanoma growth.* Cell Rep, 2016. **14**(11): p. 2599-610.

56. Li, W.Q., et al., *Sildenafil use and increased risk of incident melanoma in US men: a prospective cohort study.* JAMA Intern Med, 2014. **174**(6): p. 964-70.

57. Loeb, S., et al., *Use of phosphodiesterase type 5 inhibitors for erectile dysfunction and risk of malignant melanoma.* JAMA, 2015. **313**(24): p. 2449-55.

58. Feil, R., *Viagra releases the brakes on melanoma growth.* Mol Cell Oncol, 2017. **4**(5): p. e1188874.

59. Huang, P.L., et al., *Hypertension in mice lacking the gene for endothelial nitric oxide synthase.* Nature, 1995. **377**(6546): p. 239-42.

60. Shesely, E.G., et al., *Elevated blood pressures in mice lacking endothelial nitric oxide synthase.* Proc Natl Acad Sci U S A, 1996. **93**(23): p. 13176-13181.

61. Buys, E.S., et al., *Gender-specific hypertension and responsiveness to nitric oxide in sGCalpha1 knockout mice.* Cardiovasc Res, 2008. **79**(1): p. 179-86.

62. Groneberg, D., et al., *Smooth muscle-specific deletion of nitric oxide-sensitive guanylyl cyclase is sufficient to induce hypertension in mice.* Circulation, 2010. **121**(3): p. 401-9.

63. Mergia, E., et al., *Spare guanylyl cyclase NO receptors ensure high NO sensitivity in the vascular system.* J Clin Invest, 2006. **116**(6): p. 1731-7.

64. John, S.W., et al., *Genetic decreases in atrial natriuretic peptide and salt-sensitive hypertension.* Science, 1995. **267**(5198): p. 679-81.

65. Lopez, M.J., et al., *Salt-resistant hypertension in mice lacking the guanylyl cyclase-A receptor for atrial natriuretic peptide.* Nature, 1995. **378**(6552): p. 65-8.

66. Feil, R., et al., *Functional reconstitution of vascular smooth muscle cells with cGMP-dependent protein kinase I isoforms.* Circ Res, 2002. **90**(10): p. 1080-6.

67. Geiselhoringer, A., et al., *IRAG is essential for relaxation of receptor-triggered smooth muscle contraction by cGMP kinase.* EMBO J, 2004. **23**(21): p. 4222-31.

68. Schlossmann, J., et al., *Regulation of intracellular calcium by a signalling complex of IRAG, IP3 receptor and cGMP kinase Ibeta.* Nature, 2000. **404**(6774): p. 197-201.

69. Koller, A., et al., *Association of phospholamban with a cGMP kinase signaling complex.* Biochem Biophys Res Commun, 2003. **300**(1): p. 155-60.

70. Surks, H.K., et al., *Regulation of myosin phosphatase by a specific interaction with cGMP- dependent protein kinase Ialpha.* Science, 1999. **286**(5444): p. 1583-7.

71. Wooldridge, A.A., et al., *Smooth muscle phosphatase is regulated in vivo by exclusion of phosphorylation of threonine 696 of MYPT1 by phosphorylation of Serine 695 in response to cyclic nucleotides.* J Biol Chem, 2004. **279**(33): p. 34496-504.

72. Somlyo, A.P. and A.V. Somlyo, *Ca2+ sensitivity of smooth muscle and nonmuscle myosin II: modulated by G proteins, kinases, and myosin phosphatase.* Physiol Rev, 2003. **83**(4): p. 1325-58.

73. Sauzeau, V., et al., *Cyclic GMP-dependent protein kinase signaling pathway inhibits RhoA-induced Ca2+ sensitization of contraction in vascular smooth muscle.* J Biol Chem, 2000. **275**(28): p. 21722-9.

74. Sawada, N., et al., *cGMP-dependent protein kinase phosphorylates and inactivates RhoA.* Biochem Biophys Res Commun, 2001. **280**(3): p. 798-805.

75. Beamish, J.A., et al., *Molecular regulation of contractile smooth muscle cell phenotype: implications for vascular tissue engineering.* Tissue Eng Part B Rev, 2010. **16**(5): p. 467-91.

76. Owens, G.K., M.S. Kumar, and B.R. Wamhoff, *Molecular regulation of vascular smooth muscle cell differentiation in development and disease.* Physiol Rev, 2004. **84**(3): p. 767-801.

77. Feil, R., S. Feil, and F. Hofmann, *A heretical view on the role of NO and cGMP in vascular proliferative diseases.* Trends Mol Med, 2005. **11**(2): p. 71-5.

78. Lincoln, T.M., et al., *Regulation of vascular smooth muscle cell phenotype by cyclic GMP and cyclic GMP-dependent protein kinase.* Front Biosci, 2006. **11**: p. 356-67.

79. Wolfsgruber, W., et al., *A proatherogenic role for cGMP-dependent protein kinase in vascular smooth muscle cells.* Proc Natl Acad Sci U S A, 2003. **100**(23): p. 13519-24.

80. Segura-Puimedon, M., et al., *Proatherosclerotic effect of the alpha1-subunit of soluble guanylyl cyclase by promoting smooth muscle phenotypic switching.* Am J Pathol, 2016. **186**(8): p. 2220-2231.

81. Lukowski, R., et al., *Role of smooth muscle cGMP/cGKI signaling in murine vascular restenosis.* Arterioscler Thromb Vasc Biol, 2008. **28**(7): p. 1244-50.

82. Dey, N.B., et al., *Inhibition of cGMP-dependent protein kinase reverses phenotypic modulation of vascular smooth muscle cells.* J Cardiovasc Pharmacol, 2005. **45**(5): p. 404-13.

83. Chamley-Campbell, J., G.R. Campbell, and R. Ross, *The smooth muscle cell in culture.* Physiol Rev, 1979. **59**(1): p. 1-61.

84. Owens, G.K., *Regulation of differentiation of vascular smooth muscle cells.* Physiol Rev, 1995. **75**(3): p. 487-517.

85. Worth, N.F., et al., *Vascular smooth muscle cell phenotypic modulation in culture is associated with reorganisation of contractile and cytoskeletal proteins.* Cell Motil Cytoskeleton, 2001. **49**(3): p. 130-45.

86. Butt, E., *cGMP-dependent protein kinase modulators.* Handb Exp Pharmacol, 2009(191): p. 409-21.

87. Gambaryan, S., et al., *Potent inhibition of human platelets by cGMP analogs independent of cGMP-dependent protein kinase.* Blood, 2004. **103**(7): p. 2593-600.

88. Marshall, S.J., et al., *GPIb-dependent platelet activation is dependent on Src kinases but not MAP kinase or cGMP-dependent kinase.* Blood, 2004. **103**(7): p. 2601-9.

89. Valtcheva, N., et al., *The commonly used cGMP-dependent protein kinase type I (cGKI) inhibitor Rp-8-Br-PET-cGMPS can activate cGKI in vitro and in intact cells.* J Biol Chem, 2009. **284**(1): p. 556-62.

90. Gambaryan, S., et al., *The oligopeptide DT-2 is a specific PKG I inhibitor only in vitro, not in living cells.* Br J Pharmacol, 2012. **167**(4): p. 826-38.

91. Burkhardt, M., et al., *KT5823 inhibits cGMP-dependent protein kinase activity in vitro but not in intact human platelets and rat mesangial cells.* J Biol Chem, 2000. **275**(43): p. 33536-41.

92. Evgenov, O.V., et al., *NO-independent stimulators and activators of soluble guanylate cyclase: discovery and therapeutic potential.* Nat Rev Drug Discov, 2006. **5**(9): p. 755-68.

93. Stasch, J.P., P. Pacher, and O.V. Evgenov, *Soluble guanylate cyclase as an emerging therapeutic target in cardiopulmonary disease.* Circulation, 2011. **123**(20): p. 2263-73.

94. Follmann, M., et al., *The chemistry and biology of soluble guanylate cyclase stimulators and activators.* Angew Chem Int Ed Engl, 2013. **52**(36): p. 9442-62.

95. Sandner, P., *From molecules to patients: exploring the therapeutic role of soluble guanylate cyclase stimulators.* Biol Chem, 2018. **399**(7): p. 679-690.

96. Tulis, D.A., et al., *YC-1-mediated vascular protection through inhibition of smooth muscle cell proliferation and platelet function.* Biochem Biophys Res Commun, 2002. **291**(4): p. 1014-21.

97. Chiche, J.D., et al., *Adenovirus-mediated gene transfer of cGMP-dependent protein kinase increases the sensitivity of cultured vascular smooth muscle cells to the antiproliferative and pro-apoptotic effects of nitric oxide/cGMP.* J Biol Chem, 1998. **273**(51): p. 34263-71.

98. Garg, U.C. and A. Hassid, *Nitric oxide-generating vasodilators and 8-bromo-cyclic guanosine monophosphate inhibit mitogenesis and proliferation of cultured rat vascular smooth muscle cells.* J Clin Invest, 1989. **83**(5): p. 1774-7.

99. Komalavilas, P., et al., *Activation of mitogen-activated protein kinase pathways by cyclic GMP and cyclic GMP-dependent protein kinase in contractile vascular smooth muscle cells.* J Biol Chem, 1999. **274**(48): p. 34301-9.

100. Ignarro, L.J., et al., *Role of the arginine-nitric oxide pathway in the regulation of vascular smooth muscle cell proliferation.* Proc Natl Acad Sci U S A, 2001. **98**(7): p. 4202-8.

101. Weinmeister, P., et al., *Cyclic guanosine monophosphate-dependent protein kinase I promotes adhesion of primary vascular smooth muscle cells.* Mol Biol Cell, 2008. **19**(10): p. 4434-41.

102. Herrington, W., et al., *Epidemiology of Atherosclerosis and the Potential to Reduce the Global Burden of Atherothrombotic Disease.* Circ Res, 2016. **118**(4): p. 535-46.

103. Doherty, T.M., P.K. Shah, and T.B. Rajavashisth, *Cellular origins of atherosclerosis: towards ontogenetic endgame?* FASEB J, 2003. **17**(6): p. 592-7.

104. Gomez, D. and G.K. Owens, *Smooth muscle cell phenotypic switching in atherosclerosis.* Cardiovasc Res, 2012. **95**(2): p. 156-64.

105. Iwata, H., I. Manabe, and R. Nagai, *Lineage of bone marrow-derived cells in atherosclerosis.* Circ Res, 2013. **112**(12): p. 1634-47.

106. Moore, K.J., F.J. Sheedy, and E.A. Fisher, *Macrophages in atherosclerosis: a dynamic balance.* Nat Rev Immunol, 2013. **13**(10): p. 709-21.

107. Libby, P., P.M. Ridker, and G.K. Hansson, *Progress and challenges in translating the biology of atherosclerosis.* Nature, 2011. **473**(7347): p. 317-25.

108. Moore, K.J. and I. Tabas, *Macrophages in the pathogenesis of atherosclerosis.* Cell, 2011. **145**(3): p. 341-55.

109. Ross, R., *Atherosclerosis--an inflammatory disease.* N Engl J Med, 1999. **340**(2): p. 115-26.

110. Nguyen, A.T., et al., *Smooth muscle cell plasticity: fact or fiction?* Circ Res, 2013. **112**(1): p. 17-22.

111. Tang, Z., et al., *Smooth muscle cells: to be or not to be? Response to Nguyen et Al.* Circ Res, 2013. **112**(1): p. 23-6.

112. Bennett, M.R., S. Sinha, and G.K. Owens, *Vascular smooth muscle cells in atherosclerosis.* Circ Res, 2016. **118**(4): p. 692-702.

113. Feil, S., F. Hofmann, and R. Feil, *SM22alpha modulates vascular smooth muscle cell phenotype during atherogenesis.* Circ Res, 2004. **94**(7): p. 863-5.

114. Rong, J.X., et al., *Transdifferentiation of mouse aortic smooth muscle cells to a macrophage-like state after cholesterol loading.* Proc Natl Acad Sci U S A, 2003. **100**(23): p. 13531-6.

115. Feil, S., et al., *Transdifferentiation of vascular smooth muscle cells to macrophage-like cells during atherogenesis.* Circ Res, 2014. **115**(7): p. 662-7.

116. Andreeva, E.R., I.M. Pugach, and A.N. Orekhov, *Subendothelial smooth muscle cells of human aorta express macrophage antigen in situ and in vitro.* Atherosclerosis, 1997. **135**(1): p. 19-27.

117. Allahverdian, S., et al., *Contribution of intimal smooth muscle cells to cholesterol accumulation and macrophage-like cells in human atherosclerosis.* Circulation, 2014. **129**(15): p. 1551-9.

118. Shankman, L.S., et al., *KLF4-dependent phenotypic modulation of smooth muscle cells has a key role in atherosclerotic plaque pathogenesis.* Nat Med, 2015. **21**(6): p. 628-37.

119. Albarran-Juarez, J., et al., *Lineage tracing of cells involved in atherosclerosis.* Atherosclerosis, 2016. **251**: p. 445-453.

120. Chappell, J., et al., *Extensive proliferation of a subset of differentiated, yet plastic, medial vascular smooth muscle cells contributes to neointimal formation in mouse injury and atherosclerosis models.* Circ Res, 2016. **119**(12): p. 1313-1323.

121. Jacobsen, K., et al., *Diverse cellular architecture of atherosclerotic plaque derives from clonal expansion of a few medial SMCs.* JCI Insight, 2017. **2**(19).

122. Ehret, G.B., et al., *Genetic variants in novel pathways influence blood pressure and cardiovascular disease risk.* Nature, 2011. **478**(7367): p. 103-9.

123. Emdin, C.A., et al., *Phenotypic consequences of a genetic predisposition to enhanced nitric oxide signaling.* Circulation, 2018. **137**(3): p. 222-232.

124. Erdmann, J., et al., *Dysfunctional nitric oxide signalling increases risk of myocardial infarction.* Nature, 2013. **504**(7480): p. 432-6.

125. Kessler, T., et al., *Functional characterization of the GUCY1A3 coronary artery disease risk locus.* Circulation, 2017. **136**(5): p. 476-489.

126. Maass, P.G., et al., *PDE3A mutations cause autosomal dominant hypertension with brachydactyly.* Nat Genet, 2015. **47**(6): p. 647-53.

127. Chen, J., et al., *Hypertension does not account for the accelerated atherosclerosis and development of aneurysms in male apolipoprotein E/endothelial nitric oxide synthase double knockout mice.* Circulation, 2001. **104**(20): p. 2391-2394.

128. Kuhlencordt, P.J., et al., *Accelerated atherosclerosis, aortic aneurysm formation, and ischemic heart disease in apolipoprotein E/endothelial nitric oxide synthase double-knockout mice.* Circulation, 2001. **104**(4): p. 448-54.

129. Kuhlencordt, P.J., et al., *Atheroprotective effects of neuronal nitric oxide synthase in apolipoprotein e knockout mice.* Arterioscler Thromb Vasc Biol, 2006. **26**(7): p. 1539-44.

130. Detmers, P.A., et al., *Deficiency in inducible nitric oxide synthase results in reduced atherosclerosis in apolipoprotein E-deficient mice.* J Immunol, 2000. **165**(6): p. 3430-5.

131. Kuhlencordt, P.J., et al., *Genetic deficiency of inducible nitric oxide synthase reduces atherosclerosis and lowers plasma lipid peroxides in apolipoprotein E-knockout mice.* Circulation, 2001. **103**(25): p. 3099-104.

132. Duda, D.G., D. Fukumura, and R.K. Jain, *Role of eNOS in neovascularization: NO for endothelial progenitor cells.* Trends Mol Med, 2004. **10**(4): p. 143-145.

133. Knowles, J.W., et al., *Enhanced atherosclerosis and kidney dysfunction in eNOS(-/-)Apoe(-/-) mice are ameliorated by enalapril treatment.* J Clin Invest, 2000. **105**(4): p. 451-8.

134. Friebe, A., et al., *Fatal gastrointestinal obstruction and hypertension in mice lacking nitric oxide-sensitive guanylyl cyclase.* Proc Natl Acad Sci U S A, 2007. **104**(18): p. 7699-704.

135. Doddapattar, P., et al., *Fibronectin containing extra domain A induces plaque destabilization in the innominate artery of aged apolipoprotein E-deficient mice.* Arterioscler Thromb Vasc Biol, 2018. **38**(3): p. 500-508.

136. Rohwedder, I., et al., *Plasma fibronectin deficiency impedes atherosclerosis progression and fibrous cap formation.* EMBO Mol Med, 2012. **4**(7): p. 564-76.

137. Glukhova, M.A., et al., *Expression of extra domain A fibronectin sequence in vascular smooth muscle cells is phenotype dependent.* J Cell Biol, 1989. **109**(1): p. 357-66.

138. Tamkun, J.W., et al., *Structure of integrin, a glycoprotein involved in the transmembrane linkage between fibronectin and actin.* Cell, 1986. **46**(2): p. 271-82.

139. Hynes, R.O., *Integrins: bidirectional, allosteric signaling machines.* Cell, 2002. **110**(6): p. 673-87.

140. Campbell, I.D. and M.J. Humphries, *Integrin structure, activation, and interactions.* Cold Spring Harb Perspect Biol, 2011. **3**(3).

141. George, E.L., et al., *Defects in mesoderm, neural tube and vascular development in mouse embryos lacking fibronectin.* Development, 1993. **119**(4): p. 1079-91.

142. Moretti, F.A., et al., *A major fraction of fibronectin present in the extracellular matrix of tissues is plasma-derived.* J Biol Chem, 2007. **282**(38): p. 28057-62.

143. Pankov, R. and K.M. Yamada, *Fibronectin at a glance.* J Cell Sci, 2002. **115**(Pt 20): p. 3861-3.

144. Hedin, U. and J. Thyberg, *Plasma fibronectin promotes modulation of arterial smooth-muscle cells from contractile to synthetic phenotype.* Differentiation, 1987. **33**(3): p. 239-46.

145. Hedin, U., et al., *Diverse effects of fibronectin and laminin on phenotypic properties of cultured arterial smooth muscle cells.* J Cell Biol, 1988. **107**(1): p. 307-19.

146. Astrof, S. and R.O. Hynes, *Fibronectins in vascular morphogenesis.* Angiogenesis, 2009. **12**(2): p. 165-75.

147. Tan, M.H., et al., *Deletion of the alternatively spliced fibronectin EIIIA domain in mice reduces atherosclerosis.* Blood, 2004. **104**(1): p. 11-8.

148. Babaev, V.R., et al., *Absence of regulated splicing of fibronectin EDA exon reduces atherosclerosis in mice.* Atherosclerosis, 2008. **197**(2): p. 534-40.

149. Thunemann, M., et al., *Visualization of cGMP with cGi biosensors.* Methods Mol Biol, 2013. **1020**: p. 89-120.

150. Nikolaev, V.O. and M.J. Lohse, *Novel techniques for real-time monitoring of cGMP in living cells.* Handb Exp Pharmacol, 2009(191): p. 229-43.

151. Thunemann, M., et al., *Transgenic mice for cGMP imaging.* Circ Res, 2013. **113**(4): p. 365-71.

152. Paolillo, M., et al., *Real-time imaging reveals augmentation of glutamate-induced Ca(2+) transients by the NO-cGMP pathway in cerebellar granule neurons.* Int J Mol Sci, 2018. **19**(8).

153. Peters, S., et al., *cGMP imaging in brain slices reveals brain region-specific activity of NO-sensitive guanylyl cyclases (NO-GCs) and NO-GC stimulators.* Int J Mol Sci, 2018. **19**(8).

154. Mohrle, D., et al., *NO-sensitive guanylate cyclase isoforms NO-GC1 and NO-GC2 contribute to noise-induced inner hair cell synaptopathy.* Mol Pharmacol, 2017. **92**(4): p. 375-388.

155. Shuhaibar, L.C., et al., *Intercellular signaling via cyclic GMP diffusion through gap junctions restarts meiosis in mouse ovarian follicles.* Proc Natl Acad Sci U S A, 2015. **112**(17): p. 5527-32.

156. Thunemann, M., et al., *Correlative intravital imaging of cGMP signals and vasodilation in mice.* Front Physiol, 2014. **5**: p. 394.

157. Tebubio. *WST-1 growth assay.* [cited 2018 02.02.2018]; Available from: https://www.tebu-bio.com/blog/2016/05/20/still-using-mtt-or-swt-1-for-cell-counting/.

158. Aceabio. *Real-time cell analysis.* [cited 2018 02.02.2018]; Available from: https://www.aceabio.com/about/real-time-cell-analysis/.

159. Limame, R., et al., *Comparative analysis of dynamic cell viability, migration and invasion assessments by novel real-time technology and classic endpoint assays.* PLoS One, 2012. **7**(10): p. e46536.

160. Miller, L. *Analyzing gels and western blots with ImageJ.* 2010 [cited 2018 02.02.2018]; Available from: http://lukemiller.org/index.php/2010/11/analyzing-gels-and-western-blots-with-image-j/.

161. Butt, E., et al., *cAMP- and cGMP-dependent protein kinase phosphorylation sites of the focal adhesion vasodilator-stimulated phosphoprotein (VASP) in vitro and in intact human platelets.* J Biol Chem, 1994. **269**(20): p. 14509-17.

162. Halbrugge, M., et al., *Stoichiometric and reversible phosphorylation of a 46-kDa protein in human platelets in response to cGMP- and cAMP-elevating vasodilators.* J Biol Chem, 1990. **265**(6): p. 3088-93.

163. Piedrahita, J.A., et al., *Generation of mice carrying a mutant apolipoprotein E gene inactivated by gene targeting in embryonic stem cells.* Proc Natl Acad Sci U S A, 1992. **89**(10): p. 4471-5.

164. Holtwick, R., et al., *Smooth muscle-selective deletion of guanylyl cyclase-A prevents the acute but not chronic effects of ANP on blood pressure.* Proc Natl Acad Sci U S A, 2002. **99**(10): p. 7142-7.

165. Sakai, T., et al., *Plasma fibronectin supports neuronal survival and reduces brain injury following transient focal cerebral ischemia but is not essential for skin-wound healing and hemostasis.* Nat Med, 2001. **7**(3): p. 324-30.

166. Ramirez-Zacarias, J.L., F. Castro-Munozledo, and W. Kuri-Harcuch, *Quantitation of adipose conversion and triglycerides by staining intracytoplasmic lipids with Oil red O.* Histochemistry, 1992. **97**(6): p. 493-7.

167. Lehners, M., *Zusammenhang zwischen cGMP-Signalgebung und dem Phänotyp von Glattmuskelzellen der Aorta.* AG. Feil, 2015.

168. Cornwell, T.L., et al., *Inhibition of smooth muscle cell growth by nitric oxide and activation of cAMP-dependent protein kinase by cGMP.* Am J Physiol, 1994. **267**(5 Pt 1): p. C1405-13.

169. Castro, L.R., et al., *Cyclic guanosine monophosphate compartmentation in rat cardiac myocytes.* Circulation, 2006. **113**(18): p. 2221-8.

170. Piggott, L.A., et al., *Natriuretic peptides and nitric oxide stimulate cGMP synthesis in different cellular compartments.* J Gen Physiol, 2006. **128**(1): p. 3-14.

171. Ridley, A.J. and A. Hall, *The small GTP-binding protein rho regulates the assembly of focal adhesions and actin stress fibers in response to growth factors.* Cell, 1992. **70**(3): p. 389-99.

172. Burridge, K. and K. Wennerberg, *Rho and Rac take center stage.* Cell, 2004. **116**(2): p. 167-79.

173. Rolli-Derkinderen, M., et al., *Phosphorylation of serine 188 protects RhoA from ubiquitin/proteasome-mediated degradation in vascular smooth muscle cells.* Circ Res, 2005. **96**(11): p. 1152-60.

174. Plow, E.F., et al., *Ligand binding to integrins.* J Biol Chem, 2000. **275**(29): p. 21785-8.

175. Lopez, M.J., D.L. Garbers, and M. Kuhn, *The guanylyl cyclase-deficient mouse defines differential pathways of natriuretic peptide signaling.* J Biol Chem, 1997. **272**(37): p. 23064-8.

176. Hahn, C. and M.A. Schwartz, *Mechanotransduction in vascular physiology and atherogenesis.* Nat Rev Mol Cell Biol, 2009. **10**(1): p. 53-62.

7 Curriculum Vitae

Hyazinth Gregor Dobrowinski

Born: 18.10.1988 Tczew (Poland)

Education

Eberhard Karls University Tübingen   *Expected Graduation Jul. 2019*

Doctoral candidate at the Interfaculty Institute of Biochemistry

Eberhard Karls University Tübingen (Grade: 1.3)   *Graduation Oct. 2013*

Master of Science in Microbiology

FHNW Muttenz, Switzerland (Grade: 4.91)   *Graduation Sep. 2010*

Bachelor of Science in Molecular Life Sciences

Justus-Von-Liebig school Waldshut-Tiengen   *Graduation Jul. 2007*

Training as assistant for biotechnology (BTA)

Publications

1   Dhayade S, Kaesler S, Sinnberg T, **Dobrowinski H**, Peters S, Naumann U, Liu H, Hunger RE, Thunemann M, Biedermann T, Schittek B, Simon HU, Feil S, Feil R. Sildenafil potentiates a cGMP-Dependent Pathway to Promote Melanoma Growth. Cell Rep, 2016. 14(11)

2   Lehners M, **Dobrowinski H**, Feil S, Feil R. cGMP Signaling and Vascular Smooth Muscle Cell Plasticity. J Cardiovasc Dev Dis, 2018. 5(2)